12-1996

Residual Strength and Fatigue Characterization of SCS-6/Ti-6-4

Sang-Myung Lee

RESIDUAL STRENGTH AND FATIGUE CHARACTERIZATION OF SCS-6/Ti-6-4

THESIS

Sang-Myung Lee
Major, ROKA
AFIT/GAE/ENY/96D-7

DEPARTMENT OF THE AIR FORCE
AIR UNIVERSITY
AIR FORCE INSTITUTE OF TECHNOLOGY

Wright-Patterson Air Force Base, Ohio

DISCLAIMER NOTICE

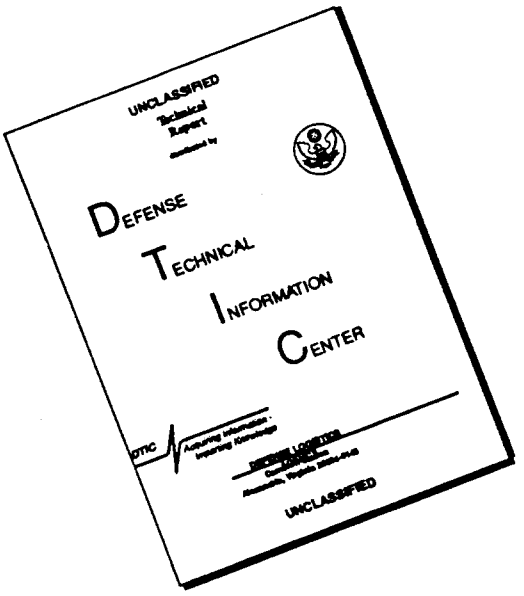

THIS DOCUMENT IS BEST QUALITY AVAILABLE. THE COPY FURNISHED TO DTIC CONTAINED A SIGNIFICANT NUMBER OF PAGES WHICH DO NOT REPRODUCE LEGIBLY.

AFIT/GAE/ENY/96D-7

RESIDUAL STRENGTH AND FATIGUE CHARACTERIZATION OF SCS-6/Ti-6-4

THESIS

Sang-Myung Lee
Major, ROKA
AFIT/GAE/ENY/96D-7

AFIT/GAE/ENY/96D-7

RESIDUAL STRENGTH AND FATIGUE CHARACTERIZATION OF SCS-6/Ti-6-4

THESIS

Presented to the Faculty of the Graduate School of

Engineering of the Air Force Institute of Technology

Air University

In Partial Fulfillment of the

Requirements for the Degree of

Master of Science in Aeronautical Engineering

Sang-Myung Lee, B.A.

Major, ROKA

December 1996

Acknowledgments

The accomplishment of this thesis would not have been possible, if it were not for the generous support of several individuals.

I would like to express my sincere gratitude to my thesis advisor, Professor Dave Robertson, who had faith and patience when others did not. He provide me with the freedom to explore almost any area I chose, even when I made mistakes and outcome was quite unclear. He always patiently waited and gently guided me in the right direction when I was going astray and managed to clear the fog. Dr. Mall, thank you for all your attention. Dr. Turcotte, thanks for looking at drafts long distance and considerate correction.

I would like to thank all of the AFIT Aerospace Department Laboratory Technicians, Dan Rioux, Jay Anderson. Especially, thanks to Mark Derisso and Shan for understanding and answering to all of my odd questions. Additionally, thank all of the ROK officers for their friendship and Col. Sun-Pil Ham for many advices.

I would like to thank my mother and my brothers, who had the most difficult time while I was studying in the AFIT as well as my mother-in-law and my sisters-in-law, who were taking care of all of my affairs during my absence.

Finally, I would like to extend appreciation and my love to my wife, Sun-Hea. She has suppressed all her desire but never failed to cheer me up while I was being extremely difficult. Thank my cute daughter, Yea-Jin. She lost a lot of time to play together with her father. Hopefully, they are going to be happy.

Sang-Myung Lee

Table of Contents

List of Figures

Page

List of Tables

Page

Abstract

Metal matrix composite have potential in a variety of aerospace applications, but they should be better understood before they can be employed. Despite the many studies that have contributed to characterizing the fatigue response of titanium alloy MMCs, few have researched the residual strength. The purpose of this study was to investigate the residual strength and the frequency effects on the residual strength of an unidirectional laminate of SCS-6/Ti-6-4, a titanium alloy matrix based composite under tension-tension, load-controlled conditions at elevated temperatures and different frequencies. Specimens were fatigued at frequencies of 1 and 0.01Hz, and at maximum stress of 900MPa with a stress ratio 0.05 and temperature of 427°C. Static tests were accomplished to obtain ultimate tensile strength. Macromechanical fatigue responses at different frequencies were compared using stress-strain plots, modulus histories and strain histories, while microscopy and fractography revealed the micromechanical behavior and damage mechanisms.

For the fatigue tests, macroscopic observation shows that fatigue life was more cycle-dependent at higher frequency and more time-dependent at lower frequency. Microscopic observation revealed that failure mode was more matrix-dominated at higher frequency and fiber-dominated at lower frequency.

There was no evidence of dependence of the residual strength on frequency. The residual strength can be considered to have a fatigue life dependency. The materials kept their strength up to approximately 80% of their lives, then catastrophically decreased at

the last 20% of the lives. But, due to the variations from specimen to specimen and plate to plate, the residual strengths were scattered. Therefore, two reasonable band curves to cover these variation characteristics of the materials, band curves had an approximately 15% difference.

1. Introduction

Advanced metal matrix composites (MMC) based on titanium alloys and Ti-Al-V intermetallic alloys reinforced with SiC fiber are promising materials for high temperature structural applications. They have a unique combination of several attractive properties, including high specific stiffness and excellent environmental stability. They can also be used at elevated temperatures without any serious degradation of mechanical properties. Potential applications of these novel materials include gas turbine engines, airframes for hypersonic aircraft and advanced energy conversion systems. Since structural components must perform under a wide range of mechanical and thermal loading conditions, a significant amount of research has been performed to characterize the performance and processing technology of MMCs.

Two significant issues in the development of these materials are the large residual stresses generated during fabrication and weak interface between the fiber and the matrix. These unique characteristics arise from a mismatch in the coefficient of thermal expansion (CTE) and the interphase or reaction zone between the fiber and the matrix. Even though fiber and matrix have low coefficient of thermal expansion (CTE), the CTE of the matrix is generally much larger than that of the fiber. This mismatch develops the residual stresses that are an important consideration in choosing fiber/matrix combinations. Research in recent years have focused on damage and fracture mechanisms of titanium MMCs under various loading conditions. Therefore, most fatigue tests have been taken to failure to analyze these characteristics of the MMCs. Few

studies have researched the responses of the residual strength and the effects of cyclic load frequency on the residual strength. In many applications, such as gas turbine engines (especially for an airplane) and some airframe parts should be replaced after a certain amount of use based on the degradation of the material's residual strength even if their conditions can be considered to be good for further use. This parameter is important to designers in order to determine the load capacity of components.

This research examined the residual strength after fatigue loading of unidirectional SCS-6/Ti-6-4 composite system consisting of Ti-6Al-4V (% wt) titanium alloy reinforced with silicon-carbide fibers (SCS-6) which have approximately 35% fiber volume fraction. A static test was performed to obtain the ultimate tensile strength under an elevated temperature (427° C) which is considered to be an application temperature for this material. Tension-tension isothermal fatigue cyclic load was applied under the load controlled mode at this temperature with a maximum stress of 900 MPa and R=0.05 up to a specific target cycle. The frequencies 1Hz and 0.01Hz were used for these tests. This maximum stress (900 MPa), which is slightly higher than the yield stress of the material ($\sigma_{yield} \cong 850$ MPa), was chosen to fail the specimens within reasonable amount of time. Plots of mean strain and modulus versus fatigue life, and stress versus strain were established to illustrate how the macromechanisms change in cyclic frequency. Fracture surfaces and specimen sections were examined microscopically to study the damage and fracture mechanism. Coupling these two data from the macroscopic and the microscopic observation helped to determine which deformation mechanisms lead to specimen failure and affect the residual strength. Finally, based on this information, the residual strength

versus fatigue life was plotted. The residual strengths of the specimen demonstrated significant scatter due to variations from specimen to specimen, and so maximum and minimum curves were used to reasonably band the scattered data. These curves indicated that the specimens held their strength up to 80% of the expected fatigue lives. The residual strength dropped catastrophically after this percent life, but the level of the specimen's strength was not affected by frequency as a function of percent life. However, it was evident that duration of the residual strength shifts from cyclic-dependent to time-dependent as the frequency is changed from high to low owing to its fatigue life dependency. Fracture surfaces from specimens tested for residual strength were also examined to quantify the fatigue area vs. static area from the fracture surfaces. Because of the variations from specimen to specimen and the fiber dominated failure mode, especially for the 0.01Hz tests, quantifying the fatigue area was difficult. Finally, this quantified fatigue area versus the residual strength was plotted. In this plot, it was observed that the residual strength decreased as the fatigue area increased even if they were not linearly fit.

The following chapters contain a description of the above mentioned efforts. First, significant contributions in MMC research are reviewed from previous studies. Second, a complete description of the test experiment and techniques used in this study are provided. Third, a discussion of the experimental results are presented. This includes examples of the mechanical response, microscopy analyses, fatigue life analyses, and residual strength analyses. Finally, some conclusions and recommendations are given.

2. Previous Work

2.1 Introduction

In contrast to "homogeneous" and "isotropic", a laminated composite material may be described by any of the following terms: homogeneous isotropic, homogeneous anisotropic, heterogeneous orthotropic, heterogeneous anisotropic, and quasi-isotropic, which involves the complexity of the mechanical constitution of the composites. Moreover, the variations of their characteristics can make their analysis difficult. Therefore, in order to fully understand the material used in this study, Having a knowledge of the fundamentals of macro-mechanical and micro-mechanical behavior is necessary. This chapter discusses previous static and fatigue studies to gain a general understanding of damage mechanisms, interfacial properties and the high temperature processing on titanium-based metal matrix composites. This chapter also reviews some important fundamentals that are pertinent to this study.

2.1 Fundamentals of Macro-mechanical Behavior

The fatigue life, modulus degradation and strain response are important factors to analyze the macro-mechanical behavior. To enhance the practicality of the analysis of these macro-mechanical behavior, various loading environments corresponding to actual applications have been carefully applied to MMC specimens. Almost all applications include quite complex load and temperature factors. These factors have been investigated both individually and in concert. Previous researchers have used various testing methods to accomplish this. For instance, static or monotonic tests,

thermal fatigue (TF), isothermal fatigue (IF) and thermomechanical fatigue (TMF) tests have all been used under many conditions to characterize these materials. The simplest of all loading conditions is a static test where increasing load or strain is applied over a range of temperatures until the composite fails. From these tests, the elastic modulus, ultimate tensile strength and yield stress or proportional limit can be characterized.

When the term fatigue testing is used, it generally refers to test performed at a constant room temperature. This test often serves as a baseline for further high temperature isothermal (IF) or thermomechanical fatigue (TMF) testing. Thermal fatigue (TF) involves cycling the temperature while the specimen stress is held constant. This is usually accomplished by varying the temperature over a specified range using the sawtooth wave function. The coefficient of thermal expansion (CTE) of the matrix is typically larger than that of the fiber. This results in fluctuating stresses at the fiber-matrix interface when the specimen is exposed to thermal cycling. In the isothermal fatigue (IF) environment, the temperature is held constant while cycling a mechanical load. Since the thermally induced stresses are constant in this case, this test environment provides an opportunity to isolate damage mechanisms due only to applied mechanical loading. The TMF test provides a controlled method which approaches the actual aerospace environment. In this case, a specimen is subjected to both thermal and mechanical fatigue. These parameters can be cycled in-phase (IP), so that the maximum (minimum) temperature and load are reached simultaneously. Also, the temperature can be cycled out-of-phase (OP), so the temperature lags the load profile by some phase angle. These cyclic profiles may become more complex by imposing hold times on the

temperature, load, or both [12]. Fatigue testing may be accomplished using either load or strain control mode. In load control mode, the load range is determined by the ratio of the maximum stress to minimum stress which is called the R-ratio ($R=\sigma_{max.}/\sigma_{min.}$). For the tension-tension test the R-ratio is greater than or equal to zero so that the specimen is not subjected to compressive stress. When either the strain control mode or tension-compression test is used, special consideration must be taken to prevent buckling. This is required during strain-control loading because matrix creep deformation will result in a relaxation of the composite stress, so compressive loads are then necessary to achieve the minimum strain level [28]. Figure 2.1 and 2.2 show typical strain versus fatigue life in load control mode, and stress histories over fatigue life in a strain control mode.

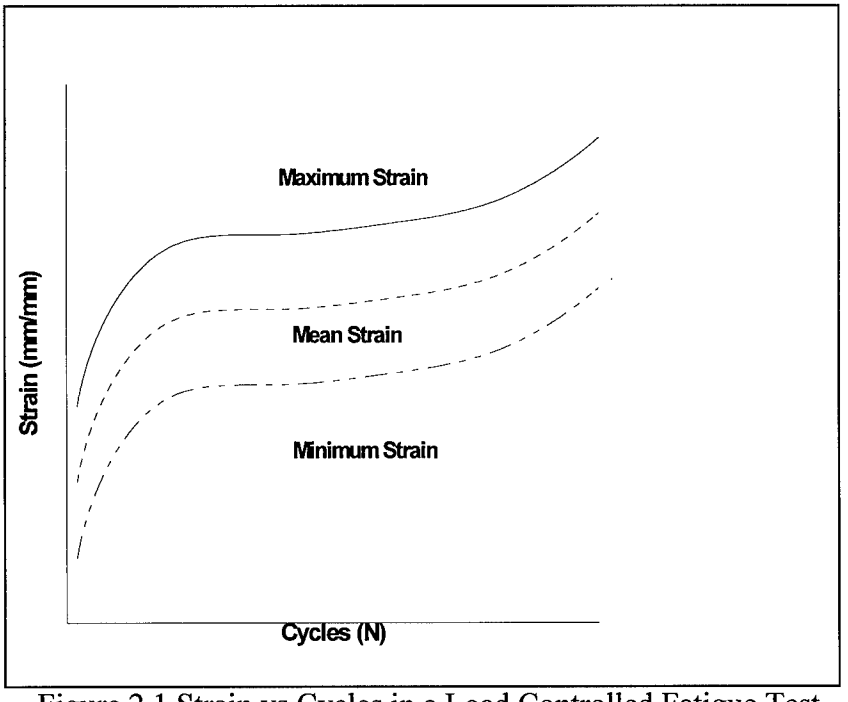

Figure 2.1 Strain vs Cycles in a Load Controlled Fatigue Test

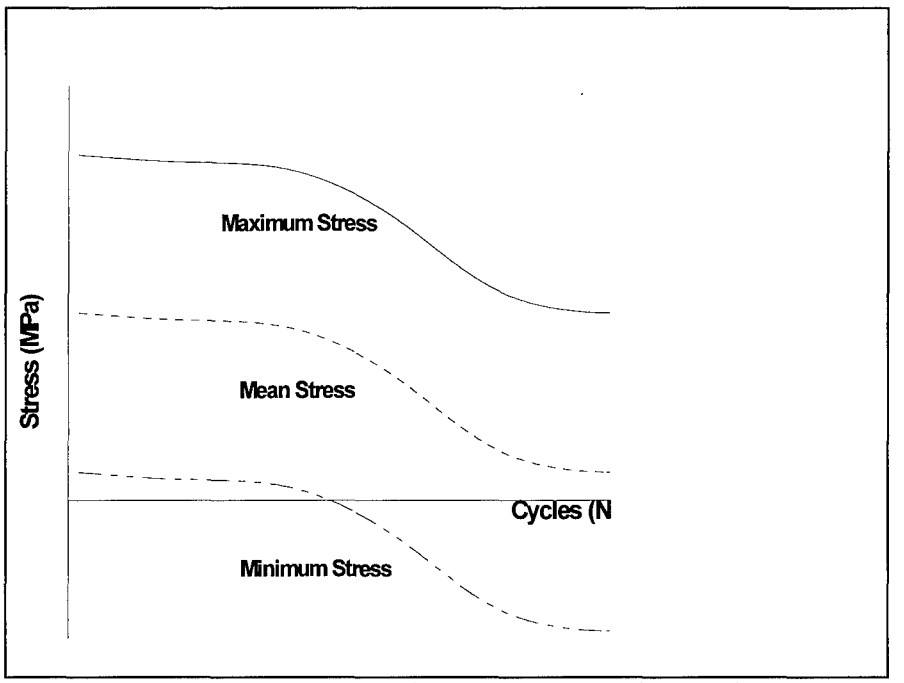

Figure 2.2 Stress vs Cycles in a Strain Controlled Fatigue Test

Following Talreja's approach [38] for unidirectional polymeric composites, fatigue life diagrams are often broken into three distinct regimes (Regime I, II and III). Region I corresponds to fiber breakage and the resulting fiber-matrix interfacial debonding. The scatter band in this region accounts for variations in fiber strength and matrix ductility. Damage in Region I is characterized as non-progressive. Region II corresponds to progressive fatigue damage. Damage mechanisms in Region II include matrix cracking and fiber-matrix interface failure. Region III corresponds to the matrix fatigue limit. In this region, matrix cracking, if it does occur, is non-propagating. Thus, the three region fatigue curve provides a useful tool for depicting a relationship between the damage mechanisms, the fatigue life, and the applied load or strain. Majumdar and

Lerch [20] also showed that the S-N curve in regime I is dominated by fiber failure, while in Regime II it is dominated by matrix failure. Regime III represents the fatigue limit of the material. These regimes are shown in figure 2.3.

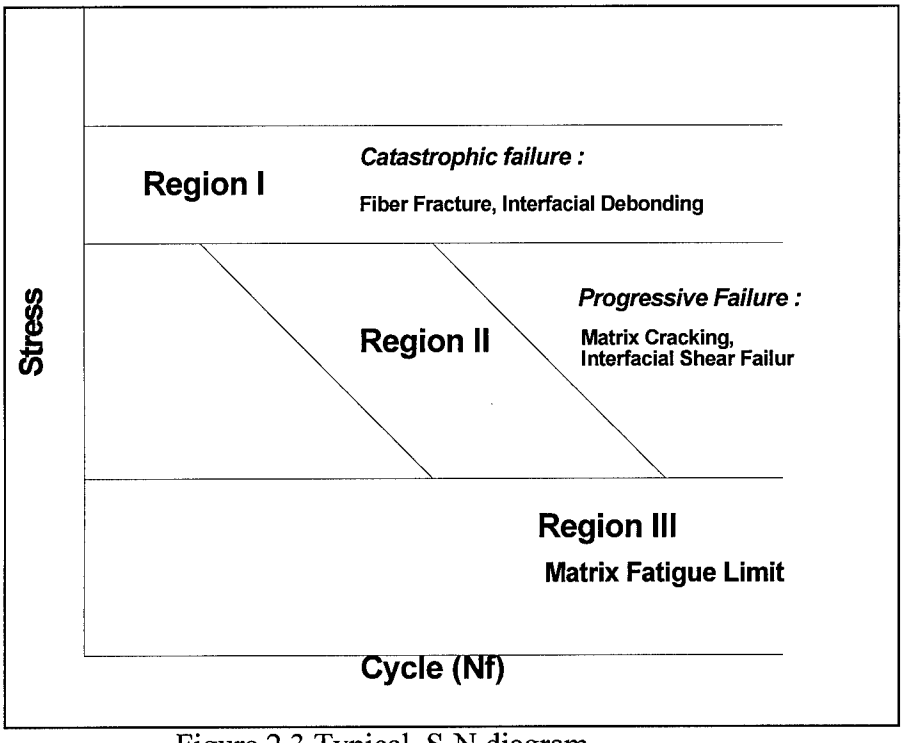

Figure 2.3 Typical S-N diagram

In addition to fatigue life, the degradation of modulus (E) or stiffness, which is defined as the slope of the elastic stress-strain curve, can be used to analyze the macro-mechanical behavior of a failed specimen. Since the applied stress remains constant for load control testing conditions, any change in modulus results in a change in strain. As the number of cycles increase, damage occurs resulting in an increase in strain range. The nature of this damage may be debonding, matrix and /or fiber cracking or matrix plasticity. Although fatigue life and modulus degradation are strong indicators that

damage has occurred, the exact nature of the damage can only be determined by micro-mechanical analysis.

2.2 Fundamentals of Micro-mechanical Behavior

Micro-mechanical analysis in the current study is broken into two separate groups: damage and plasticity. Damage mechanisms include matrix cracks, fiber breaks, and fiber-matrix debonding. Plasticity includes slip band formation, crack nucleation and fatigue striations, which are similar to slip bands. The type of damage in each specimen is dependent upon the applied stress level.

Damage is defined by the creation of new free surfaces from fiber and matrix crack growth. Cracks may originate within the fiber and matrix itself or they may originate from fiber-matrix interfaces. Fiber cracks may cause debonding between the fiber and matrix. This debonding prevents the fibers from transferring any load to the matrix. Debonding may also occur from low interface strength caused by poor material processing. Debonding of this nature provides numerous crack initiation sites within the matrix. The two types of debonding are important in determining what causes failure. Extreme necking around fibers due to fiber overload causes debonding and fiber cracks. Debonding that shows less necking indicates destruction of the fiber-matrix interface due to low interface strength. Matrix cracks are likely to originate from this region whereas fiber cracks may be nonexistent.

Plasticity includes the formation of slip bands and fatigue striations as well as microvoid coalescence. Slip bands are caused by dislocation motion along closely-packed crystallographic planes called slip planes [19]. The ridges or steps formed by

slip bands are seen as parallel lines on the surface and remain after unloading. Slip bands created by fatigue are called fatigue striations. The striations run parallel to the crack growth direction, thereby indicating where cracks originated and in what direction they were moving [17]. Each striation represents the incremental advance of the crack front as a result of one cycle. The extent of the advancement varies with stress range, i.e. higher stress ranges result in larger spaces between striations. Microvoid coalescence also indicates plastic behavior [17]. Furthermore, it indicates ductile failure. This behavior is most easily found in regions containing high concentrations of matrix necking. Microvoid coalescence appears as a dull, dimpled surface and is caused by necking of the matrix material around tiny voids created in material processing [17].

In composite materials, the damage mechanisms and plastic behavior may be interdependent. Pre-existing matrix cracks will result in the plastic deformation of the material just ahead of the crack tip, thereby creating slip bands or fatigue striations. Alternatively, the formation of slip bands in composites may cause cracks. Debonding may also lead to the formation of matrix cracks. In strong, complex alloys, planar slip is prevalent and surface nucleation of cracks by slip processes is retarded. In these materials, the stress concentration produced by the interaction between slip bands and second phase particles, i.e. inclusions or precipitates, can crack or debond the particle and produce internal fatigue cracks [6]. Similar behavior may be expected in a MMCs where the fibers act the interspersed precipitate. Hence, debonding between the fiber and matrix may cause internal cracks. This will be shown later in the discussion of the micro-mechanic behavior of the tested material.

2.3 Recent Studies In Metal Matrix Composite Testing

Jeng, et al.[13] studied tensile behavior in SCS-6 fiber reinforced Ti-6-4, Ti-15-3, Ti-25-10 matrix composite. They conclude that the stress-strain response, the crack growth and the fracture behavior are strongly influenced by the strength of the fiber, the toughness of the matrix and the interfacial shear strength. They also found that the strength decreases as the thickness of the reaction zone increases.

Jeng, Alassoer and Yang [14] conducted low cycle fatigue tests of SCS-6 fiber reinforced Ti-6-4, Ti-15-3, Ti-25-10 matrix composite with 35 fiber Vol%. In their study, the fatigue damage of the SCS-6 fiber-reinforced titanium matrix composites was classified into three regimes: (1) fiber breakage dominated (non-progressive failure), (2) interface, matrix cracking and fiber breakage (progressive failure), and (3) matrix cracking dominated. They showed that the SCS-6/Ti alloy matrix composites do not exhibit a "self-similar fatigue growth" behavior and the low cycle fatigue life is controlled by (1) crack initiation at the surface defects and interfacial reaction layer, (2) crack propagation rate in the matrix and (3) the properties of the fibers.

Sami, et al.[5] tested a 16-ply layup with a 40 Vol% SCS-6 fiber-reinforced Ti-6-4 matrix alloy under strain-controlled fatigue at room temperature and elevated temperature in air environment and made comparison with load-controlled fatigue tests. The fatigue behavior was characterized by three basic regimes of damage development corresponding to three distinctive regions of the strain-life curve: Region(1) is the low cycle fatigue range where high stresses and strains approach the strength distribution scatterband of the fiber. Region(2) is intermediate fatigue life region where the stresses

and strains are insufficient to result in extensive fiber failures. Region(3) is high cycle fatigue region, where the fatigue stresses and strains are below the matrix fatigue crack initiation stress. They also found that early fatigue damage took place on the first few cycles in transverse test orientation and the low transverse strength and the brittle nature of the fiber-matrix interface are the two main contributors to the low strain-life behavior of this MMC when loaded normal to the fiber direction.

Jeng, et al.[15] used an 8-ply unidirectional SCS-6 fiber-reinforced Ti-6-4 composite with 35 Vol% for thermal-mechanical fatigue behavior(TMF) and isothermal fatigue behavior(TF) . The maximum cyclic temperature varied from 370°C to 650°C and maximum applied stresses ranged from 828 to 1180 MPa. They concluded that matrix cracking with fibers bridging in the wake of the crack tip is the major damage mechanism of this MMC tested at high temperature isothermal fatigue and TMF and that environmental-assisted matrix cracking, oxidation of the outer carbon layer and formation of thermal pits on the fiber surface are the main damage mechanisms for high temperature with oxidizing environment.

Bhatt and Grimes [4] compared axial, low cycle fatigue properties of 25 and 44 Vol% SiC/Ti-6-4 composites measured at 650°C with the fatigue properties of unreinforced Ti (6Al-4V) at the same temperature. At this temperature, the author found significant improvement in the composite's life over the Ti-alloy's life. Since the modulus of the fiber is reduced to less than that of the matrix and the residual stresses in the composite are relived at 650°C, the composite specimens lasted longer than the monolithic specimens. As with room temperature testing, all cracks initiated on the

specimen surfaces at broken and fragmented fibers, while interior fibers only failed near advancing cracks.

R.N. Pittman [29] studied the frequency effects on the fatigue behavior of a unidirectional 8-ply SCS-6/Ti-6-4 composite at elevated temperature. He applied four different frequencies (0.01, 0.1, 1 and 10Hz) and also applied three stress levels with stress ratio of 0.05 as well as compared isothermal tests at 427°C with 370°C and 538°C. He found that fatigue life was more cycle-dependent at higher frequencies and more time-dependent at lower frequencies due to the possibilities both more oxidation progress during longer exposure to the high temperature and more creep at lower frequencies. He also found that frequency effects were magnified as temperature increased.

Barney, et al.[3] investigated fatigue crack growth resistance of six-ply SiC/Ti-6-4 with a through-thickness cut notch under cyclic loading. In their study, all tests were performed in three point bending. They concluded that a reduction in the fatigue crack growth rate as the value of the nominal ΔK_{app}(nominal applied stress intensity range) increased can be caused by the effective stress intensity range at the crack tip, ΔK_{tip}, decreasing i.e. the presence of unbroken fibers bridge the crack faces and provide crack tip shielding. At the high stress ratio (R=0.5) and high $\Delta K_{app} \approx 18$ MPa$\sqrt{m}$ at ambient temperature fatigue crack growth rates increase with nominal ΔK_{app} increases due to lack of fiber bridging. At the lower mean stress (R=0.1), there is a marked improvement of the crack growth resistance of the composite system for a given level of ΔK_{app} due to sufficient fiber crack bridging by intact fibers. They concluded that the

crack growth resistance of SiC/Ti-6-4 at ambient temperatures is markedly superior to that of the unreinforced alloy and is highly dependent on both the initial applied stress intensity range and mean stress as well as increased fiber failure occurs as a result of increased initial applied stress intensity range, increased mean stress and at the elevated test temperature of 500°C.

Sen-Tzer Chiou [34] investigated the residual strength of the unidirectional and cross-ply laminates of SCS-6/Ti-15-3, metal matrix composite at the elevated temperature of 427°C under tension-tension load controlled mode. The tests were performed under the following conditions : σ_{max}=900MPa and 10Hz for the unidirectional specimen, σ_{max}=300MPa & 400MPa and 5&10Hz for the cross-ply specimens. He found that the residual strength results for specimens under both the different test conditions and the specimens having different fiber direction had similar trends, where all residual strength decrease slowly with cycles and then dropped catastrophically near the end of the fatigue life due to the fiber bridging the critical matrix cracking.

Schmidt, C.G., et al. [32] performed residual strength testing of a thermomechanically-fatigued SCS-6 fiber-reinforced Ti-15Mo-3Nb-0.2Si metal matrix composite under the conditions, σ_{max}=800MPa, R-ratio=0.1, load frequency=1cycle/180sec, thermal frequency=1cycle/180sec: out of phase to the load cycle. He assessed the residual strength after thermomechanical fatigue from a quantitative analysis of the fracture surfaces and the individual contributions to the total residual strength of the composite. On the base of estimations following the load paths:

(1) fibers that were not broken during thermomechanical fatigue loading, (2) the matrix that did not fail due to thermomechanical fatigue loading, (3) the regions of the matrix that failed in shear as fatigue cracks linked together during the final stages of fracture, (4) the friction between the matrix and fibers that were broken during fatigue, he showed that the sum of the estimated contributions of the four sources of the residual strength would be in good agreement if the accuracy of the counting of the estimated number of fiber that broke during thermomichanical fatigue could be improved.

3. Experimental Set-up and Procedures

In order to facilitate a better understanding of the present experimental work, this chapter provides more complete information about the material, test equipment, set-up, and procedures used in this study.

3.1 Material

The material for this study was a unidirectional fiber reinforced SCS-6/Ti-6AL-4V Metal Matrix Composite. The composite was produced by hot pressing an eight ply sandwich structure of alloy (90% Titanium, 6% Aluminum and 4% Vanadium: by weight) and aligned continuous Silicon-Carbon fibers (SCS-6) . This foil fiber processing produced a well compacted unidirectional composite with a fiber volume fraction of approximately 0.35. This material was manufactured by Textron Specialty Materials Inc.

To provide a better understanding of the macro and micro-mechanisms of the matrix under the elevated temperature test, it is helpful to review the general characteristics and fracture properties of Ti-6-4 Titanium Alloy.

Titanium possesses a hexagonal close packed crystal structure at temperatures up to 882°C, above which it undergoes an allotropic transformation to b.c.c. structure. The transition temperature is strongly influenced by the presence of impurities and alloying elements. The chemical composition (wt %) of titanium and some of its alloys are shown in table 3.1. The alloying elements affect the transition temperature as follows: C, N,

and O increase the transition temperature and are referred to as α stabilizers while Cr, Fe, Mo and V decrease it and are called β stabilizers. Tin and zirconium are known as neutral elements. The relative amounts of α and β stabilizers in an alloy determine whether its microstructure is predominantly single-phase α, two phase α+β or single phase β. The mechanical properties of titanium and its alloys are strongly dependent on the processing history and the resulting microstructure [18].

Table 3.1 Chemical composition (wt %) of titanium and some of its alloys

Material	C	N	O	H	Fe	Al	Zr	Mo	V	Sn
CP titanium	0.01	0.02	0.14	0.002	0.10					
Ti-5Al-2.5Sn		0.002	0.174		0.314	5.10				2.72
Ti-6Al-5Zr-0.5Mo-0.25Si		0.01	0.14	0.003	0.024	6.18	5.27	0.28		
Ti-15Mo	0.048		0.165	0.015				12.8		
Ti-6Al-4V	0.048	0.013	0.137	0.006	0.197	6.49			4.36	

Ti-6Al-4V is an α+β titanium alloy. Such alloys are used either in the solution treated and aged condition or annealed condition. Solution treating is carried out high in the α+β field followed by quenching in water or oil. As a result of quenching , the β phase present at the solution treatment temperature may be retained or partly transformed during quenching. Aging of the quenched product is carried out in the temperature range of 753K-923K which results in precipitation of α and produces a fine mixture of α and β in the retained or transformed β phase. Annealing may be carried out in the temperature range 973-1073K. The microstructure consists of equiaxed primary α grains interspersed with β particles [18].

Figure 3.2 shows the fracture map for Ti-6Al-4V. In the map, the alloy fails in the familiar ductile manner causing the development of a "cup" and "cone" in the necked region of the tensile specimen below $0.25T_m$ (210°C) and at high stresses ($>10^{-2}$ E). Transgranular creep fracture occurs at intermediate temperatures, 0.25-0.5 T_m (210-700°C) and lower stress ($<10^{-2}$ E). Above 0.5 T_m (~ 700°C), Ti-6-4 undergoes, during tensile testing, dynamic recrystallization and neck down nearly to a point with corresponding values of reduction in area exceeding 95% [18].

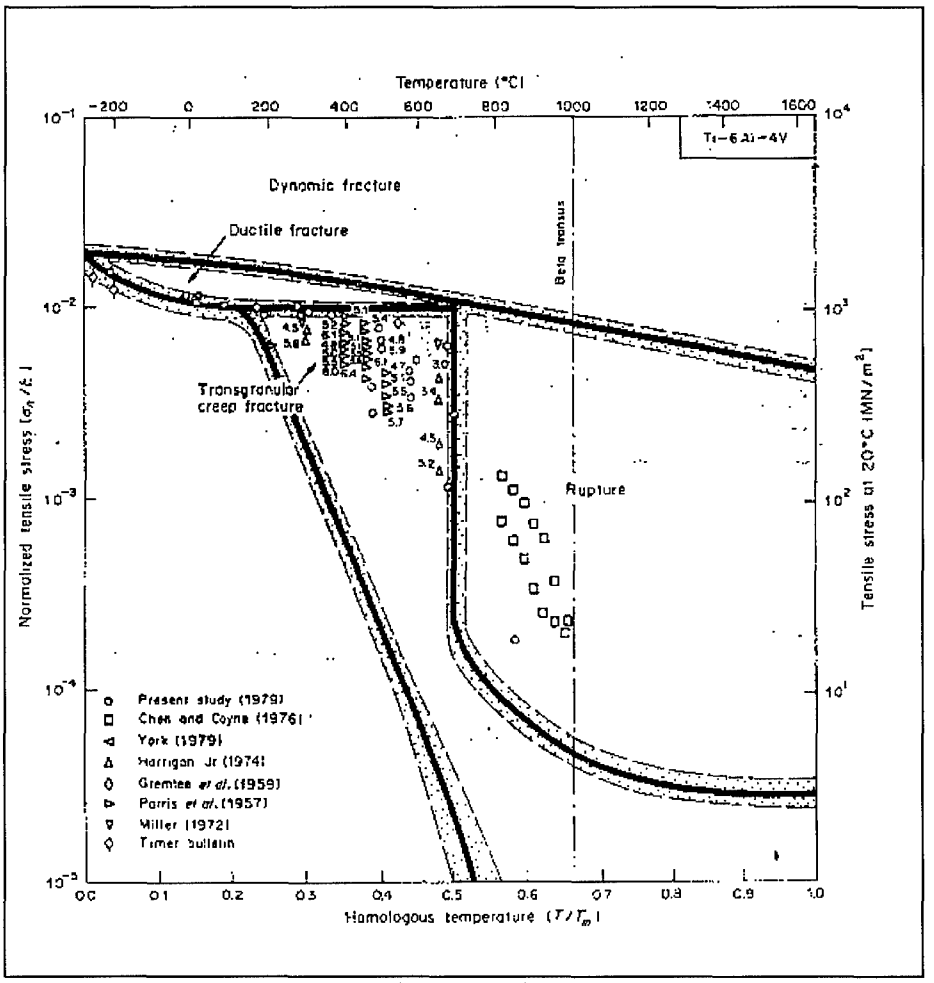

Figure 3.1 Fracture Mechanism Map for α+β Alloy Ti-6Al-4V [18]

Each fiber has a carbon core which acts as a substrate for surrounding layers of silicon carbide. Table 3.2 shows Young's modulus (E), coefficient of thermal expansion (α), and yield stress (σ_{ys}.) of the composite's constituents at room temperature [29]. Properties of the composite were calculated using the rule of mixtures approximation [24].

Table 3.2 SCS-6/Ti-6.4 Constituent Properties

Constituent	E (GPa)	α (10^{-6} /°C)	σ_{ys} (MPa)
SCS-6 fiber	400	4.9	
Ti-6-4 matrix	110	7.5	1089
$[0]_8$ Laminate	212	6.6	1163

A unique loading condition that MMCs experience arises from the large difference in coefficient of thermal expansion between the fiber and matrix. After cool down from high temperature processing, large residual shear stresses along the fiber/matrix interface can be a source of damage in the as received composite, and can accelerate interfacial cracking during fatigue testing [29].

3.2 Specimen Design & Preparation

The specimens of the present study were supplied by Textron Specialty Materials Division, Textron Inc. For all tests, dogbone specimens were used. This geometry improved the chance of failure within the gage length. Both rectangular and dogbone specimens have been used by previous researchers. For instance, Gayda and Gabb [9] performed load control tests on the unidirectional SCS-6/Ti-15-3 MMC at elevated

temperature using both geometries and showed that the mechanical response and fatigue life of SCS-6/Ti-15-3 was independent of specimen design [8]. However, dogbone specimens must be machined to proper dimensions to prevent stress concentrations or induced shear stresses. If the shoulder radius is too small, the chance of failure outside the gage length may increase. Some researchers have sought to quantify this by using a finite element analysis (FEA) to determine the shoulder shear stress for varying radii of curvature [22]. The shoulder radius of the specimens used in the present study is listed in Figure 3.2. This geometry produced a high level of success for failure within the gage length.

The MMC plates were produced by hot isostatic pressing (HIP-ing) alternating layers of fibers and matrix together with 35Mpa pressure at 815°C. Each plate was inspected for internal fiber damage, gross matrix cracking and ply delamination using ultrasonic immersion through transmission testing. No processing damage was revealed from this evaluation.

Specimens were initially cut into rectangular coupons with a low-speed diamond saw and then further machined into the "dogbone" shapes shown in Figure 3.2. The nominal dimensions of the rectangular specimens were 101.60 mm x 12.70 mm, and the dogbone width was 9.2 mm at the ends and 7.5 mm in the gage section.

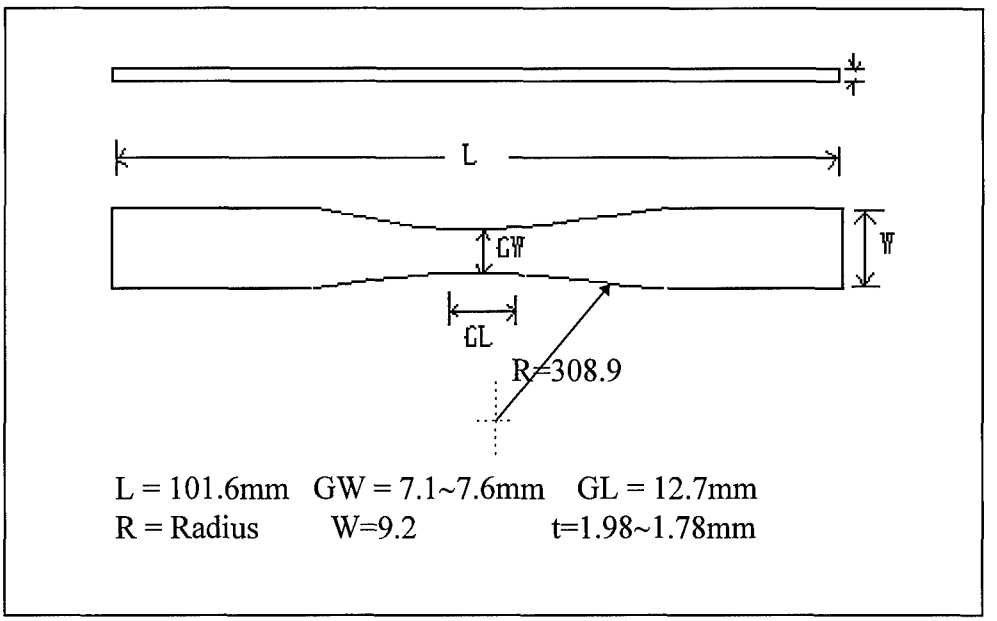

Figure 3.2 Specimen Geometry

The specimen edges were machined using a diamond encrusted blade and then heat treated to simulate a secondary processing cycle that this composite would be expected to undergo in an aerospace application. For this heat treatment the specimens were wrapped in Tantalum foil and placed in a 0.0133 Pa vacuum environment. Chamber temperature was increased to 677°C at 10°C/min. and held constant for 60 min. Temperature was then ramped to 843°C at 10°C/min and held constant for 120 min. Next, the temperature was decreased to 316°C at 3°C/min. at which point the oven power was cut and the specimens cooled to room temperature at 1.6°C/min. Finally, specimen edges were ground and polished in order to remove burs and damage from cutting.

Polishing of the curved edges on the dogbone specimen required the development of a hand polishing technique. Several specimens could be polished simultaneously by gluing them together. Dummy specimens were glued to the outside to prevent edge rounding. Fragments accumulated during the machining process on both edges were

eliminated by using boron carbide powder, low grit silicon carbide paper, and a hand-held rotary tool. Once these fragments were removed, a nylon pad was used in conjunction with a diamond paste and slurry (45, 15, and 3 μm) to achieve a smooth surface. The final polishing step consisted of using Mastermet and a neoprene pad to produce a mirror-like finish. The last two steps were applied only to one edge for the purpose of taking edge replicas. Tabs were applied to some specimens to prevent slip or fracture near the grip using a high temperature application epoxy. Once in position, the tabs were clamped and placed in a furnace at 57°C for one hour or more.

3.3 Test Setup

All of the isothermal fatigue and static tests were conducted on a servo-hydraulic test stand (Material Test System 810) equipped with a 5 kip load cell. For the test, a mechanical actuator, load and temperature controllers, a data acquisition system and water cooler were required. Each of these subsystem will be discussed in this section.

The specimen was aligned longitudinally in the hydraulic grips of a Material Test System (MTS) hydraulic actuator to ensure all stresses would act in the fiber direction. The grips held about 19~20mm (0.75in) of the specimen at each end. The load actuator was rated for 24.5kN, and 18MPa grip pressure was applied. A ±22.2 kN load cell was employed for the controller's ±10 volt range. An MTS rod, air cooled, extensometer measured the displacement inside the 12.7mm (0.5in) gage length. This device was placed on the specimen edge, and the rods were changed periodically due to dulling or

chipping. Each time rods were replaced the extensometer was recalibrated to ensure accurate strain measurements.

The temperature environment was controlled with two 1000watt, tungsten filament, water cooled, parabolic strip heaters (lamps). The heaters were controlled by a Micricon controller [25]. The heaters were slightly offset (the upper lamp was positioned at one end of the specimen's gage length and the lower lamp positioned the other end of the specimen's gage length) in order to maintain temperature equilibrium throughout the gage section. Three chromel-alumel thermocouples were used as temperature feedback transducers. Two of them (under the upper and lower lamp) were spot welded to the specimen surface directly below the lamps. The temperature of each lamp could be independently controlled by the Micricon controller which maintained a temperature in the gage section within ±2°C of the target level. Another thermocouple was welded in the middle of the gage section under the upper lamp and was used as part of the data acquisition subsystem.

The test profile was maintained by a Zenith 386DX, 16MHz personal computer using a program called LABoratory Material Analysis and Testing Environment (MATE developed by the University of Dayton Research Institute) data acquisition software. Input information included the maximum desired stress, load ratio (R), specimen area, temperature, test frequency, fatigue waveform type (triangle waveform was used) and data acquisition interval. The data acquisition system can also be controlled in the program. The user may specify a cycle interval at the end of which data is to be taken. One thousand pairs of voltage data are gathered on any given cycle. Also, for each test,

all information entered by the user such as sample number, cycle count, actual maximum stress, measured elastic modules and actual load ratio for the corresponding cycle are written to a file.

The program also inquires as to the calibrations of the load and strain cards inserted into the test stand. All specifications were then sent to the micro-profiler which ultimately drives the load cell. The test apparatus is shown in Figure 3-3.

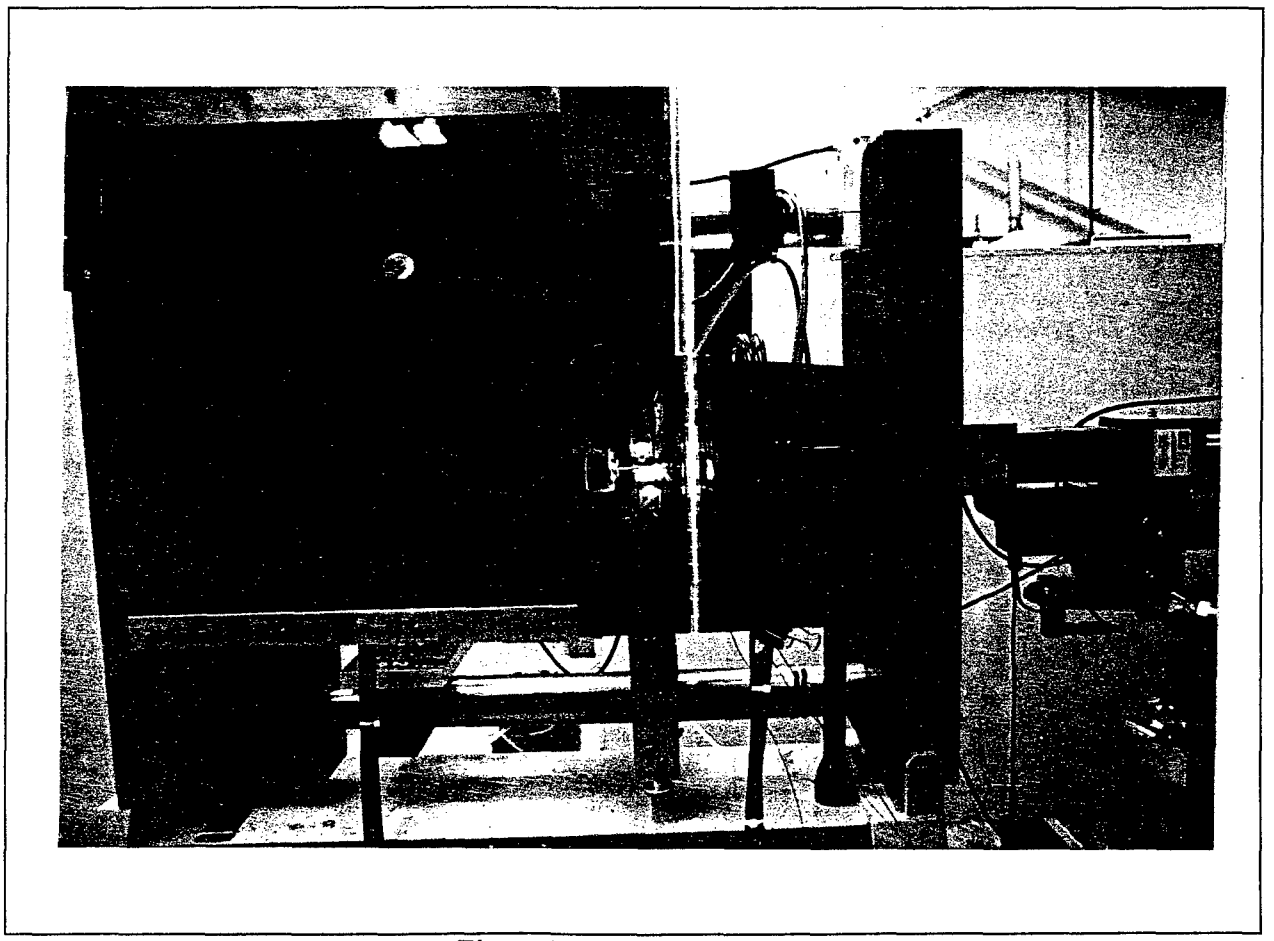

Figure 3.3 Test Setup

Use of a welding guide (protective sheet) was found to be benificial in this study since frequent rewelding on the specimen may cause some damage on the surface of the specimen. Rewelding may be required for several reasons. For instance, rewelding is necessary if the initial welding site is not properly selected, because temperature control of the specimen is difficult. Rewelding is also necessary when an observation is required to measure the crack size on the surface of the specimen, or when a thermocouple falls off due to weak welding (rarely occurred in the present study). A welding sheet made from stainless steel was applied to specimens machined from the third plate (the specimens investigated in this study were produced from three different plates). Three thermocouples were spot welded to the outside of the welding sheet; two were used to control temperature generated by parabolic lamps and one was used to relay temperature data back to the computer. A temperature ramp-up time of 10 minutes was used to allow the temperature to diffuse through the welding sheet. Preliminary testing of temperature differences between the outside of the welding sheet and the specimen at the end of the ramp-up time showed that the temperature detected on the welding sheet was 3-5°C higher than the temperature measured on the specimen surface. In order to obtain the desired specimen temperature in the specimen, 430°C was entered instead of 427°C when the welding guide was used. Figure 3.4 shows the design of the welding guide and its setup.

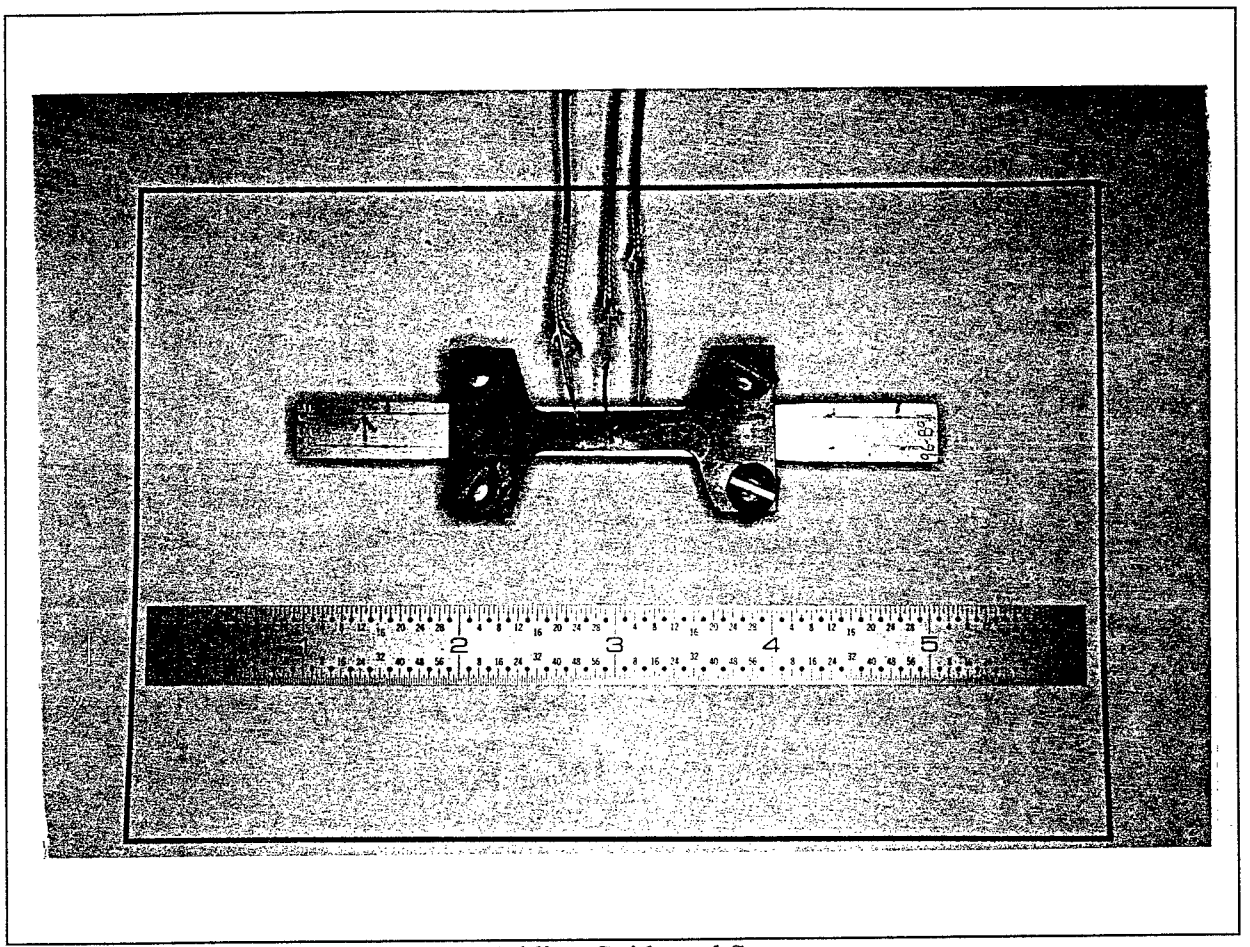

Figure 3.4 Welding Guide and Setup

3.4 Tests / Procedures

Experimental procedures for this research involved performing initial material measurements (young's modulus at elevated temperature and coefficient of thermal expansion), fatigue tests, propagation measurements, static tests to get residual strength, and micromechanical inspection of the fractured specimens.

3.4.1 Material Measurements

To determain the cross-sectional area of the specimens a micrometer was used to measure the width and thickness at three points (center of the specimen, and a half gage length (6.35mm) from the center in each direction). The average width and thickness was used for the area measurement. At elevated temperature (427°C), Young's modulus and the material strength was measured performing a monotonic tensile test under the strain control (strain rate was 0.001) and under the load control (load rate was 150MPa). A typical stress-strain curve for a monotonic tensile test of the MMC composite at elevated temperature is shown in Figure 3.5. The figure shows that the maximum stress (900MPa) is slightly beyond the linear region. Thus, this specimens were being deformed gradually during the fatigue tests.

A modulus check was performed on several specimens before applying the fatigue loading. A 45 MPa load was applied in this case. The results are shown in table 3.3 and Figure 3.6. The coefficient of thermal expansion (CTE) was also measured. The temperature in the gage section was ramped up to the target level (427°C) in 120 sec and

held for three to five minutes. When the welding sheet was used, another three minute were needed to reach temperature equilibrium.

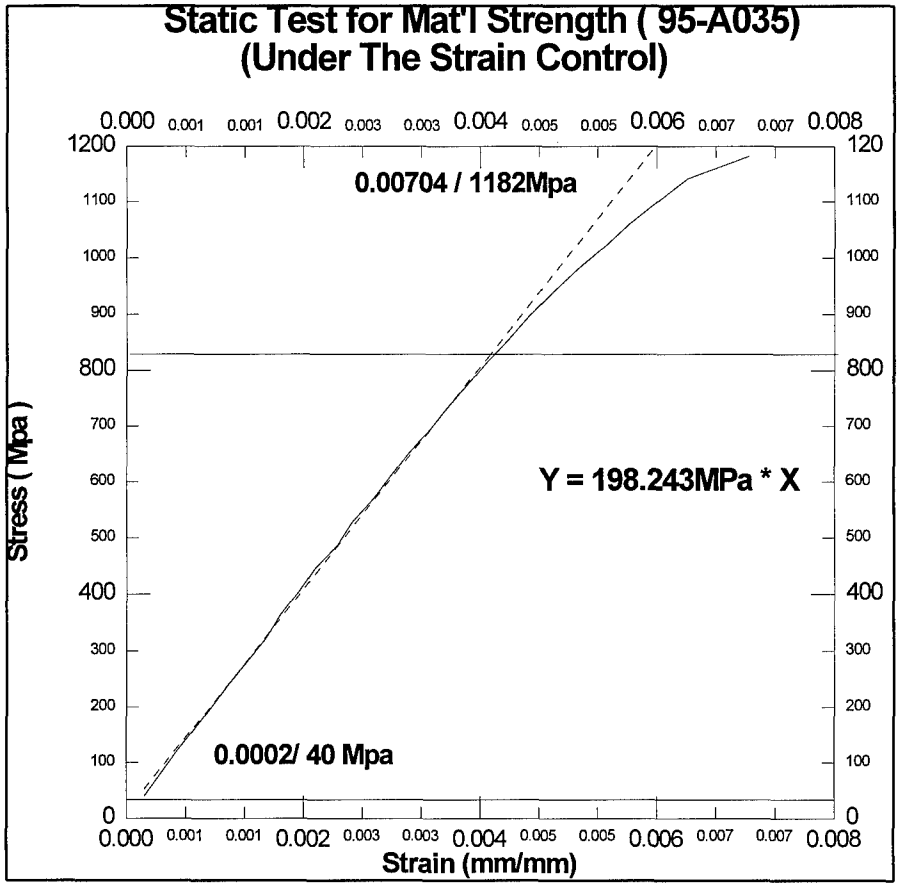

Figure 3.5 Tensile Response of the Composite at 427°C

The extensometer displacement was then recorded to calculate thermal strain and the coefficient of thermal expansion (α):

$$\varepsilon_T = \frac{\delta}{GL} \tag{3.1}$$

$$\alpha = \frac{\varepsilon_T}{\Delta T} \tag{3.2}$$

where ε_T is thermal strain, δ is extensometer displacement, GL is gage length and ΔT is the change from room temperature to test temperature.

Table 3.3 Modulus Taken From the Monotonic Tests

Parent Plate	5-2L ~ 5-7L	7-2L ~ 7-7L	10-1L ~ 10-7L	Total
Specimens	035 ~ 040	061 ~ 066	884 ~ 891	20
Average (E)	187 GPa	214 GPa	199 GPa	200 GPa

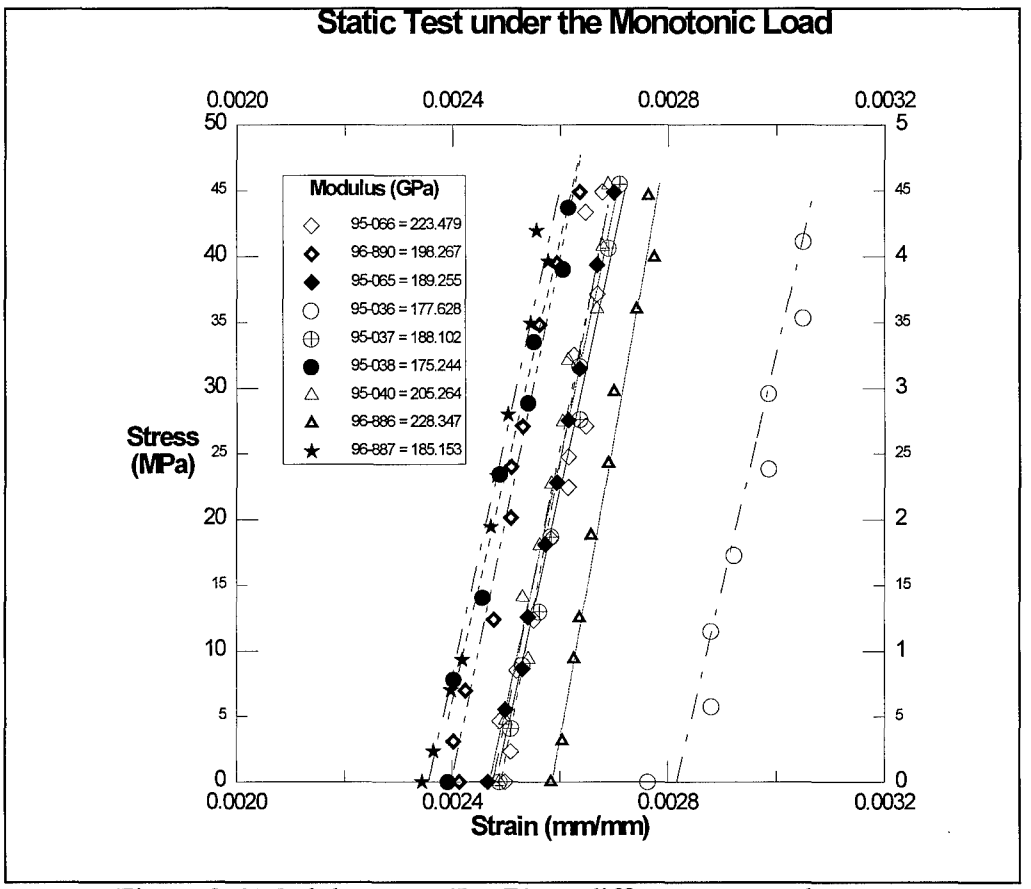

Figure 3.6 Modulus Tests For Three different parent plates

3.4.2 Fatigue Testing

The present study involved fatigue testing through a specified number of cycles followed by a static load to failure. The target cycle at which the test was stopped before the final static load to failure was chosen at approximately 30%, 50%, 70% or 80% of the number of cycles to fatigue failure. In order to ensure proper operation, all test conditions were monitored closely throughout the test. For instance, load wave form, measured temperature, modulus, load ratio and cycle number were continually monitored. Also, because of increasing strain with cycles, checking the maximum and minimum strain displayed by the MTS machine was found to be a good method of controlling the maximum cycles applied to each specimen. The strain limit was set relatively low, so the test would stop rather than continuing on to fatigue failure. The Data Acquisition Cycle (DAC) interval was also adjusted to collect data more frequently as the test neared its planned completion. The fatigue portion of the tests were considered complete when the target cycle was reached, when the strain exceeded the strain limit, or when the specimen fractured into two pieces. In many cases, the specimen suddenly failed without indication of strain increase or modulus decrease. Discussion of this will be provided in the next chapter.

Each test was stopped one or two times during the fatigue loading in order to check the crack propagation on specimen surfaces and edges. Knowledge about surface and edge crack growth and which crack caused the final fracture was regarded as important information especially when compared with modulus drop or residual strength. In many cases, the specimen was removed from the stand for observation under a

scanning electronic microscope(SEM) and an optical microscope, before the fatigue test was resumed.

Table 3.4 summarizes the test plan. A total of eighteen tests were completed. The purpose of the present investigation was to study the degradation of residual strength with fatigue cycling. In addition, an assessment of the time-dependent effects was desired. Therefore, two test frequencies were chosen (1Hz and 0.01Hz). A maximum stress level of 900MPa was chosen so that the failure mechanisms would be in the transition region between matrix and fiber dominated [14].

Table 3.4 Test Plan

Specimen ID	Parent Plate	Shape of Specimen	Size (th*wd) (mm*mm)	Freq (Hz)	Test Type
95 - A 034	PRDA 5-1L	Dogbone	1.7932*7.6039	10	fatigue-RS
95 - A 035	PRDA 5-2L	Dogbone	1.7831*7.2626	Static	fatigue-RS
95 - A 036	PRDA 5-3L	Dogbone	1.8524*7.1349	1	fatigue-RS
95 - A 037	PRDA 5-4L	Dogbone	1.8762*7.1306	1	fatigue-RS
95 - A 038	PRDA 5-5L	Dogbone	1.9168*7.1636	1	fatigue-RS
95 - A 039	PRDA 5-6L	Dogbone	1.9355*7.1382	1	fatigue-RS
95 - A 040	PRDA 5-7L	Dogbone	1.9473*7.1196	1	fatigue-RS
95 - A 061	PRDA 7-2L	Dogbone	1.9525*7.2027	1	fatigue-RS
95 - A 062	PRDA 7-3L	Dogbone	1.9431*7.0621	0.01	fatigue-RS
95 - A 063	PRDA 7-4L	Dogbone	1.9397*7.2356	0.01	fatigue-RS
95 - A 064	PRDA 7-5L	Dogbone	1.9414*7.2898	0.01	fatigue-RS
95 - A 065	PRDA 7-6L	Dogbone	1.9399*7.2542	0.01	fatigue-RS
96 - A 066	PRDA 7-7L	Dogbone	1.8991*7.2314	1	fatigue-RS
96 - 884	PRDA 10-1	Rect.	1.9888*7.4862	Static	Static
96 - 885	PRDA 10-2	Dogbone	1.8728*7.4863	1	fatigue-RS
96 - 886	PRDA 10-3	Dogbone	1.8567*7.4777	Static	fatigue-RS
96 - 887	PRDA 10-4	Dogbone	1.8593*7.5226	1	fatigue-RS
96 - 888	PRDA 10-5	Dogbone	1.8669*7.5252	1	fatigue-RS
96 - 889	PRDA 10-6	Dogbone	1.8821*7.5217	0.01	fatigue-RS
96 - 890	PRDA 10-7	Dogbone	1.8703*7.5040	0.01	fatigue-RS
96 - 891	PRDA 10-8	Dogbone	1.8745*7.4981	0.01	fatigue-RS

A load ratio of 0.05 (defined by $R = \sigma_{min} / \sigma_{max}$ where σ_{max} = maximum stress and σ_{min} = minimum stress) was chosen to prevent any compressive stress during the load controlled fatigue test. The temperature was held constant at 427°C for all tests.

3.4.3 Post-Failure Analysis

The first step taken after test was to reduce the data produced by the MATE software. As mentioned earlier, each data file included around 50-100 subdata files. Each subdata file contained 1000 load-displacement points. FORTRAN programs were written to create stress-strain data files from load-displacement data files. The maximum, minimum and mean strain as well as modulus histories with successive cycles were extracted from these individual files. Modulus values were normalized by the specimen's initial modulus and cycle number was normalized by the number of cycles to failure. This was done to better compare the modulus history curves among different test conditions. For strain history comparisons, cycle number was again normalized by the number of cycles to failure.

In this study, microscopic observation was performed before both before and after the specimen fracture. Some specimens were examined to check for any micromechanical changes and cracks on the surface and edge after a certain specific cycle or completion of a fatigue test. On the other hand, every specimens were examined for damage mechanisms after failure. To prepare the specimens for microscopic observation, they were transversely sectioned into 3 pieces using a low speed diamond saw. Figure

3.7 shows sectioned locations for the fractography and microscopy samples. These pieces were used as sources for fracture surface, polishing and etching respectively.

Fractographic analysis was achieved by analyzing the fracture surface. The sample was ultrasonically cleansed and mounted on a small pedestal with conductive paint adhesive. The sample was then placed in the SEM where its fracture surface features were observed. Much information about both damage and fracture mechanisms can be gained from this fractographic analysis.

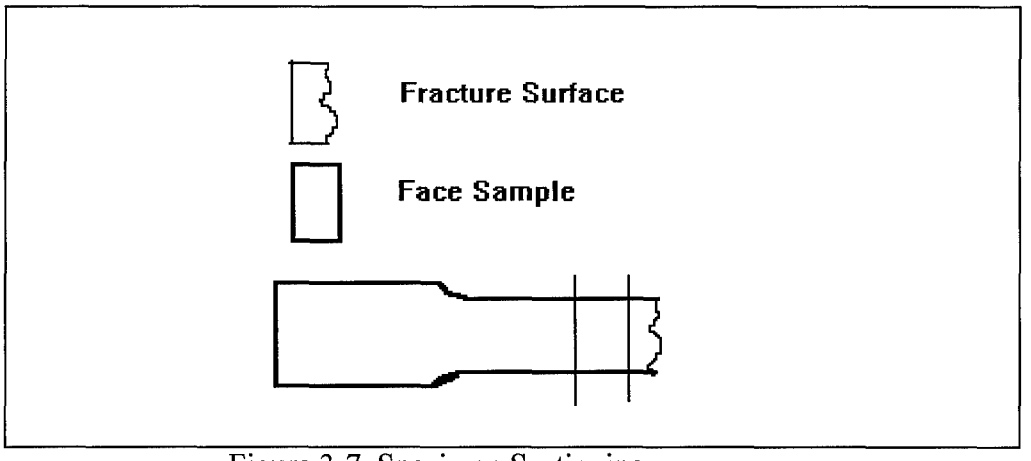

Figure 3-7 Specimen Sectioning

Microscopy was accomplished by studying the polished specimen face surface under an optical microscope. Another transverse cut in the specimen was made with the low speed diamond saw about 8-10 mm below the location of the first cut. The polishing procedure followed below step outlined below [25]. The goal was to polish down to the first layer of fibers.

Polishing steps

A. Rough polishing

Under a Buehler number 8 platen mounted on Buehler Maximet

(1) A 45 micron diamond suspension was applied to remove any deep scratches from the surface and allow the first matrix layer to be ground down to the first layer of fibers.

(2) 15 and 9 micron diamond suspensions on nylon and silk platens were applied to get an even surface.

(3) 6 and 3 micron diamond suspensions on nylon and silk platens were applied to remove fine scratches on the surface and most pits in the matrix.

B. Fine polishing

Under a series of Buehler Vibromets

(1) 1 micron diamond paste mixed with Hyperez OS lubricant onto a perforated texmet cloth was applied for 20-30 minutes on this vibromet.

(2) 0.5 micron diamond paste mixed with Hyperez OS lubricant on a nylon cloth over a perforated texmet cloth was applied for at least eight hours.

(3) 0.06 micron Colloidal Silica Neutral Solution (MasterMet) on a micron cloth was applied for approximately one hour.

Samples were then ultrasonically cleansed in distilled water and then with acetone. They were then ready to be investigated for matrix cracking, fiber damage and fiber/matrix interface debonding under an optical microscope.

Sometimes polishing technique may cause some damage on the sample. Therefore, much care was required to reduce possible damage. Etching the specimens was also performed. To etch the sample, an acid based solution of 10% molybdic acid and 90% distilled water was used. The optical and SEM were used to investigate the microstructure, damage mechanism and development of matrix slip bands of etched samples.

4. Results and Discussion

In this chapter, the results from experimental work are presented. The monotonic tests on the virgin specimens provided information on the modulus, material ultimate tensile strength and thermal coefficient of expansion. The fatigue and residual strength tests provided information on how the strength degraded with successive cycles as well as strain and modulus histories. Investigation of the damage progression through microscopic evaluation, and quantitative assessments of how this damage relates to residual strength was also undertaken.

4.1 Monotonic loading responses

To obtain the Young's modulus, yield point, and ultimate tensile strength of the specimens, three different methods were performed. First, specimens were randomly selected from each plate and tested under static load of 45MPa to check modulus and make sure the test setup. Second, the modulus was also obtained from the first cycle of all fatigue tests. Third, two specimens machined from different plates were loaded to obtain the ultimate tensile strength. Table 4.1 shows the summary of Young's modulus and ultimate tensile strength as well as the coefficient of thermal expansion (CTE) at the desired test temperature (427°C). The mean moduli measured from the 45 MPa load as opposed to the first cycle of the fatigue test have approximately a 5%~14% variation. The moduli of these specimens were banded between approximately 175 GPa and 223 GPa at 427°C. Figure 4.1 show the stress strain responses of different specimens when

subjected to a 45MPa stress. The coefficient of thermal expansion varied from 5.5815×10^{-6}/°C to 6.417×10^{-6}/°C at 427°C with a mean value of 5.5725×10^{-6}/°C.

Table 4.1 Material properties obtained from monotonic test

Plate ID	Specimen ID	$\sigma_{Max/Ult}$ (MPa)	Thermal Strain at 427°C	$\Delta\varepsilon_{max}$ (10^{-6}/°C)	Modulus (GPa)	Modulus (GPa) @ 1st Cys
1	95-035	1182(Ult)	0.00238	5.574	*	200.258
1	95-036	900	0.00274	6.417	180.747	182.059
1	95-037	900	0.00248	5.808	188.102	198.698
1	95-038	900	0.00246	5.761	175.244	189.450
1	95-039	900	0.00248	5.808	*	208.230
1	95-040	900	0.00244	5.714	205.264	195.023
1	**Average**	**------**	**0.002497**	**5.847**	**187.339**	**195.619**
2	95-061	900	0.00268	6.276	*	190.645
2	95-062	900	0.00248	5.808	*	187.819
2	95-063	900	0.00254	5.948	*	194.311
2	95-064	900	0.00265	6.206	*	187.596
2	95-065	900	0.00237	5.550	206.367	189.939
2	95-066	900	0.00237	5.550	223.476	194.731
2	**Average**	**------**	**0.00252**	**5.889**	**214.921**	**190.840**
3	96-884	**	**	**	**	**
3	96-885	900	0.00241	5.644	*	191.922
3	96-886	900	0.00238	5.574	228.347	199.488
3	96-887	900	0.00234	5.480	185.153	194.892
3	96-888	1355.8(Ult)	0.00244	5.714	*	201.644
3	96-889	900	0.00237	5.550	*	197.480
3	96-890	900	0.00236	5.527	198.267	197.712
3	96-891	900	0.00246	5.761	*	214
3	**Average**	**-----**	**0.00239**	**5.6071**	**203.922**	**199.591**
Total	**Average**		**0.00246**	**5.7725**	**200**	**194.447**

* No data obtained, ** Bad test

Figure 4.2 and 4.3 show the stress-strain response of the first cycle from each test (fatigue and residual strength). The moduli taken from these stress-strain curves are more

consistent from specimen to specimen. Also, the moduli found from the 1Hz tests (192.2 GPa) and the moduli of the 0.01 Hz tests (196.8 GPa) is well within plate to plate and specimen to specimen variation. Deviation from linear-elastic behavior was found to occur between 820 ~ 870 MPa.

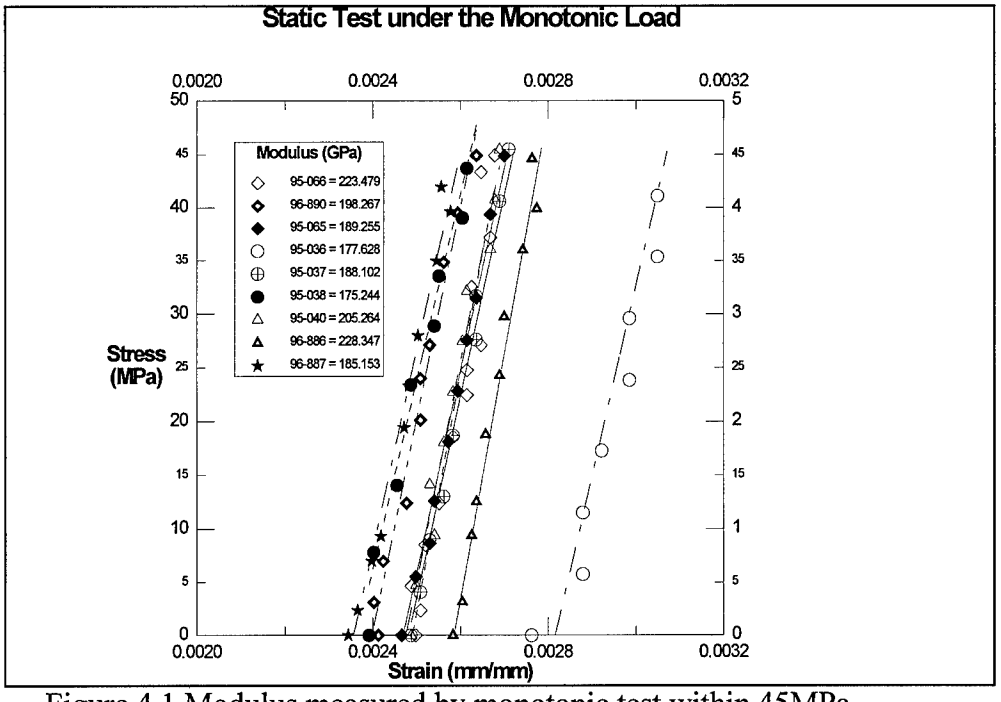

Figure 4.1 Modulus measured by monotonic test within 45MPa

Table 4.2 and Figure 4.4 show the elastic moduli, ultimate tensile strength and strain-to-failure of the composite. The composite exhibited an initial linear elastic region followed by a non-linear stress-strain behavior. The transition from linear to non-linear occurred between a strain level 54 ~ 55% of strain-to-failure. This is most likely due to yielding of the matrix and the possible formation of microcracks in the interfacial reaction zone.

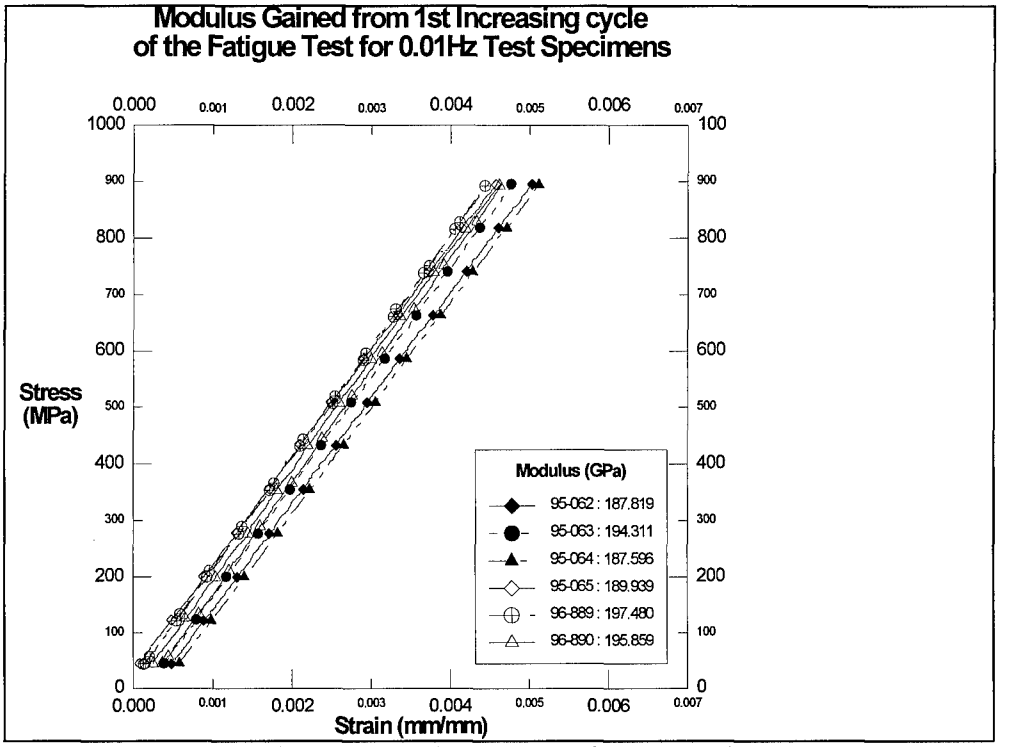

Figure 4.2 Modulus measured at the first fatigue cycle under 0.01Hz.

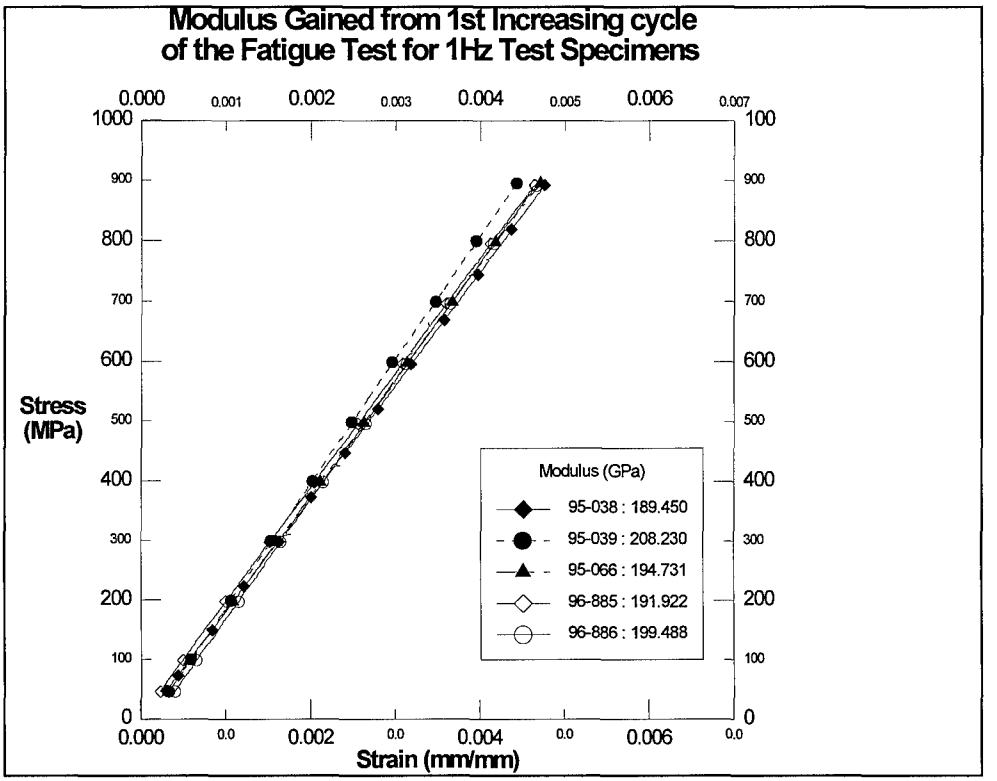

Figure 4.3 Modulus measured at the first fatigue cycle under 1Hz.

Table 4.2 Results of ultimate tensile test

Specimen ID	Modulus (GPa)	σ_{Ult} (MPa)	Yield Strain	Strain at Failure	Thermal Strain	$\Delta\varepsilon_{max}$ (10^{-6}/°C)
95-035	200.258	1182	0.0039	0.00704	0.00238	5.574
96-884	**	**	**	**	**	**
96-888	201.644	1355.8	0.0043	0.00801	0.002471	5.787
Average	200.951	1268.9	0.0041	0.00753	0.00243	5.6805

** Bad data

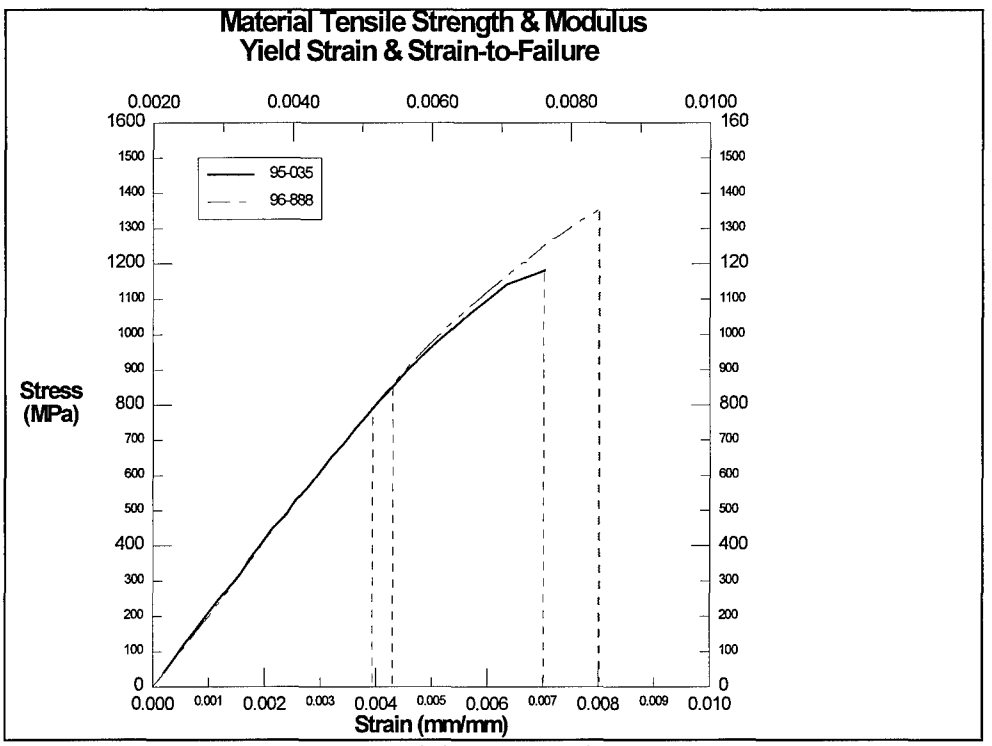

Figure 4.4 Strength, Yield point and Strains , T=427°C

4.2. Fatigue Tests

In this section, the eight specimens that experienced fatigue are discussed. Due to specimen-to-specimen variation, most of the fatigue to failure were obtained as a

byproduct when the residual strength tests failed without warning prior to reaching the target cycle. Any strain and modulus change over the fatigue life of the specimen was studied for the macroscopic response. As stated in the previous chapter, during each test intermittent recordings of the load-displacement were corrected as recordings of the stress-strain by the FORTRAN program after ending the tests. Based on these stress-strain data, the FORTRAN Program produced maximum-strain, minimum-strains, mean-strains and moduli corresponding to maximum and minimum-stresses. Figures of stress-strain response, mean strain history comparisons and modulus history comparisons are presented to interpret fatigue damage accumulation mechanisms in each test as evidenced by cyclic load peak strain shift and/or hysteresis loop response and effective composite elastic modulus changes. Comparisons are made in two different frequencies. All these data were plotted as a function of number of cycles to failure. The figures presented here are almost consistent with the matrix dominated mode observed by Pittman who tested the same material [31]. For the present study, only frequency (f) was varied. Maximum stress (σ_{max}), temperature (T), load ratio (R), load wave type and specimen geometry were held constant.

4.2.1 Macroscopic Observations

4.2.1.1 1Hz Frequency Tests

Table 4.3 shows the fatigue life and where the specimens fractured. The gage length was 12.7 mm (0.5 in). Middle means the center of the gage length and Inside means that the specimen fractured within the gage length. Each number indicates the

fracture location outside the gage length. Figure 4.5 is a photograph of two fractured specimens.

Table 4.3 Results for 1Hz fatigue test

Specimen ID	Temp (°C)	σ_{max} (MPa)	Freq (Hz)	Cycles (N)	Distance Outside Gage Section(mm)
95-A036	427	900	1	30697	Middle
95-A037	427	900	1	31058	Inside
95-A039	427	900	1	48102	Inside
95-A061	427	900	1	8004	1.558
95-A066	427	900	1	28708	3.969

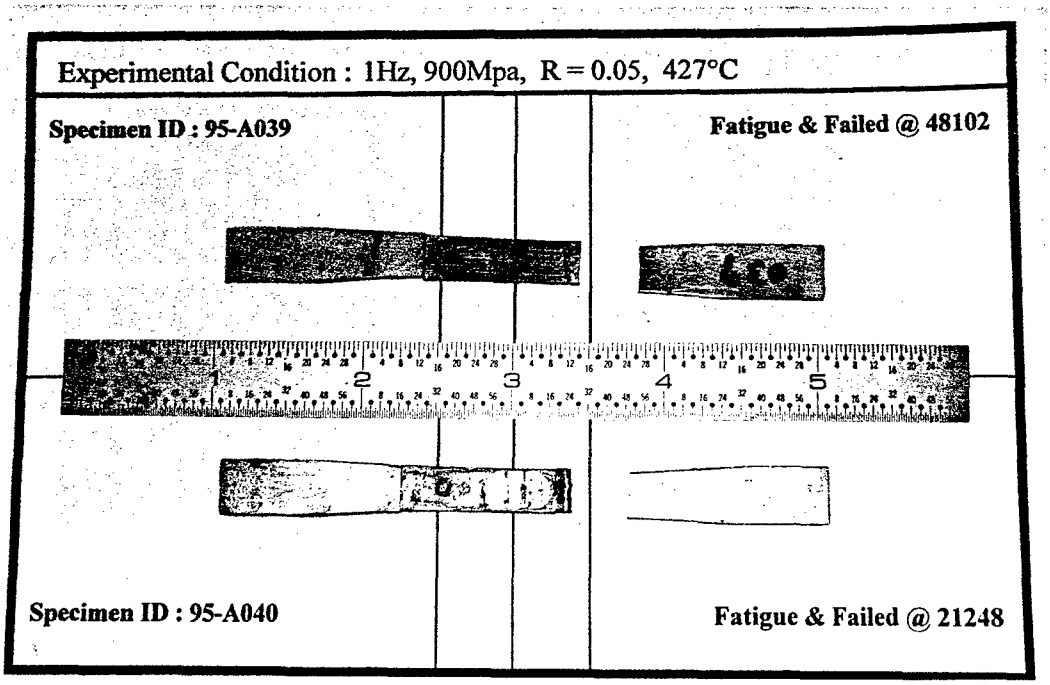

Figure 4.5 Fractured Specimens (95-039 &95-040)

Figure 4.6 illustrates the mean strain and modulus history of each specimen tested under 1Hz frequency. Fatigue cycles are normalized by dividing each cycle number (N) by the number of cycles to failure (N_f). Young's modulus is also normalized by dividing the current modulus (E) by the initial modulus (E_i). Mean strain is not normalized and is defined as the average of the maximum strains and minimum strains over the test cycles. Mean strains have similar increasing trends in the specimens tested. There was very little increase in strain over the entire fatigue life. The most rapid increase in strain occurred within the initial 3~5% of the life. The change in moduli basically mirrored the change in strain for each specimen. Only the initial 3~5% of the life did not experience much if any change in modulus. This indicates that the change in strain in the first few cycles was due to plastic deformation because the minimum strain increased at the same rate as the maximum strain. After 80% of the life, the modulus began to decrease at a relatively greater rate. This reduction in stiffness suggests fatigue damage. Also, one possible reason specimen 95-037 has a greater change in strain and modulus than the other specimens is more than one dominant crack within the gage length. As these two cracks progressed and combined, the effect on the strain and modulus change with subsequent cycles would essentially double over that observed from a single dominant crack.

Figure 4.7 illustrates the stress-strain response at a few selected cycles for a specimen tested at 1Hz frequency. This figure shows a typical matrix dominant failure mode. During each cycle, a linear stress-strain response was observed. The up-loading

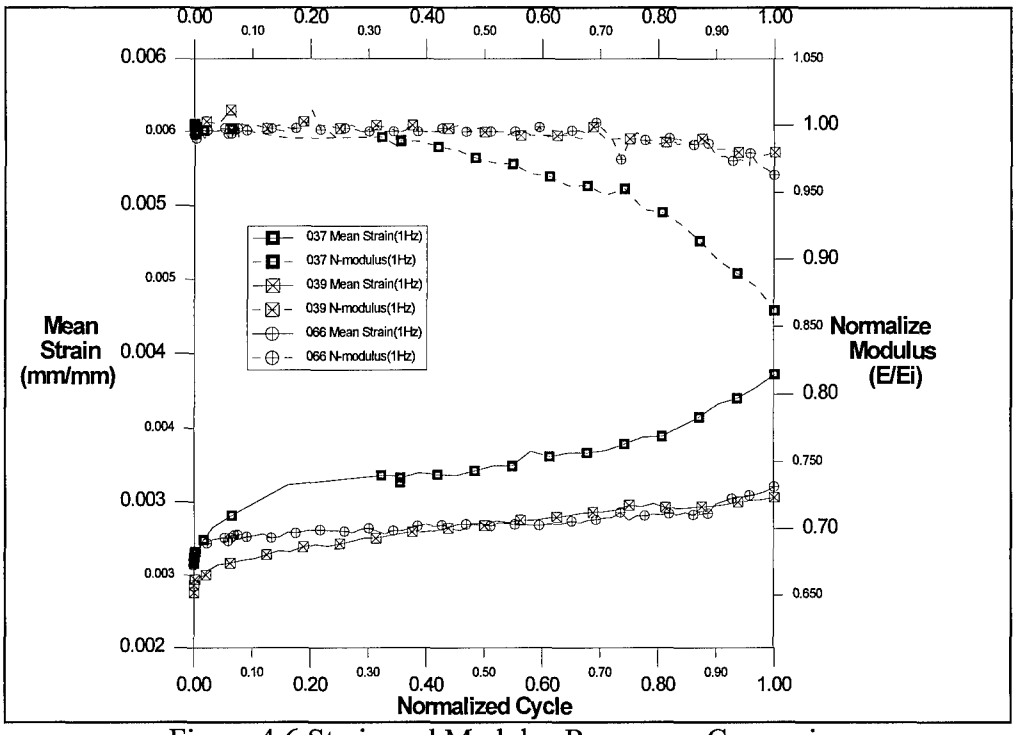

Figure 4.6 Strain and Modulus Responses Comparisons

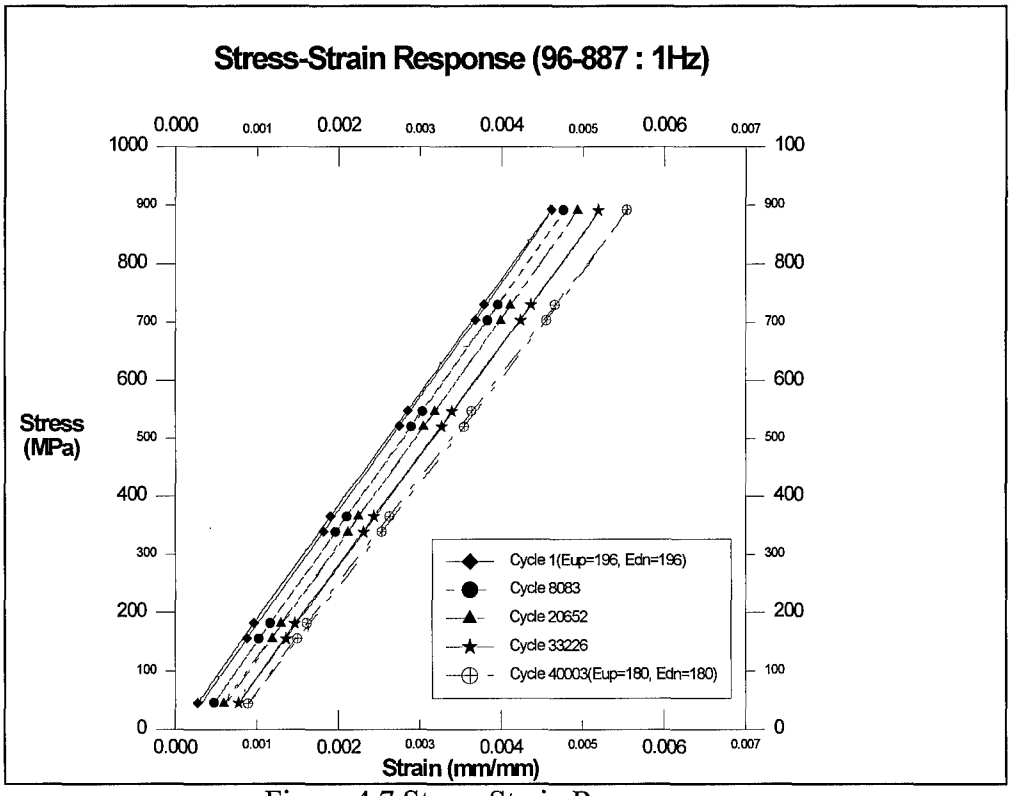

Figure 4.7 Stress-Strain Responses

modulus of the first cycle and the down-loading modulus of the last cycle were 195 GPa and 180 GPa respectively. The maximum strain rises at a greater rate than the minimum strain after 60~70% of the life and the modulus begins to droop. The maximum stress of 900 MPa is not enough to break the fibers. Interfacial debonding and matrix cracking propagate while the fibers bridge the matrix crack. For these kinds of damage mechanisms, matrix cracking is the main source of stiffness reduction.

4.2.1.2 0.01Hz Frequency Tests

Table 4.4 shows where the 0.01Hz specimens fractured in the fatigue to failure tests. The gage length was 12.7 mm (0.5 in). Figure 4.8 is a photograph of two fractured specimens. The specimen 95-063 failed at only 21% of specimen 95-064's life and only 14% life compared to the specimen 95-712, which was tested by Robert N. Pittman [28]. Even though it was considered a bad test, it presented a trend in the microscopic observation discussed later that led to the use of the protective welding guide or sheet.

Table 4.4 Results for 0.01Hz fatigue test

Specimen ID	Temp (°C)	σ_{max} (MPa)	Freq (Hz)	Cycles (N)	Distance Outside Gage Section(mm)
95-063	427	900	0.01	1552	Middle
95-064	427	900	0.01	7283	1.588
95-712*	427	900	0.01	10827	---

* Specimen tested by Pittman

Figure 4.9 shows the strain and normalized modulus vs. normalized cycle. In comparison to the 1Hz test, the trends in strain and modulus are very similar. The modulus displays a slight drop after ~ 80% of the life while the strain increased slightly in almost a linear fashion. The maximum and minimum strain increased at approximately the same rate for most of the test. This behavior is also shown in the stress-strain response

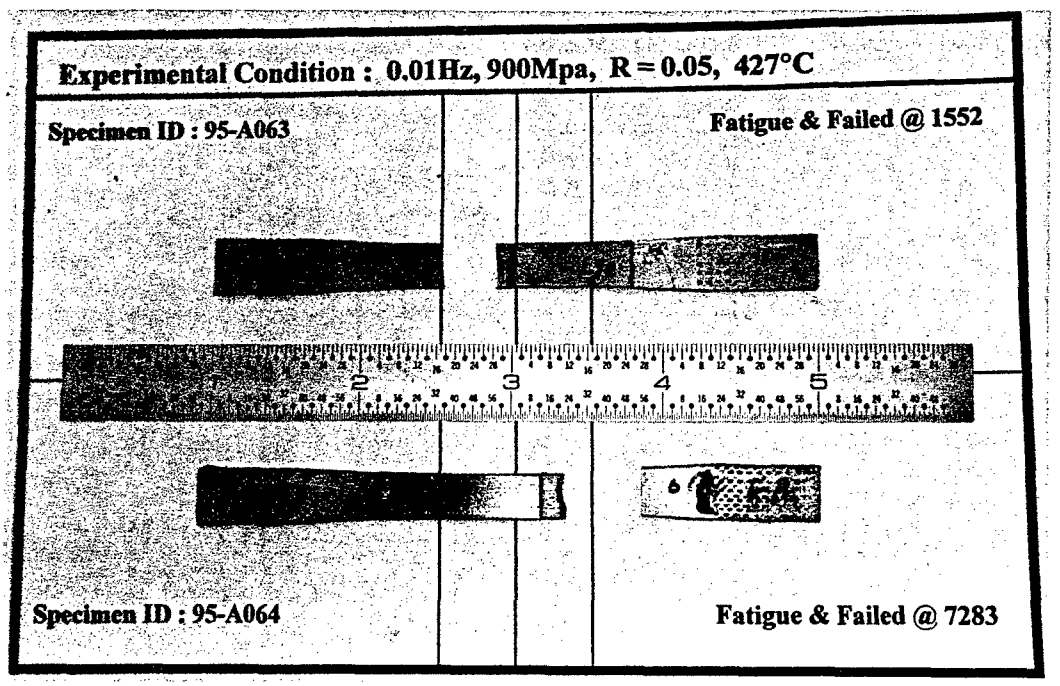

Figure 4.8 Fractured Specimens (95-063 & 95-064)

(Figure 4.10). The increasing modulus from approximately 90% of the life cycles observed in one of the tests can be explained, as a fracture location appeared 1.588 mm out of gage length. When the specimen is fracturing outside the gage length the extensometer will not experience the increased displacement due to the crack.

In Figure 4.10 both the up-loading and the down-loading modulus at the first cycle and at the last cycle were 187 GPa and 189 GPa respectively. These strain and modulus trends did not agree with the response that Pittman observed with specimen 95-712 at same test condition (σ_{max} = 900 MPa Frequency = 0.01 Hz, Temperature = 427°C, R-ratio = 0.05). In his study, a greater strain increase was observed at 0.01Hz than the strain tested at higher frequency due to additional influence of creep. Similar to

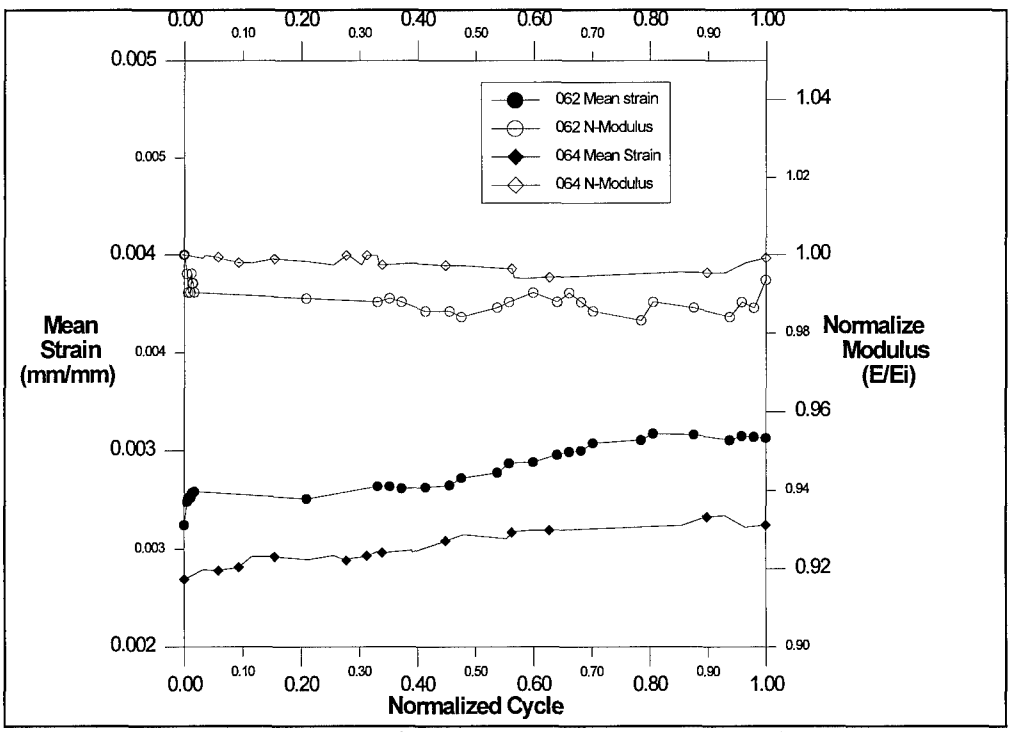

Figure 4.9 Strain and Modulus Responses Comparisons

the 1Hz results, in this range of applied cyclic stress (900 MPa) the possibility of fiber breakage is small. However, the applied maximum stress of the composite is higher than the cracking stress of the interfacial reaction layer. Therefore, during the initial fatigue loading the brittle layer can crack at the edges and center parts of the specimen. The number of fatigue crack initiation sites at the interface increase as the fatigue cycles increases.

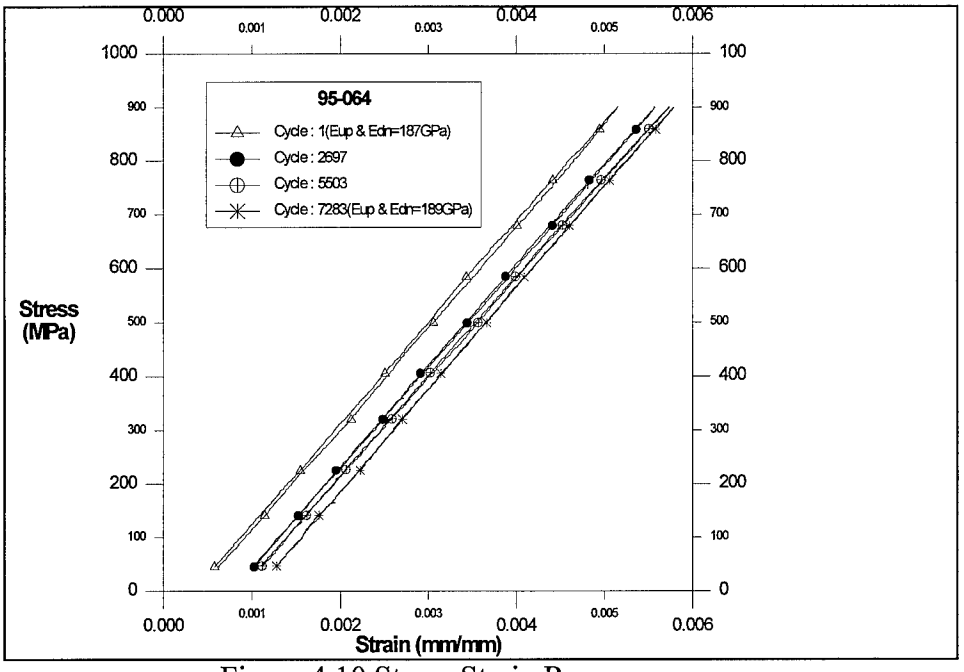

Figure 4.10 Stress-Strain Responses

4.2.2 Microscopic Observations

This section provides the physical evidence of the damage mechanisms. Pittman [28] studied the frequency effect under the same test condition. In his study, comparisons were made in three maximum stress categories: fiber-dominated mode (1200 MPa), matrix-dominated mode (800 MPa and 900 MPa), and mixed-mode (1050 MPa) at various frequencies (10 Hz, 0.1 Hz, 0.01Hz). Herein, the microscopic results

(fractography and microscopy) for the fatigue test were basically consistent with his observation. The fracture surface provides the evidence for determining failure mechanisms. On the other hand, microscopy reveals the condition of the fibers and matrix directly behind the fracture surface. As discussed in chapter three, specimens were sectioned so that the face could be ground and polished down to the first layer of fibers. Each sample was about 1~ 1.5 cm long. Additionally, the etched sample was sectioned about 2 cm long from behind the other fracture surface to compare with the polished sample. This microscopic analysis coupled with the mechanical response provided the complete characterization of damage and deformation mechanisms of the specimens tested in fatigue (900 MPa, 1Hz or 0.01Hz, 427°C, R=0.05).

4.2.2.1 1Hz Frequency Tests

Six specimens were analyzed at this frequency. In the previous section, Table 4.3 shows that their fatigue life varied from 8004 to 48102. The specimens that had a relatively short life were found to be damaged by the thermocouple welding. Figures 4.11 and 4.12 show the evidence of the welding effect. Almost all welding sites had a surface crack which propagated inward though the thickness as the specimens were fatigued. In order to avoid this effect, the welding guide was used for some specimens of the 0.01Hz test.

Figure 4.13 depicts a flat matrix-cracking region on the fracture surface of the specimen which had the longest fatigue life. The entire fracture surface was very irregular but consisted of five matrix cracking planes, both edges and both surfaces had

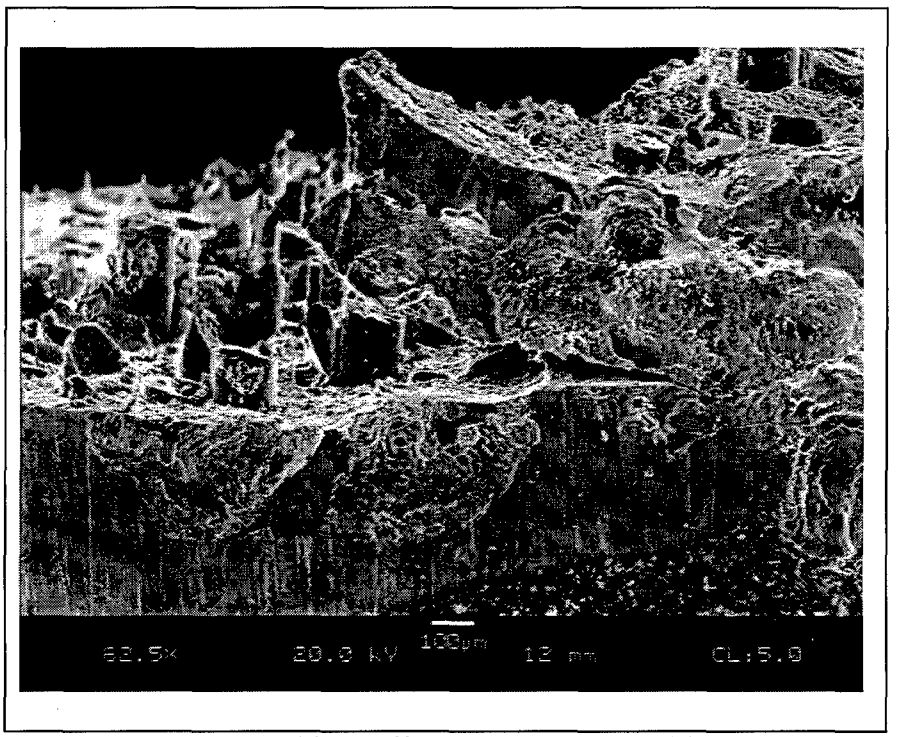

Figure 4.11 Welding Effect (Surface crack initiated)

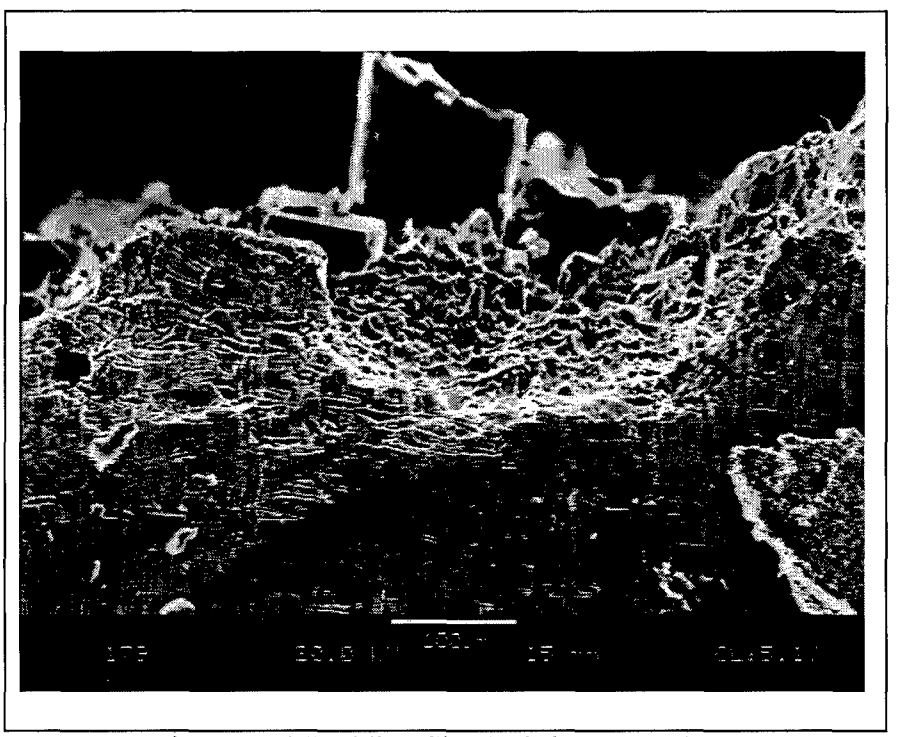

Figure 4.12 Welding Site (Brittle Fracture)

different crack planes. The offset between each crack plane varied from 0.4 mm ~ 1.0 mm. Fibers in each crack region cleaved at or near the matrix surface and no severe necking or ductility was present around the fiber. Only a few significant pull-out length were scattered onto each crack plane. The fact that five matrix crack planes formed on this specimen as well as its long life indicates the fibers effectively bridged the matrix cracks. This bridging prevented only one crack from becoming dominant.

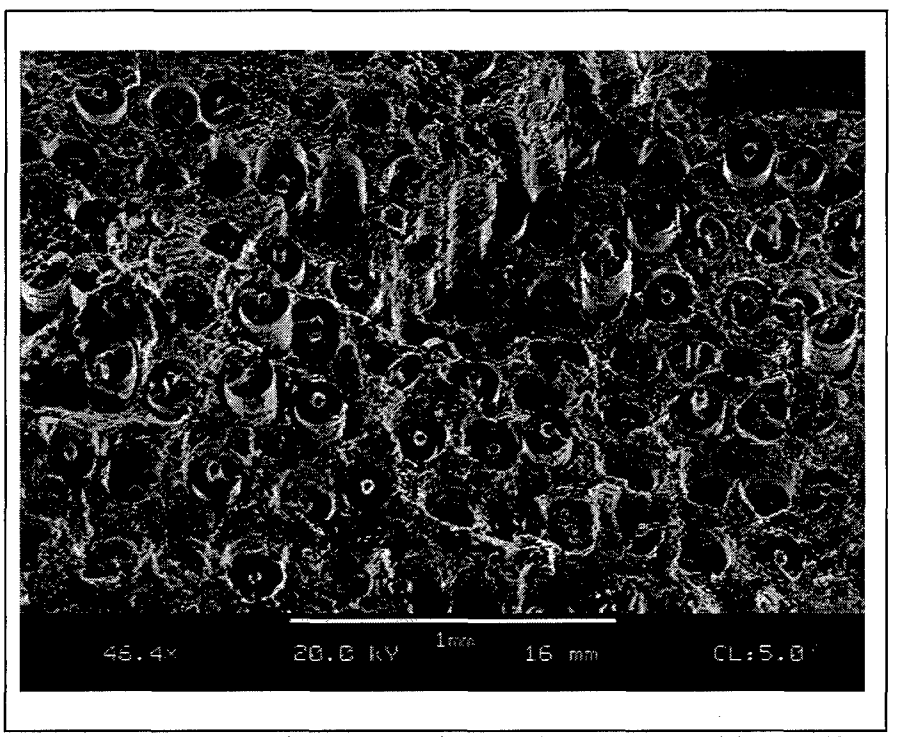

Figure 4.13 Correlated Two Flat Matrix Cracking with an Off-Set

Figure 4.14 shows the microscopy, which revealed the condition of the fibers and matrix directly behind the fracture surface. The specimen was sectioned so that the face could be ground and polished down or etched to the first layer of fibers. There were several surface cracks on both sides of the specimens that originated at damage sites on the edge or surface of the specimen. Figure 4.15 and 4.16 clearly show the crack

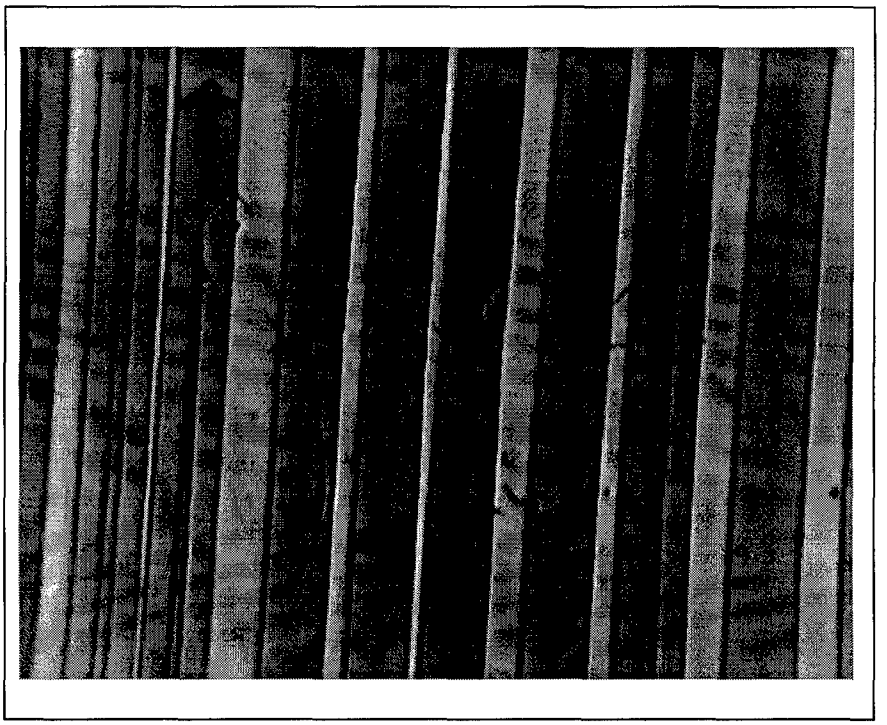

Figure 4.14 Interior Matrix Crack

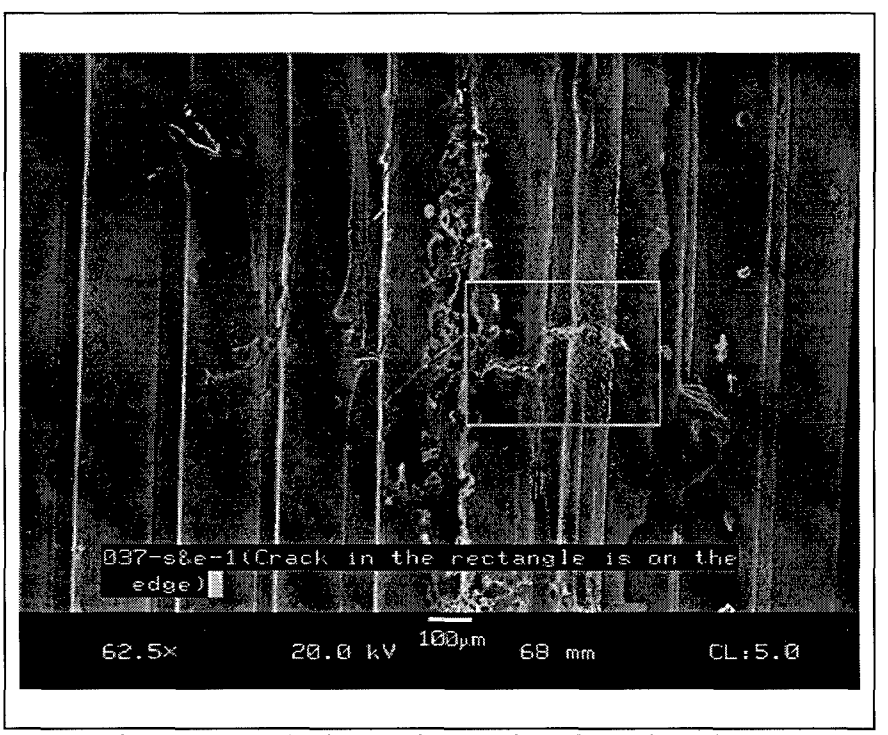

Figure 4.15 Matrix Crack Growing along the Edge

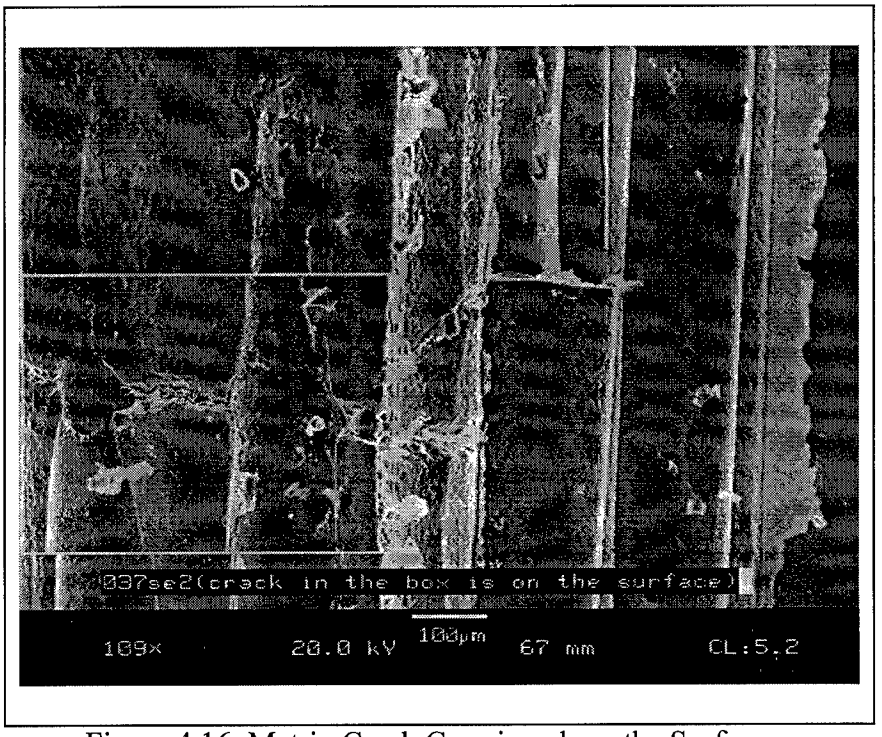

Figure 4.16 Matrix Crack Growing along the Surface

initiation site which originated from the edge. These cracks crossed the fibers with no evident fiber damage. In the Figure 4.17, the matrix crack crossed six fibers and only one fiber was fractured. Figure 4.18 shows that two fibers fractured on the matrix cracking site. In most cases of matrix-dominated fatigue response, matrix cracks continue to grow perpendicular to the loading direction and the fibers remained in the crack plane without breakage. When the fibers can no longer support the increased stress, they fracture near the matrix-cracking surface.

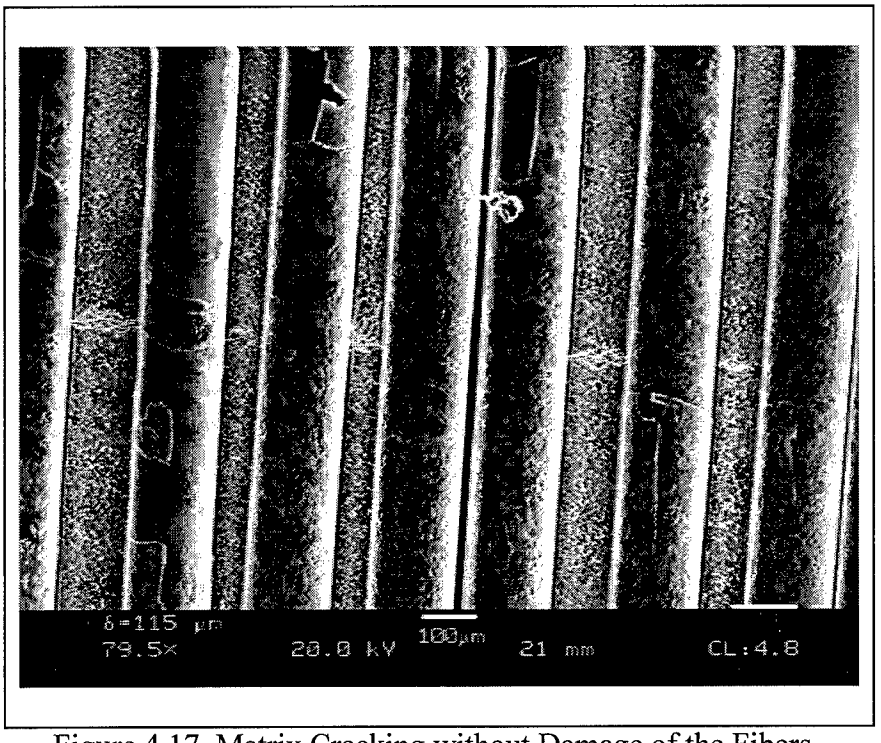

Figure 4.17 Matrix Cracking without Damage of the Fibers

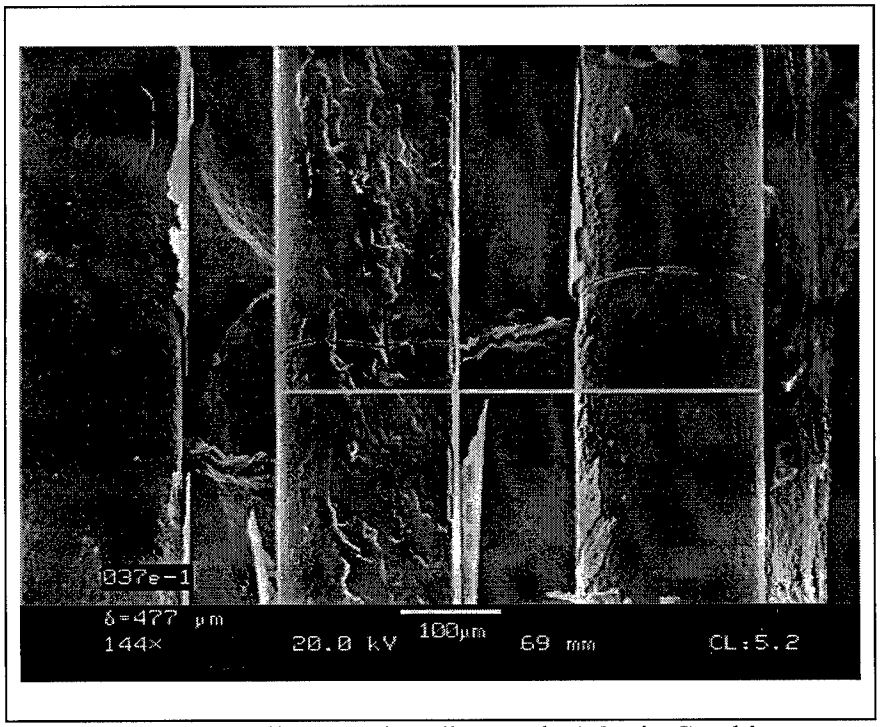

Figure 4.18 Fiber Cracks adjacent the Matrix Cracking

4.2.2.2 0.01Hz Frequency Tests

Two specimens were fatigued to failure at this frequency. In the previous section, Table 4.3 listed the fatigue lives of these specimens, 1552 and 7283, which represent only 14% and 67% of the fatigue life of 95-712 (10827) tested by Pittman. The additional damage caused by the remachining and the welding are possible reasons for the decreased life. Figure 4.19 shows the evidence of the welding damage.

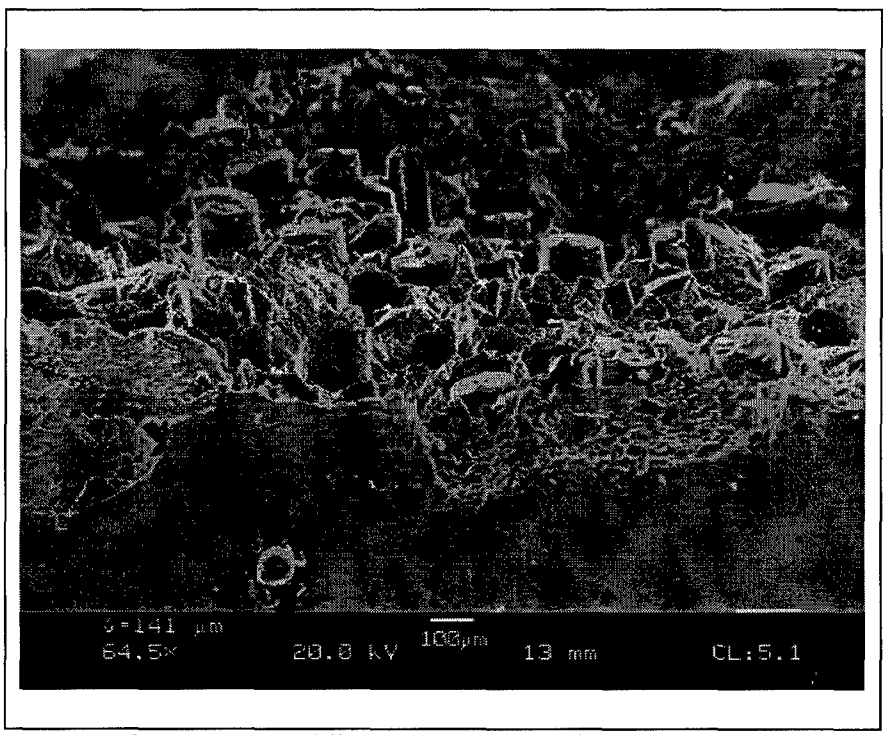

Figure 4.19 Welding Damage Site of 0.01Hz Test

Figure 4.20 depicts a flat matrix-cracking region on the fracture surface of the specimen 95-064. The amount of cracking with this pattern occupied only 6% ~ 7% over the entire fracture surface, and this cracking area initiated from the surface damaged by the welding. The fracture surface could be divided into three distinct damage

mechanisms. First, in the matrix cracking area, intergranular decohesion was observed. This mechanism is evidenced by gaps between the grains and a well-defined, faceted grain boundary. Figure 4.21 shows intergranular decohesion observed around a fiber. Second, a transition area was found. Figure 4.22, shows that the intergranular decohesion area transits to the transgranular cleavage area. . Third is a totally ductile fracture area. Figure 4.23 shows that, in addition to the matrix cracking already discussed, a ductile region existed where the dominant failure mechanisms were fiber-matrix interface damage, matrix necking and void-coalescence. At this frequency (0.01Hz), a fiber-dominate failure mode is prevalent with over 90 % of the fracture surface exhibiting ductile failure. Several fibers damaged by oxidation were randomly found throughout the fracture surface.

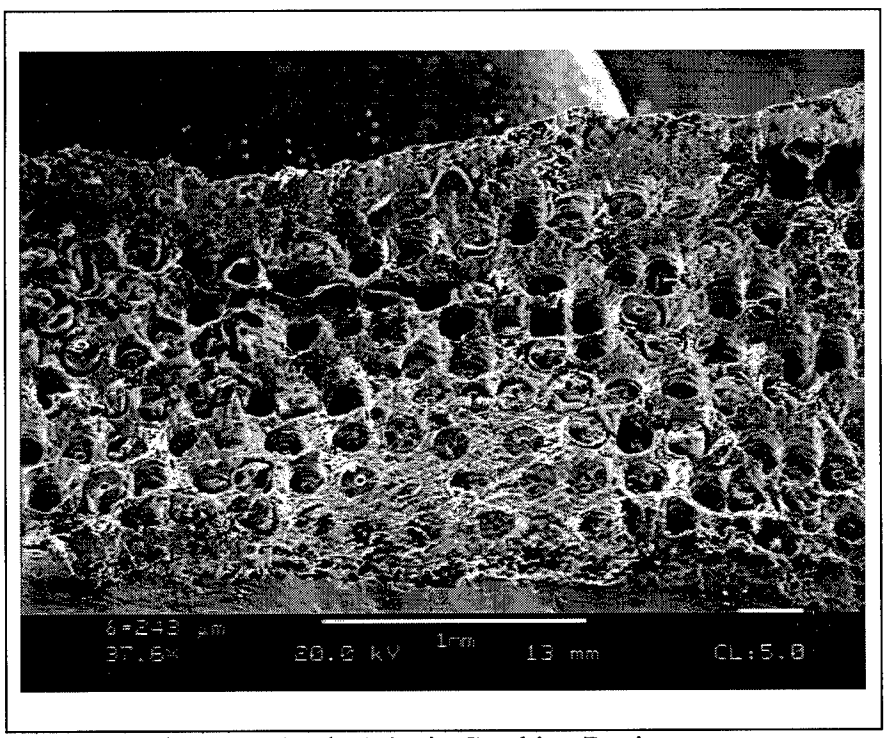

Figure 4.20 Flat Matrix Cracking Region

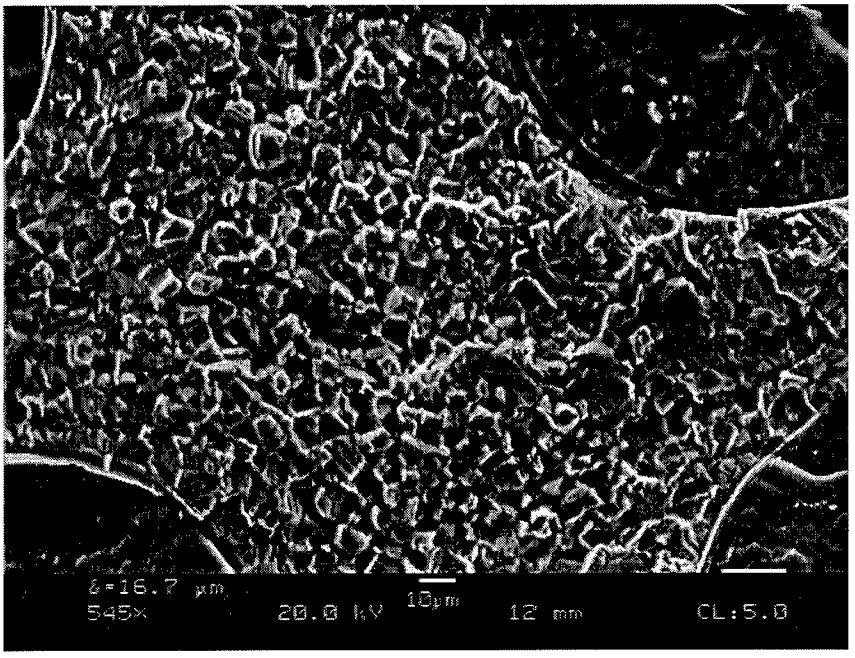

Figure 4.21 Intergranular Decohesion Region

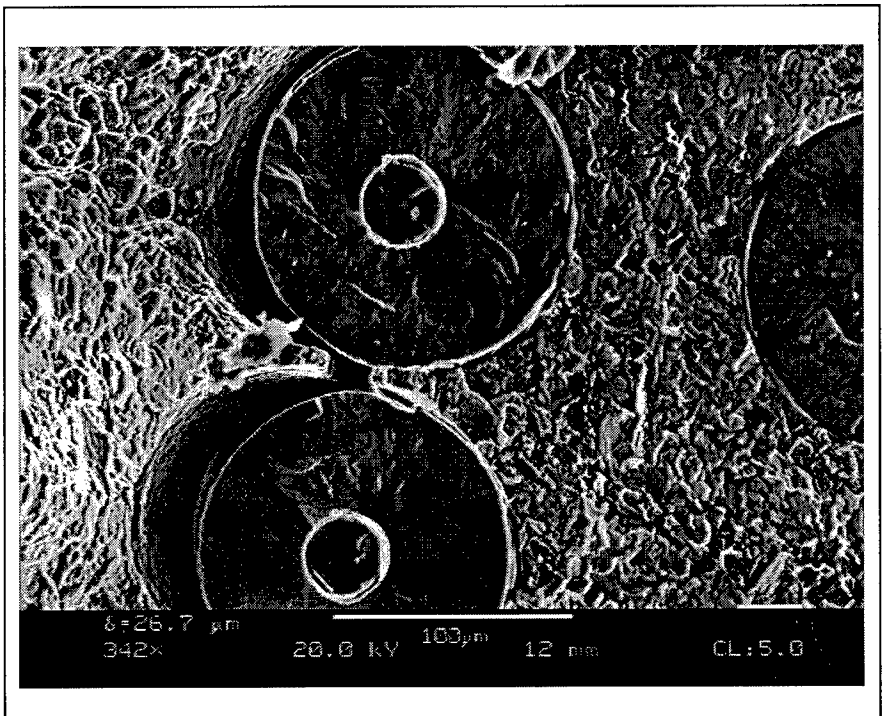

Figure 4.22 Transition Region from Intergranular to Transgranular

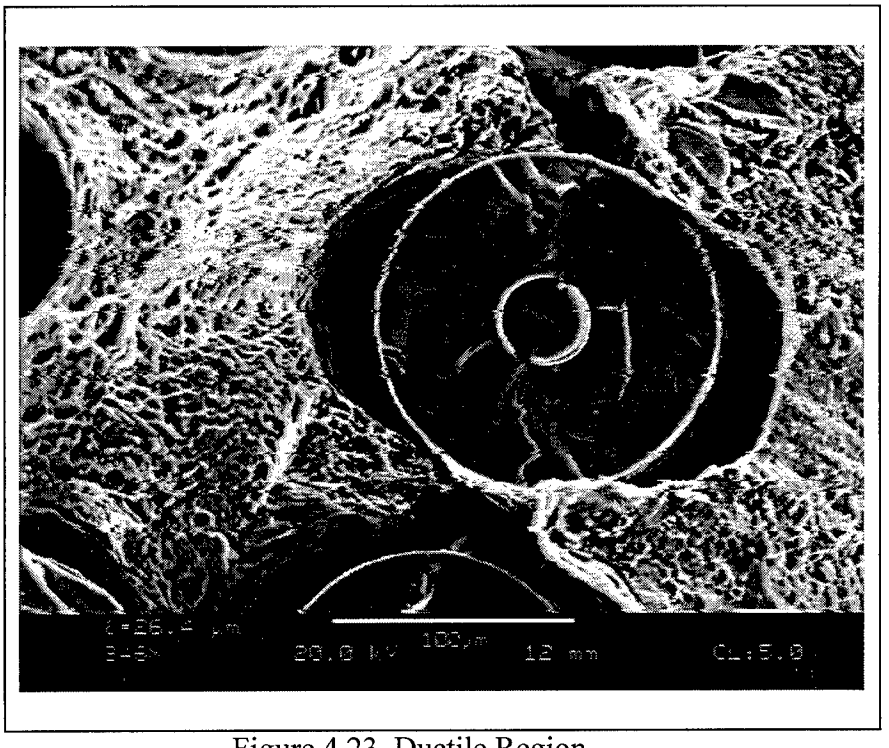

Figure 4.23 Ductile Region

4.3 Residual Strength

The objective of this section is to characterize the residual strength degradation with successive cycles for unidirectional SCS-6/Ti-6-4. In fact, it is not clear as to what kinds of dominant damage mechanisms are responsible for the reduction in residual strength nor how these damage mechanisms cause the final failure of the composite laminate. In this chapter, degradation in strength with cycles for selected fatigue loads will be mapped, and the constituent damage through microscopic evaluation will also be qualified. Finally, frequency effects will be evaluated using normalized residual strength vs. percent life data.

4.3.1 Macroscopic Observations

4.3.1.1 1Hz Frequency Tests

The test results are listed in the Table 4.5. In this table, the moduli were measured either on the last cycle (if the specimen failed in fatigue) or during the final tensile tests of the residual strength. This table shows that the moduli measured both at the last fatigue cycle and at monotonic tensile test after fatigue loading are consistent. The drop ratio in the last column of the table was calculated by dividing the residual strength with the ultimate tensile strength 1355.8 (specimen ID : 96-888). Although modulus degradation and strain increase is indicative of specimen damage, only a slight correlation was found between these quantities and the residual strength. However, they are very important elements to estimate the life of the composite.

Table 4.5 Test Results of 1Hz R.S. Tests

Plate ID	Test Mode	Specimen ID	Cycles (N)	Modulus (E_f ,E_m)	σ_{res} (MPa)	$\sigma_{res}/\sigma_{ult}$ (%)
#1	Static	95-A035	0	201	1182 (Ult)	87.2
#1	Fatigue	95-A036	30697	143*	900	66.4
#1	Fatigue	95-A037	31058	171	900	66.4
#1	Fatigue	95-A039	48102	194	900	66.4
#1	Fatigue	95-A040	21248	177	900	66.4
#2	Fatigue	95-A061	8004	187	900	66.4
#2	Fatigue	95-A066	28708	190	900	66.4
#1	***Residual***	***95-A038***	19792	184,183	***1126 (Res)***	83.1
#3	***Residual***	***96-885***	12505	194,196	***1431.4(Res)***	106
#3	***Residual***	***96-886***	25007	197,199	***1277.2(Res)***	94.2
#3	***Residual***	***96-887***	40003	182,181	***940.77(Res)***	69.4
#3	Static	96-888	0	201	***1355.8(Ult)***	100
#3	Static	96-884	0	---	**	**

* too low (bad data), ** not obtained

(E_f ,E_m: The modulus measured at the last fatigue cycle : the modulus measured at monotonic test for the residual strength test)

The modulus and strain change measured just before the test was stopped to get the residual strength are listed in the Table 4.6. In this table, the specimens 038 and 039 were machined from the same plate and the other three (885, 886, 887) were prepared from a different plate. The ultimate tensile strength of the plate was 1182 MPa for the 038 and 039 and 1355.8 MPa for the others. Even though the strain increased 27.3% for the fatigue failed specimen 039, the modulus dropped by only 2.51%. The table shows that each residual strength test was performed at 26%, 41%, 51% and 83% of the life and the modulus of each specimen dropped 0%, 4.17%, 1.5%, 7.14% and 2.51%, respectively. On the other hand, the strain also increased 7.1%, 18.6%, 4.6%, 30.3%, respectively. It is difficult to directly relate the drop in modulus and the increasing rate of strain to the degradation of residual strength. However, up to 52% of the fatigue life, the modulus dropped by about 1.9% and the specimens held at 92.4% of their residual strength on average.

Since each test was stopped at a specific number of cycles to allow the specimen to be examined by the SEM, the specimen must be cooled down. This cooling may cause some damage on the coupon due to the differences of the coefficient of thermal expansion between matrix and fibers. For the present study, this possibility was ignored. Figure 4.24 shows the stress-strain response of selected cycles and the final static tensile load of a residual strength test. The last cycle modulus was 182 GPa while the modulus of the final tensile test was 181 GPa. This confirms that no additional damage was incurred from cool-down to examine the specimen before the final tensile load to failure.

Table 4.6 Changes of Modulus, Strain and R.S. of 1Hz Test at Various life

Plate ID	ID	$\frac{N_{last}}{N_f}$ (%)	$E_{initial}$ (GPa)	E_{last} (GPa)	E_{drop} (%)	$\varepsilon_{initial}$	ε_{finial}	ε_{drop} (%)	σ_{res} (%)
#3	885	26.0	194	194	0.00	0.00247	0.00265	7.3	106
#1	038	41.1	192	184	4.17	0.00254	0.00302	18.6	83.1
#3	886	51.9	200	197	1.50	0.00242	0.00253	4.6	94.2
#3	887	83.2	196	182	7.14	0.00248	0.00323	30.3	69.4
#1	039	100.0	199	194	2.51	0.00230	0.00294	27.8	66.4

Figure 4.25 was plotted from the data based in Tables 4.5 and 4.6. The specimen 96-888, which was tested to measure the material's ultimate strength, was used to normalize the residual strength and the specimen 95-039 was considered as the

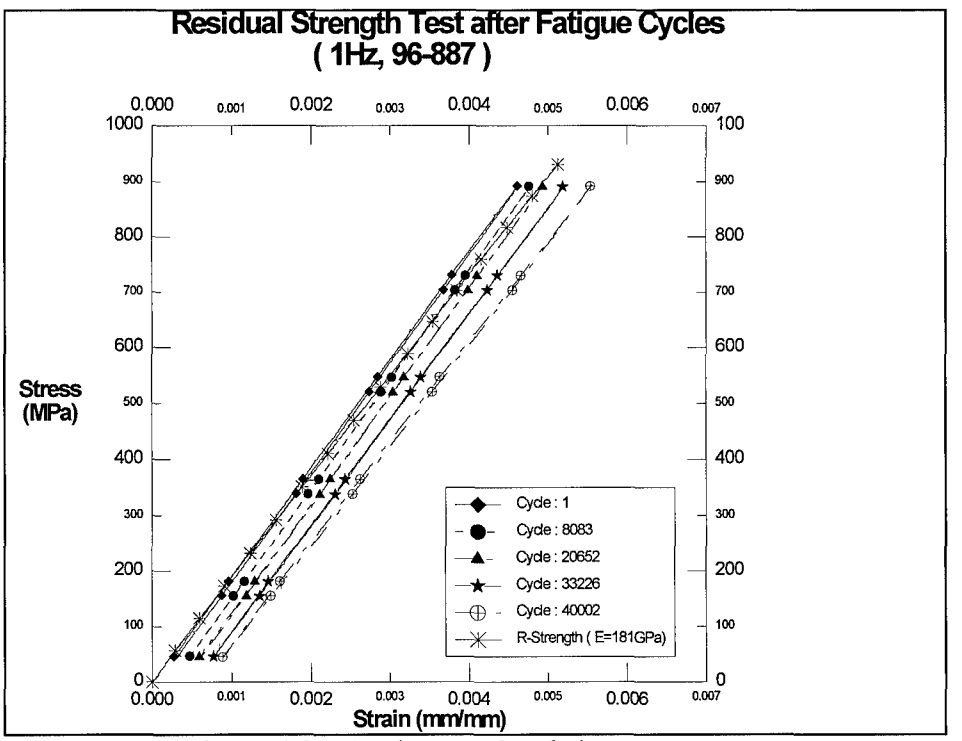

Figure 4.24 Static test after fatigue test

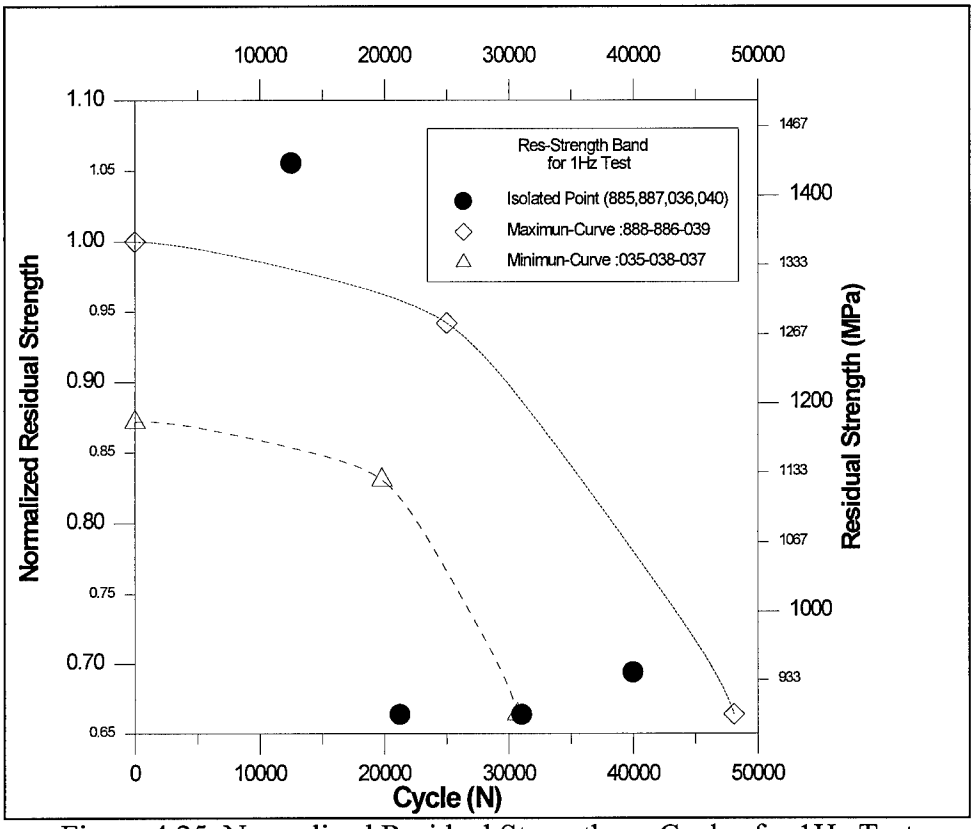

Figure 4.25 Normalized Residual Strength vs. Cycles for 1Hz Tests

maximum fatigue life. Because of the variation from specimen to specimen and bad test results, some data were not included to optimize the plot. For instance, the residual strength (1431.4 MPa) of specimen 96-885 was considered greater than reasonable and 95-040 as a case short of the proper range. The microscopic observations discussed later will point out more specific reasons for not using certain data points.

A maximum and minimum curve to band the data is presented in Figures 4.26 - 4.28. The maximum fitting curve was linked with the specimen which has a higher ultimate tensile strength (96-888) and the specimen which has the longest fatigue life (95-039). The minimum fitting line was made by linking the 95-035 which has a lower

ultimate strength and the 96-036 which experienced lower fatigue life. The other data were isolated within or outside the band.

Two methods for normalizing the residual strength were chosen. The first involves simply dividing by the material's ultimate strength and is displayed in many figures. Alternatively, the difference between the residual strength and maximum stress of the fatigue loading was normalized with the difference between the ultimate strength and maximum fatigue stress. The two methods are thus represented by

$$N.R.S._1 = \frac{\sigma_{R.S.}}{\sigma_{ult.}} \tag{4.1}$$

$$N.R.S._2 = \frac{\sigma_{R.S.} - \sigma_{Fat.}}{\sigma_{ult.} - \sigma_{Fat.}} \tag{4.2}$$

where $\sigma_{R.S.}$ is the residual strength, $\sigma_{Fat.}$ is the maximum stress during fatigue cycling, and $\sigma_{ult.}$ is the ultimate strength. The scale of the graph makes it clear which method is used for a given plot as $N.R.S._2$ will show fatigue failure as zero while $N.R.S._1$ will not. As discussed above, both the maximum and minimum curves in residual strength are decreasing only slightly (less than 10 %) up to around 50% of the fatigue life and then begin to drop catastrophically. The specimen 96-887 inside the band near the end of the life shows clearly how the residual strength drops rapidly near the end of the fatigue life. For the present study, this rapid drop could occur anywhere after 50% of the expected life. In Figure 4.26, the normalized residual strength data is plotted vs. the logarithm of the cycle. This is how S-N data is normally viewed, and thus, was plotted here to provide an indication of how the residual strength appears on such a basis.

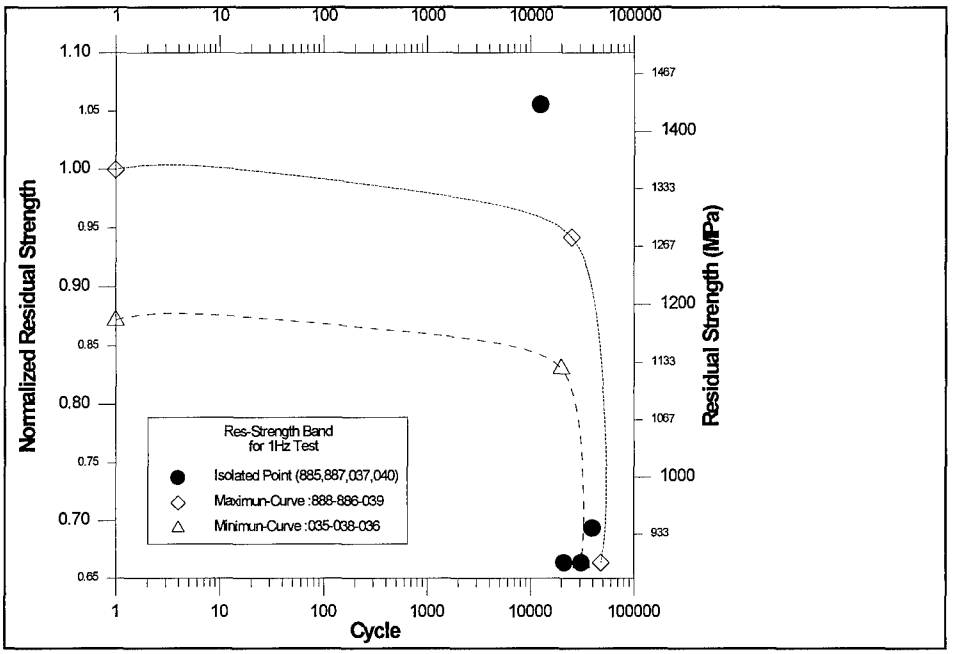

Figure 4.26 Normalized Residual Strength vs. Logarithm Cycles

Figure 4.27 used the ultimate strength from Pittman's test to normalize the data. In this plot, every residual strength tested in this study can be included without isolating any data. Figure 4.28 plots the residual strength in MPa above the fatigue maximum stress vs. the logarithm of cycles. This provides a clear indication of the data scatter without any normalization. As a further comparison, to minimize the plate-to-plate variation, the specimens from the same plate were normalized separately. Figure 4.29 presents such a plot where the residual strength was normalized. This reduces some of the data scatter. However, a couple points still remain outside the chosen maximum and minimum curve bands. A normalized cycles vs. normalized residual strength plot is presented in Figure 4.30.

This figure shows that the residual strength held about 80% of its strength up to near 50% of the fatigue life and then critically dropped. These curves are fairly consistent with the figure 4.25. Figure 4.31 presents the same data on a logarithm scale of the cycles.

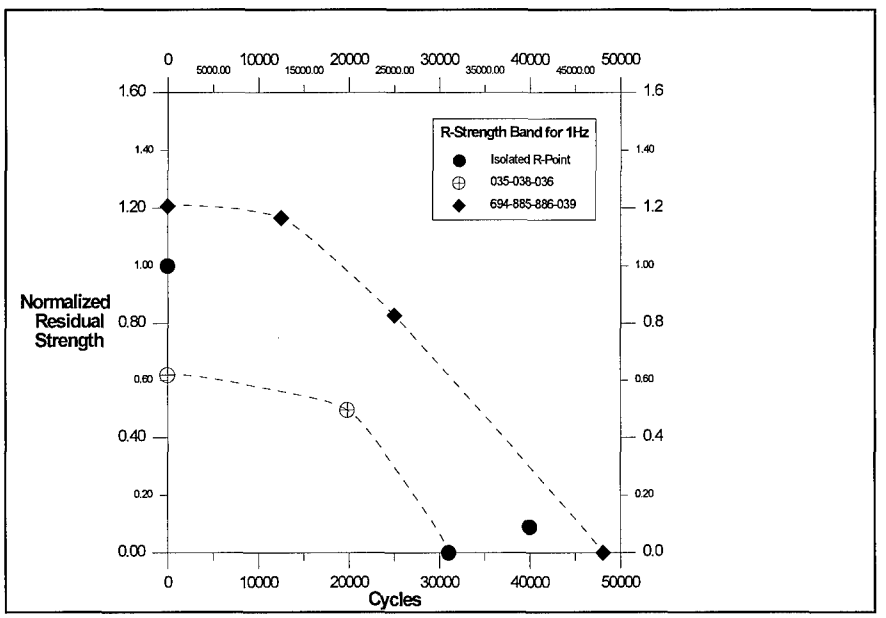

Figure 4.27 Normalized Residual Strength vs. Cycles

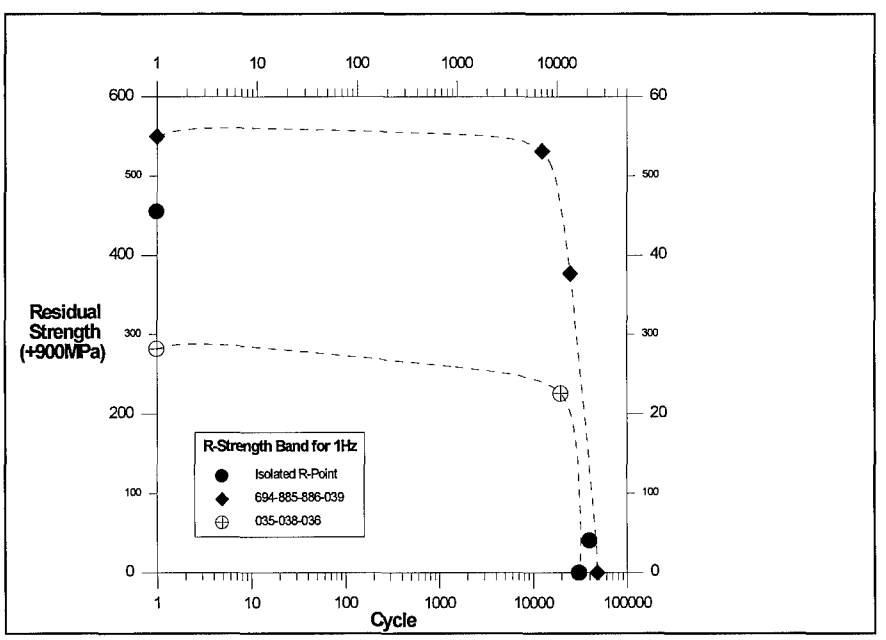

Figure 4.28 Residual Strength vs. Logarithm Cycles

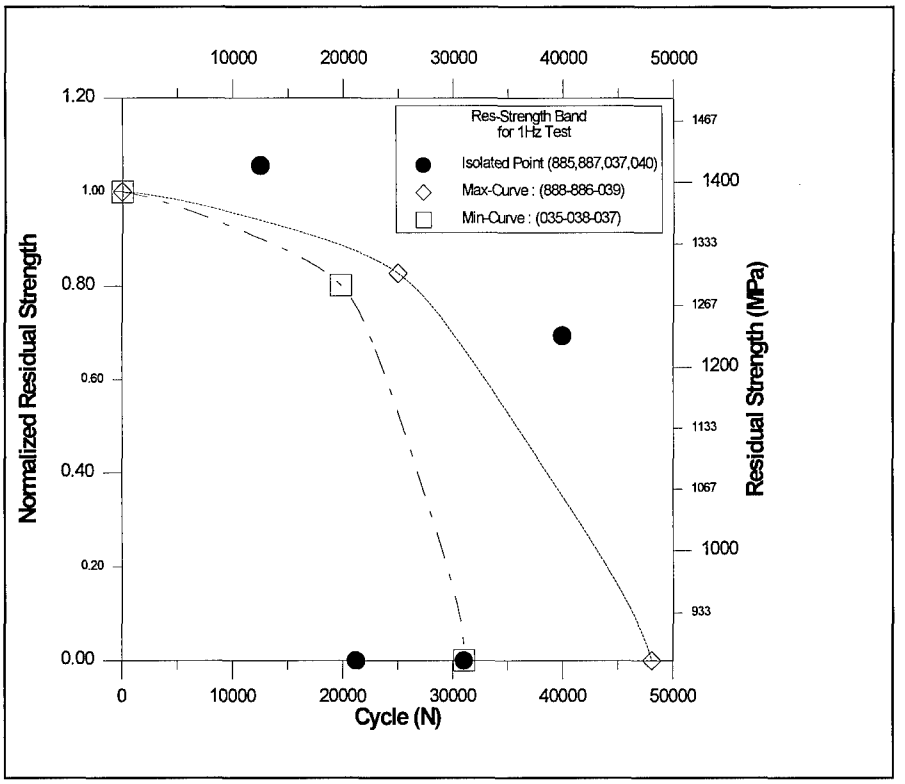

Figure 4.29 Normalized Residual Strength vs. Cycles

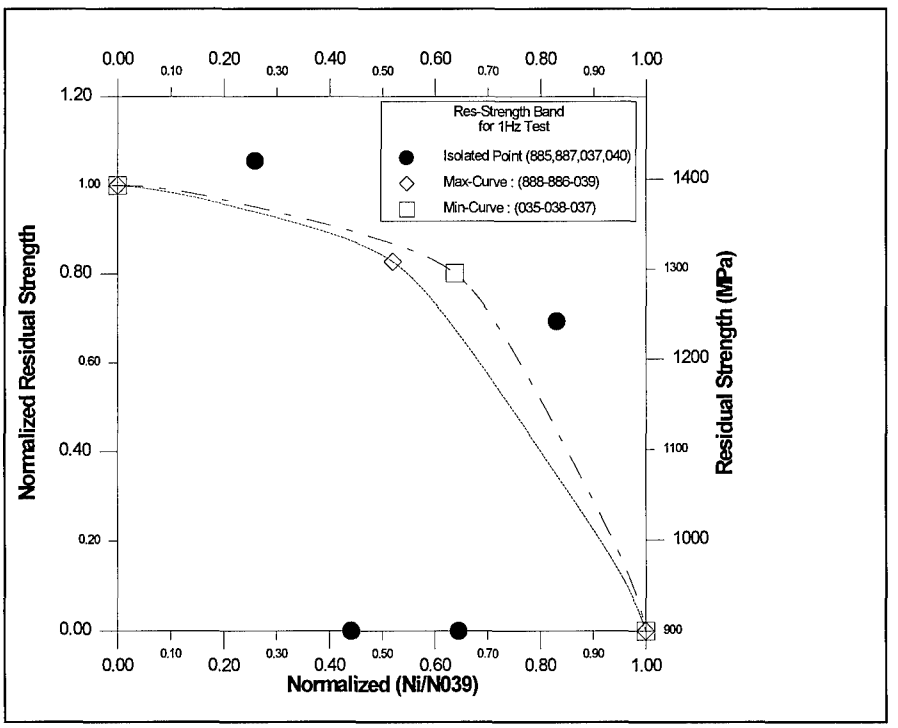

Figure 4.30 Normalized Residual Strength vs. Normalized Cycles

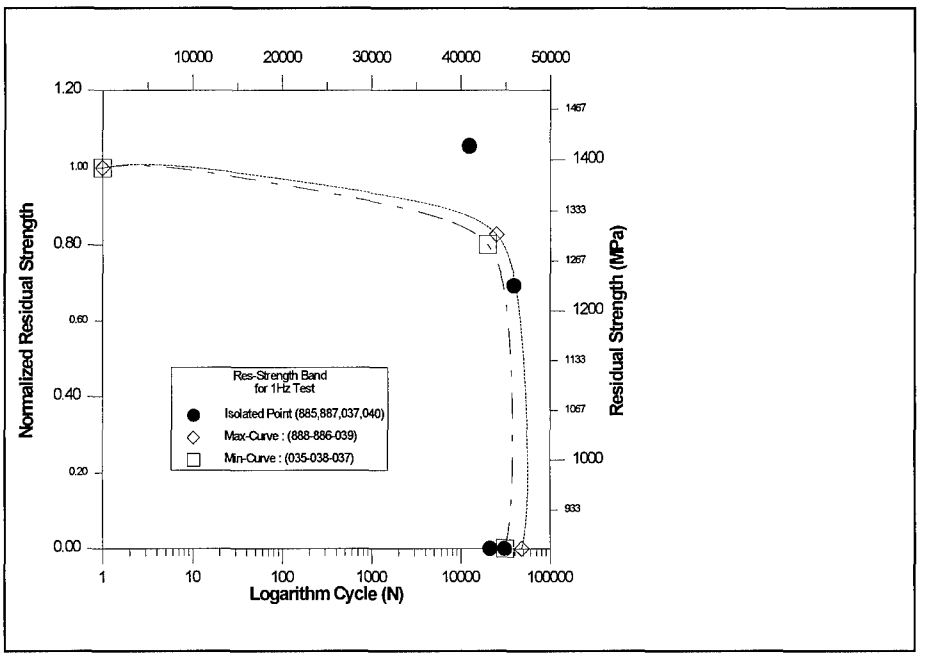

Figure 4.31 Normalized Residual Strength vs. Logarithm Cycles

4.3.1.2 0.01Hz Frequency Tests

The results of the 0.01Hz frequency tests are listed in the Table 4.7. In the Table 4.7, the two different moduli were measured when the specimens were failed and then the monotonic tension tests were performed for the residual strength. This table also shows how much the residual strength dropped ($\sigma_{res}/\sigma_{ult}$) as a percent and the number of cycles applied. The drop ratio of the residual strength was based on the ultimate tensile strength 1355.8 (specimen ID : 96-888). The specimen ID (95-712) which was previously tested by Pittman is listed as a reference for the number of cycles to failure.

The specimens 062 ~ 065 were machined from one plate. Also, specimens 888 ~ 890 were machined from a single plate while specimen 035 was machined from a different plate. In general, the specimens machined from plate # 1 have relatively lower lives. When compared with the life cycles of specimen 95-712, the moduli of the specimens

Table 4.7 Test Results of 0.01Hz R.S. Tests

Plate ID	Specimen ID	Cycles (N)	N_{end}/N_f (%)	Modulus (E_f ,E_m)	σ_{res} (MPa)	$\sigma_{res}/\sigma_{ult}$ (%)
#2	95-063	1552	14.3	193	900 (Fat)	66.4
#2	95-064	7283	67.2	169	900 (Fat)	66.4
#4	95-712	10827	---	---	900 (Fat)	66.4
#3	96-889	5003	46.2	196,197	1238 (Res)	91.3
#2	95-062	5222	48.2	191,190	992 (Res)	73.2
#2	95-065	7247	66.9	185,191	1129 (Res)	83.3
#3	96-890	9003	83.2	195,197	1250 (Res)	92.2
#3	96-891	10003	92.4	214,214	1264 (Res)	93.2
#1	95-035	0	---	201	1182 (Ult)	---
#3	96-888	0	---	201	1355 (Ult)	100

machined by different plates varies less than 4%. where two values of E are given, the first was obtained from the last fatigue cycle and the second from the monotonic test.

Table 4.8 shows that each residual strength point was performed at 46%, 48%, 67% and 83% of the life of specimen 95-712 and each specimen had residual strength 91%, 73.2%, 83.3% and 92.2%, respectively. The percent drop in the modulus and residual strength at the given number of percent life cycles as well as the mechanical strain measured at the last fatigue cycle are listed in the Table 4.8. It is easily seen that the modulus drop or strain increase can not be linearly related to the strength degradation.

However, if the two specimens 063, 889 were neglected, the modulus follows the same trend as the drop ratio of the residual strength. Up to 50% of the fatigue life, the residual strength fell around 27% while the modulus

Table 4.8 Changes of Modulus, Strain and R.S. of 0.01Hz at various life

Specimen ID	N_{end}/N_f (%)	Initial Mod (GPa)	Last Mod (GPa)	Mod Drop (%)	σ_{res} (MPa)	σ_{res} Drop (%)
063	14.3	196	193	-1.6	900	33.6
064	67.2	200	184	-8.0	900	33.6
712*	100	189	157	16.9	900	33.6
889	46.2	199	196	-1.51	1238	8.7
062	48.2	190	170	-10.5	992	26.8
065	66.9	197	185	-6.09	1129	16.7
890	83.2	199	195	-2.01	1250	7.8
891	92.4	214	214	0	1264	6.8

* Specimen tested by Pittman

decreased to 3.54% of its initial value. The specimen 063 was regarded as a bad data point due to the welding effect, which caused additional damage on the surface. This damage will be briefly discussed in the microscopic evaluation.

Similar to the 1Hz test, every fatigue test at 0.01Hz was stopped at a specific number of cycles to allow the specimen be examined by the SEM. Any possible damage due to the thermal stress caused by the differences of the coefficient of thermal expansion in between matrix and fibers was ignored.

Figure 4.32 shows the stress-strain curves of selected cycles along the final tensile load to failure for specimen 890. The modulus measured at down loading of the last cycle was 195 GPa and the modulus of the static test for the residual strength was 197

GPa. This figure shows that the specimens tested at 0.01Hz did not experience additional damage even though the temperature is cooled down to the room temperature after the last cycle and then reheated to 427C before the tensile test to failure. It was considered that this thermal reheating did not effect on the residual strength of the present study.

Figure 4.33 presents the residual strength data for the 0.01Hz specimens. The ultimate tensile strength of 96-888 was used as a denominator to normalize the residual strength. Some data points were not included due to extensometer or grip slip problems causing bad results. Also, as discussed in the microscopic evaluation, some points were thrown out due to problems with the thermocouple welds.

Similar to the 1Hz test response, the 0.01Hz test results are plotted with selected maximum and minimum curves to band the data. This band pictorially represents how the strength of the material degrades during fatigue and provides a region within which it is likely the material will fail. Figure 4.34 reproduces the data on a logarithmic scale of the cycles.

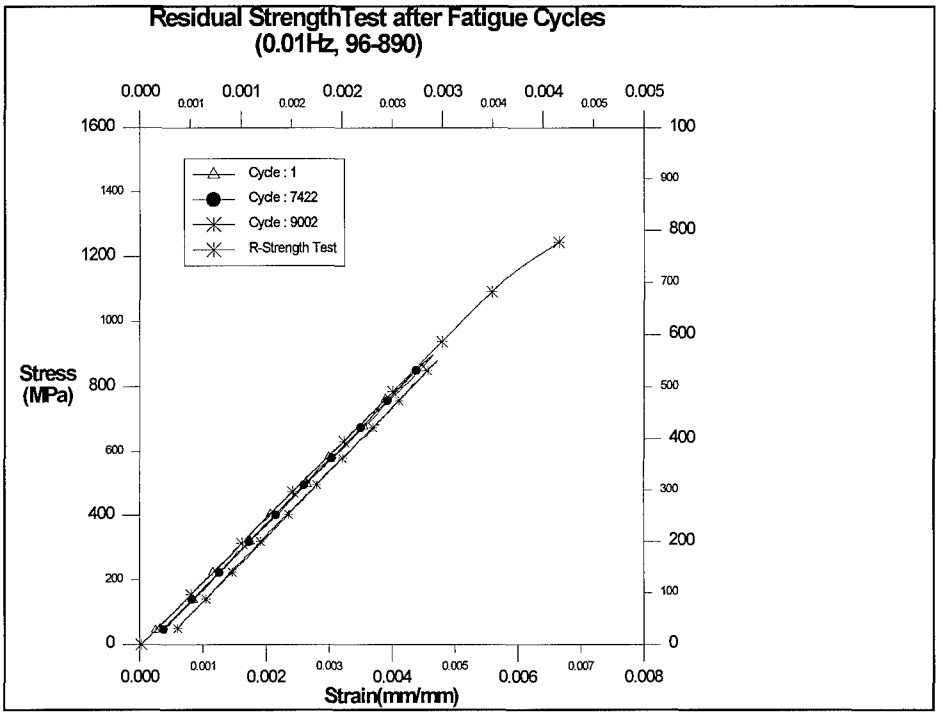

Figure 4.32 Static Test after Fatigue Test

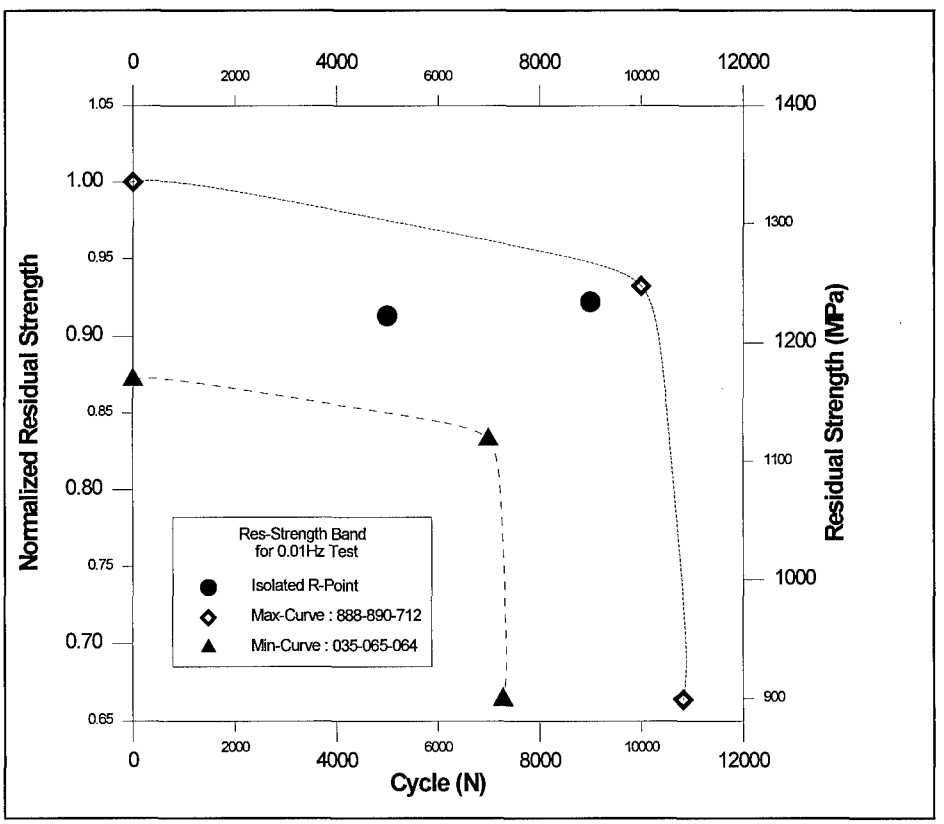

Figure 4.33 Residual Strength vs. Cycles

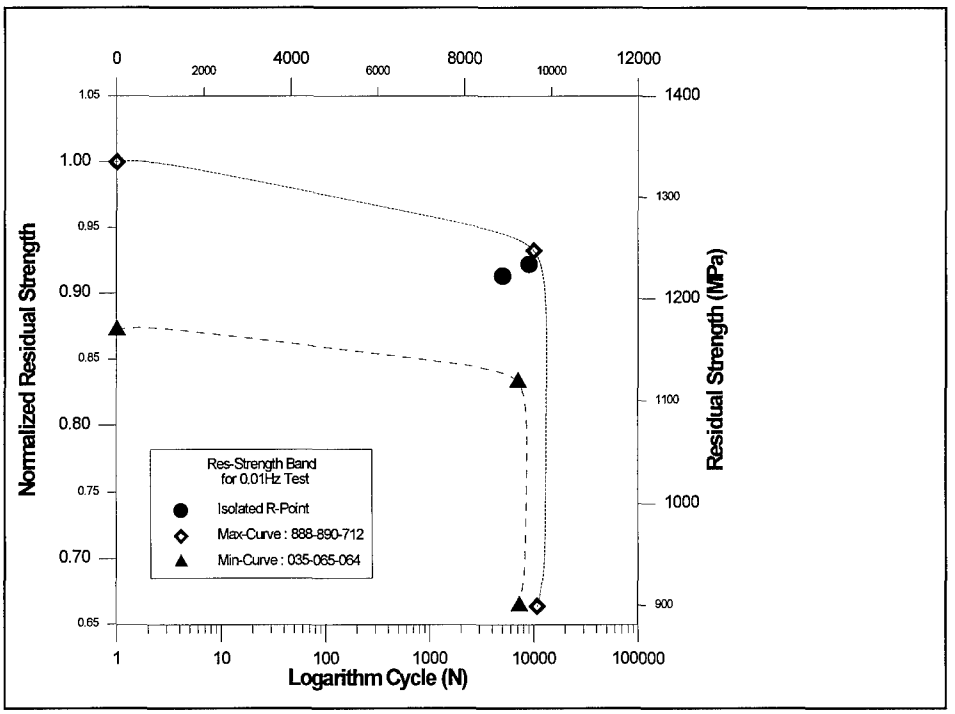

Figure 4.34 Normalized Residual Strength vs. Logarithm Cycles

Figures 4.35 and 4.36 plot the data using the second normalization procedure where the maximum fatigue stress (900 MPa) was subtracted off (4-2). Second, a 900 MPa was subtracted from the residual strength, and then the residual strength of the specimens (96-889, 96-890 and 95-062, 95-065) was divided by both 96-888 (1355.8 MPa) and 95-035 (1182 MPa), respectively. This was done to eliminate plate-to-plate variations. For the minimum band curve, the average of both 95-712 and 95-064 were selected as the expected life. The "knee" point of the maximum band curve is about 27% higher than the minimum.

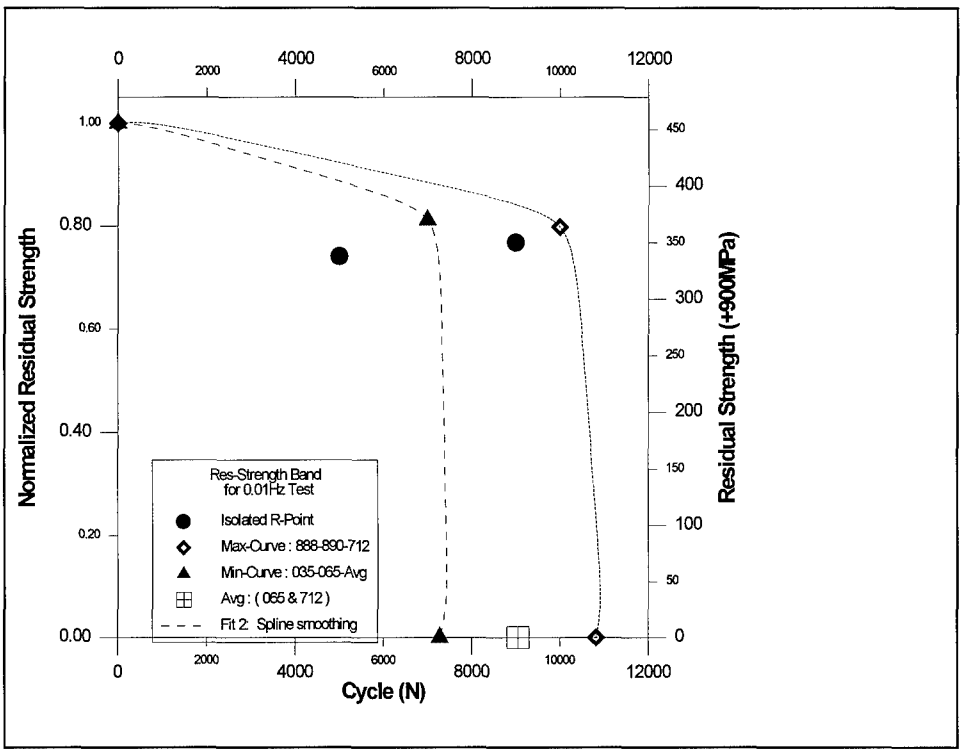

Figure 4.35 Normalized Residual Strength vs. Cycles

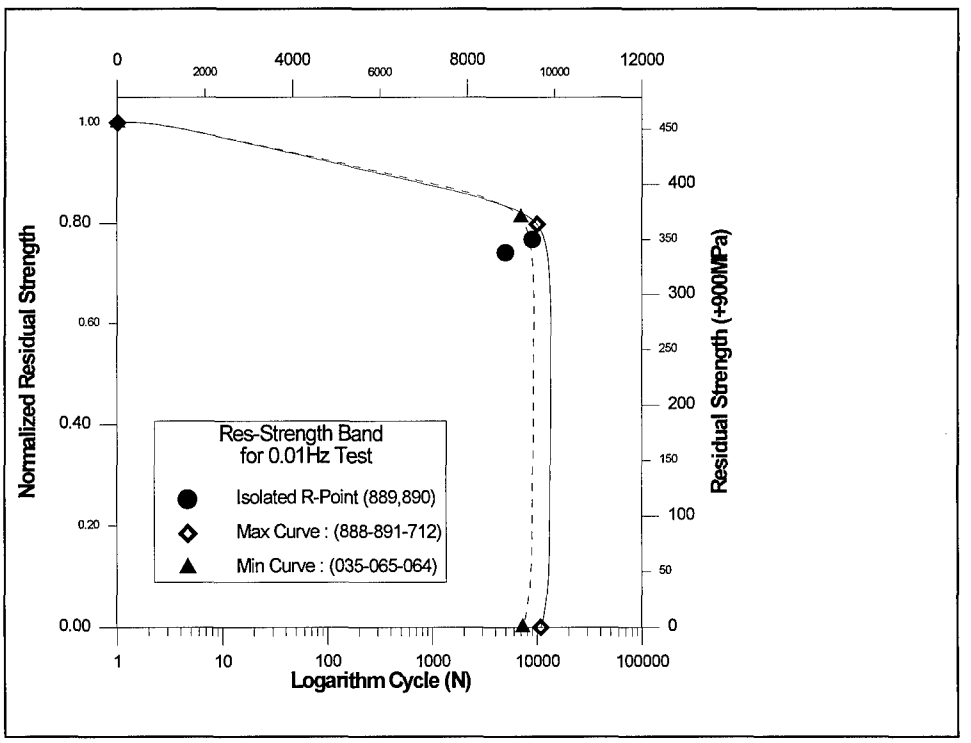

Figure 4.36 Normalized Residual Strength vs. Logarithm Cycles

In Figure 4.37, both axes of Figure 4.35 were normalized by the values described above. As indicated in the failure, the residual strength decreases gradually until it degrades by approximately 30% at around 80% of the fatigue life, then it begins to drop catastrophically.

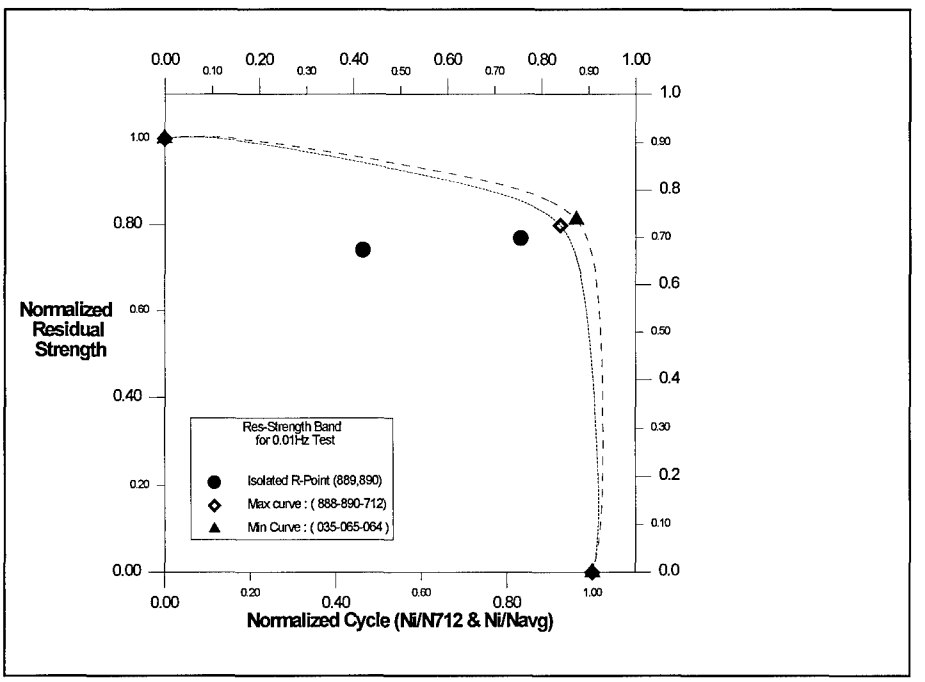

Figure 4.37 Normalized Residual Strength vs. Normalized Cycles

4.3.2 Microscopic Observations

A static load was applied to the specimens for obtaining the residual strength at a specific target cycle. Therefore every specimen used for this residual strength test had experienced fatigue load as well as a static load. These two different loads effect the damage mode on the fracture surface. Simular to the 1Hz

residual strength tests, the microscopy observation will be made for each sample, which was etched, polished and mounted. The fracture surface and microscopy provides the evidence for determining failure mechanisms with the mechanical responses. Finally, frequency effect will be discussed in addition to the differences between the various residual strength fracture surfaces.

4.3.2.1 1Hz Frequency Tests

Residual strength was successfully obtained from four specimens at this frequency. Welding guide was used to protect the specimens from the welding damage except specimen 95-038. Each test was stopped at about 26%, 41%, 52% and 83% of the fatigue life. Figure 4.38 shows the irreguar shape of the surface fractured by the static test only. Almost all fatigue cracks initiated at the surface or edge where some damaged area from the machining or welding is located. In contrast, upon tensile loading, the failure is transferred to adjacent fibers which are unable to handle the additional load. The interface between the two cracked fibers debonds and the matrix necks down in a ductile overload failure. This leads to further fiber fracture and matrix yielding. As a result, the composite exhibits a non-linear stress-strain behavior and the fracture surface is relatively flat. The fracture of the composite is initiated by fiber fracture which initially occurs randomly in the composite because of the statistical scatter of the fiber strength. So, the fracture surface exhibits irregular shape (fiber pulled out or down) with severe ductilitity (void-coalescence and matrix necking). These tensile loading mechanisms can be easily found on the fracture surface of the specimen tested for the residual strength.

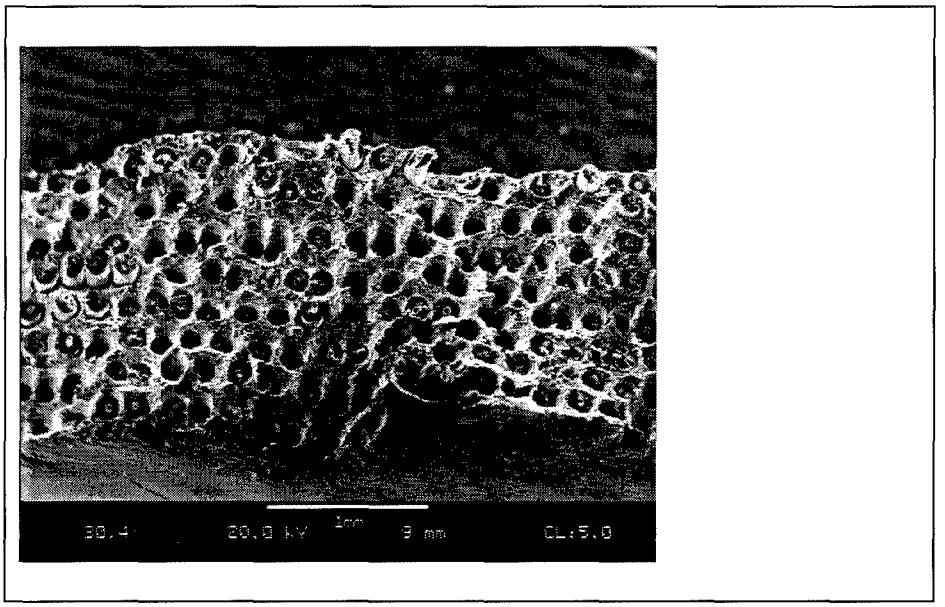

Figure 4.38 Ductile Region on the Static Test

Four specimens were successfully tested for residual strength at the 1Hz frequency. Each test was stopped at about 25 %, 40 %, 50 % and 80 % of the fatigue life. Figure 4.39 and 4.40 shows the typical fracture surfaces of the specimens tested at1Hz in fatigue followed by the static load to failure (residual strength test). The main distinction of the fracture surface between the ultimate strength test and residual strength test is the addition of a fatigue crack region. In spite of its matrix-dominated characteristics, obtaining a quantitative measure of the fatigue area over the whole fracture surface is difficult due to the material's irregularity. The fatigue area was calculated by counting the fiber numbers which had no ductility (necking and void coalesence) and dividing them by the total fiber numbers (38 on length × 8 on width ≅ 300). The specimen in Figure 4.40 had several welding sites on its surface, and the matrix cracked along these

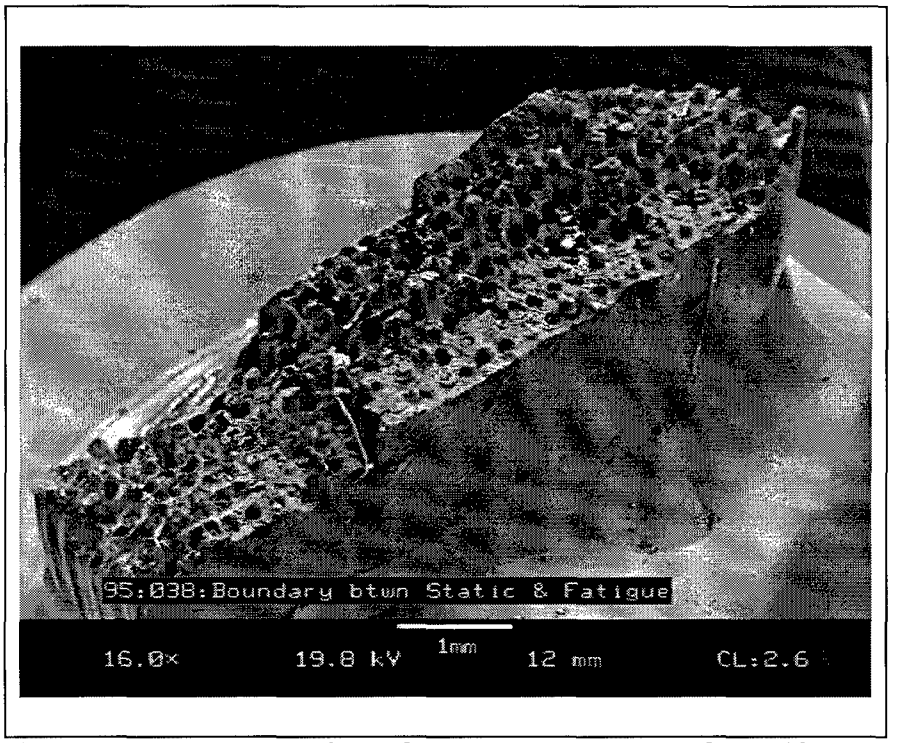

Figure 4.39 Fracture Surface of the R.S. Test at 26% of the Life

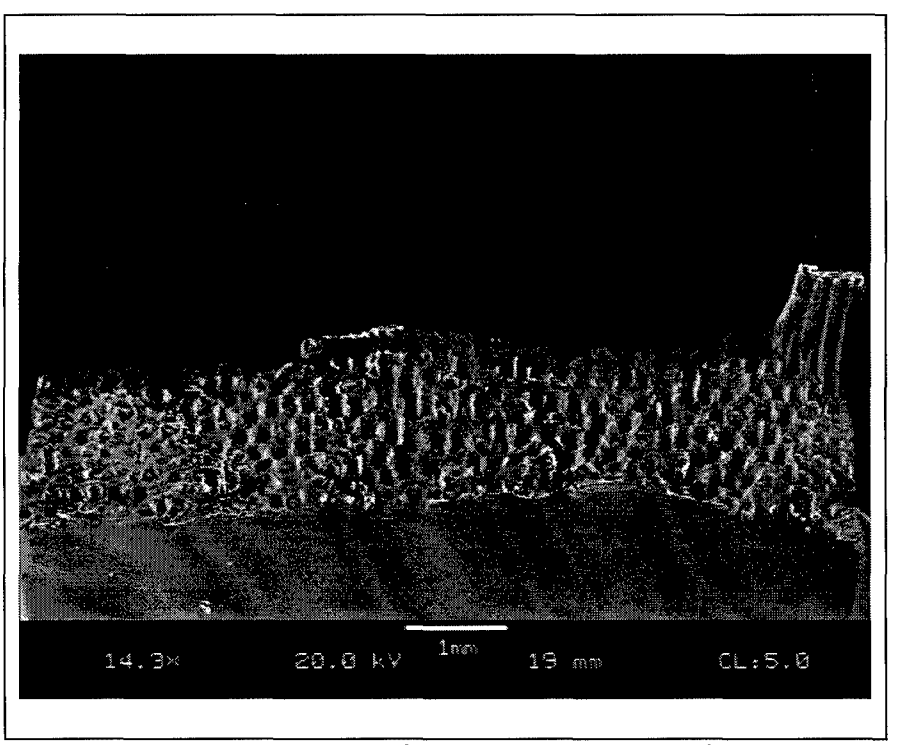

Figure 4.40 Fracture Surface of the R.S. Test at 41% of the Life

welding sites as well as from both edges. The fatigue area is very flat and represented about 40 % of the total area. The other 60% represents the tensile overload region.

Figures 4.41 and 4.42 depict the fatigue and static areas with magnification ×515 and ×525 respectively. In Figure 4.41 (fatigue area), the fibers broke near the matrix surface demonstrating some fiber pullout and no necking or ductility was present. It shows that the fibers bridged the crack as it advanced, but as the matrix stress was transfered to the fibers, they eventually broke. The presence of fibers broken above and below the cracking surface indicates that the advancing crack caused the fiber/matrix interface to fail first, and then the fiber cracked at a point along the interface separation. In Figure 4.42 (static area), fiber breakage, fiber-matrix debonding and matrix ductile overload is evident.

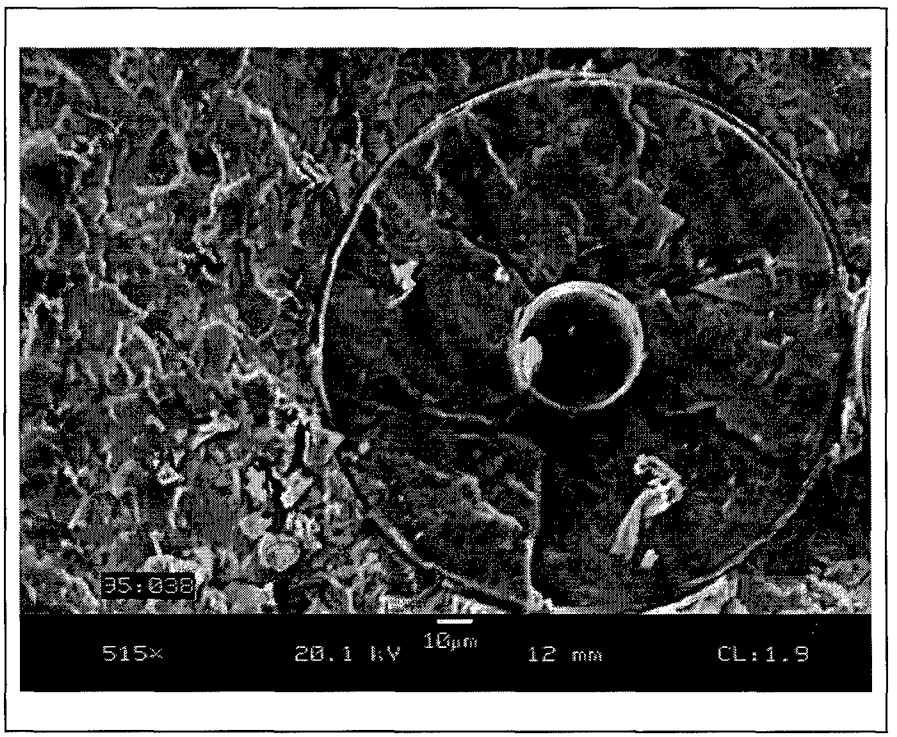

Figure 4.41 Fatigue Area (Flat Matrix Cracking)

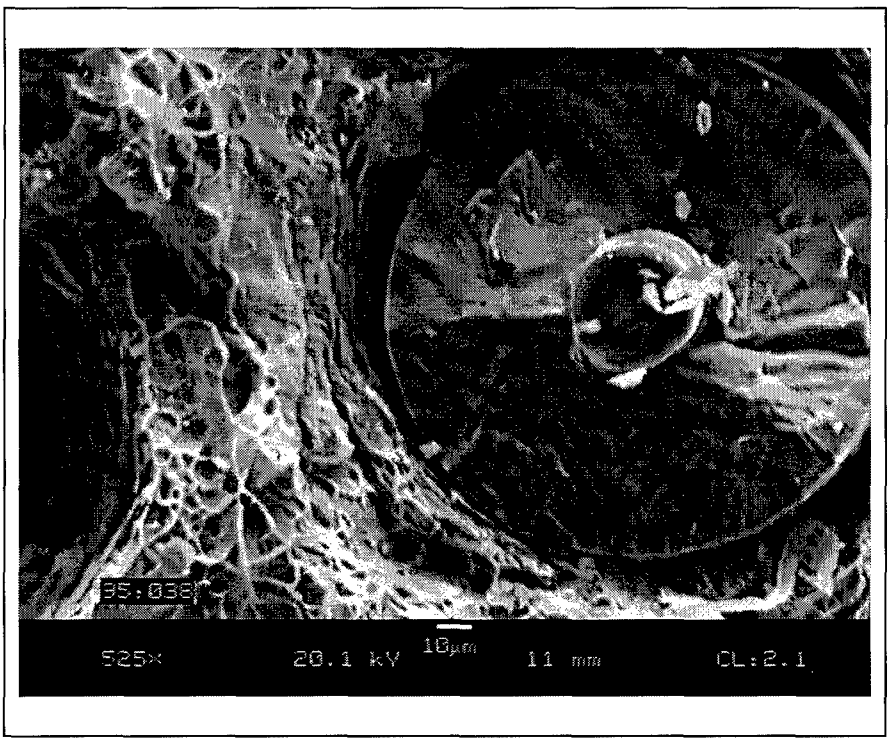

Figure 4.42 Static area (Severe Ductility)

The percentage of the fracture area dominated by fatigue or by overload for individual specimens are presented in Table 4.9 and Figure 4.43. Except for specimen 95-A038, the portions of the fatigue area are well consistent with the residual strength.

Table 4.9 Measured Data of the Fatigue and Static Area

Specimen ID	Applied Cycles	Applied Cycles (%)	Fatigue Area (%)	Static Area (%)	Residual Strength (MPa)
95-038	19792	40	40	60	1126
96-885	12505	25	23	77	1431
96-886	25007	50	30	70	1277
96-887	40003	80	60	40	941

The plots based on this estimation of the fatigure area are represented in Figures 4.43 and 4.44. They show that the residual strength vs. increased fatigue area reveals a

smooth logarithm trend and a smooth exponential trend for static area vs. residual strength. This trend illustrates that the drop in residual strength is directly related to the fatigue crack propagation, as expected, rather than the percent of expected cycles to failure.

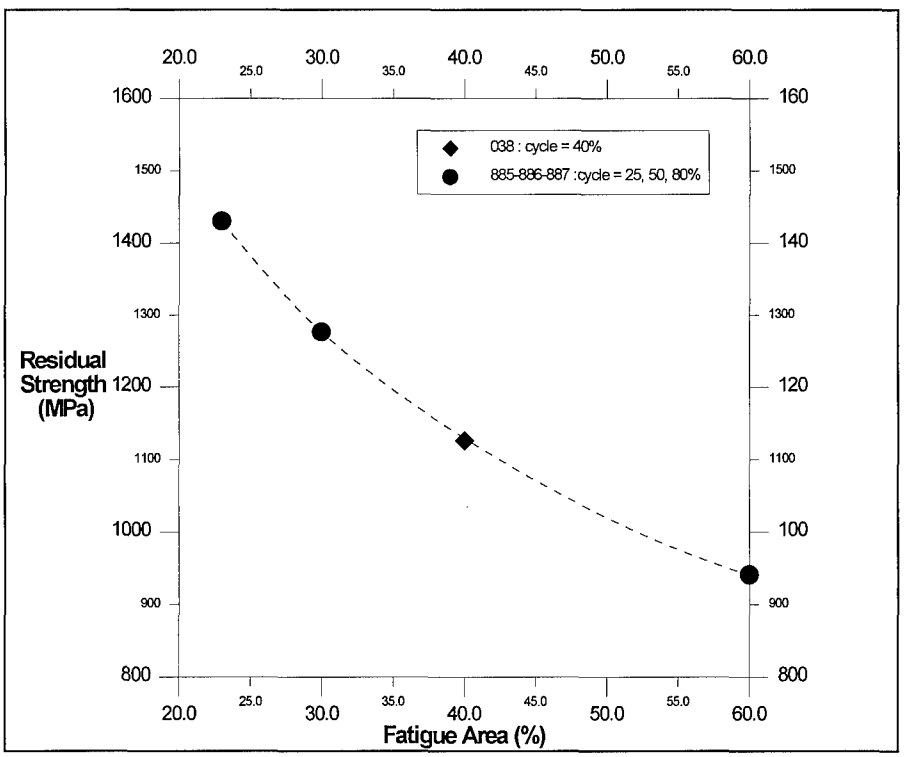

Figure 4.43 R.S. vs. Quantified Fatigue Area.

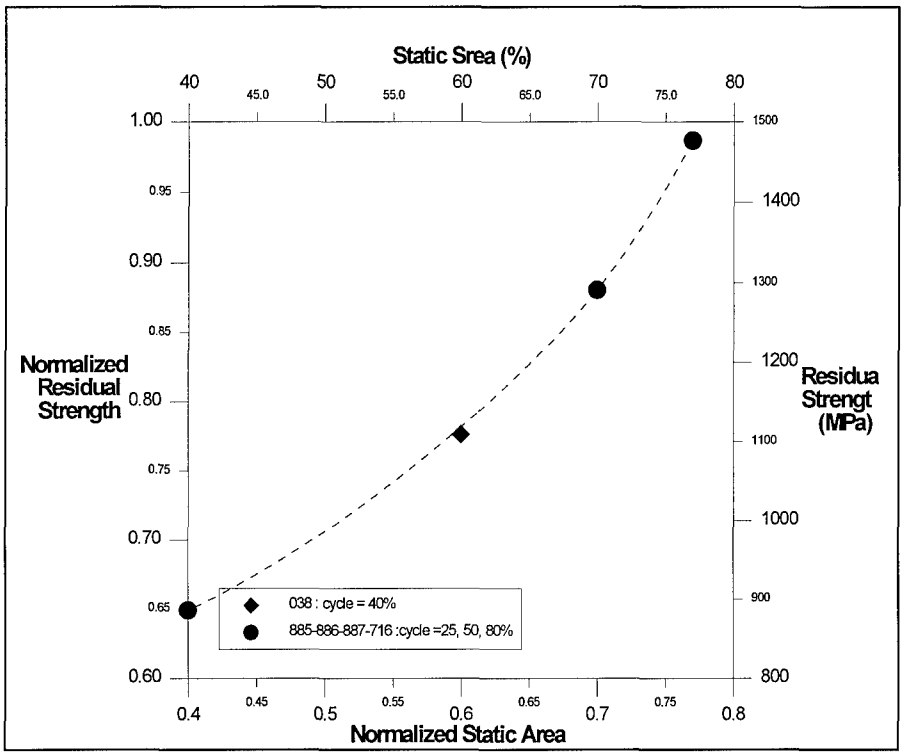

Figure 4.44 Normalized R.S. vs. Quantified Static Area.

4.3.2.2 0.01Hz Frequency Tests

Four specimens were tested for gaining the residual strength at this frequency. Welding guide was used to protect the specimens from the welding damage except specimen 95-062. Each test was stopped at about 46%, 58%, 67% and 83% of the fatigue life. Figure 4.45 shows one of the typical fracture surfaces at this test condition. As discussed in the previous chapter, the fatigue area under the 0.01Hz fatigue load had experienced more of a fiber-dominated mode than the 1Hz tests. In contrast to the other specimens tested at 0.01Hz frequency, 95-A062 was affected by damage initiation at the welding sites which are easily seen Figure 4.46. The other welding site also had about a

3 mm surface crack. The 1 mm flat area in the right hand side (Figure 4.45) also had a surface damage caused from a welding site. Figures 4.47 and 4.48 were taken at the cycle number 5222 and after fracture due to the static load.

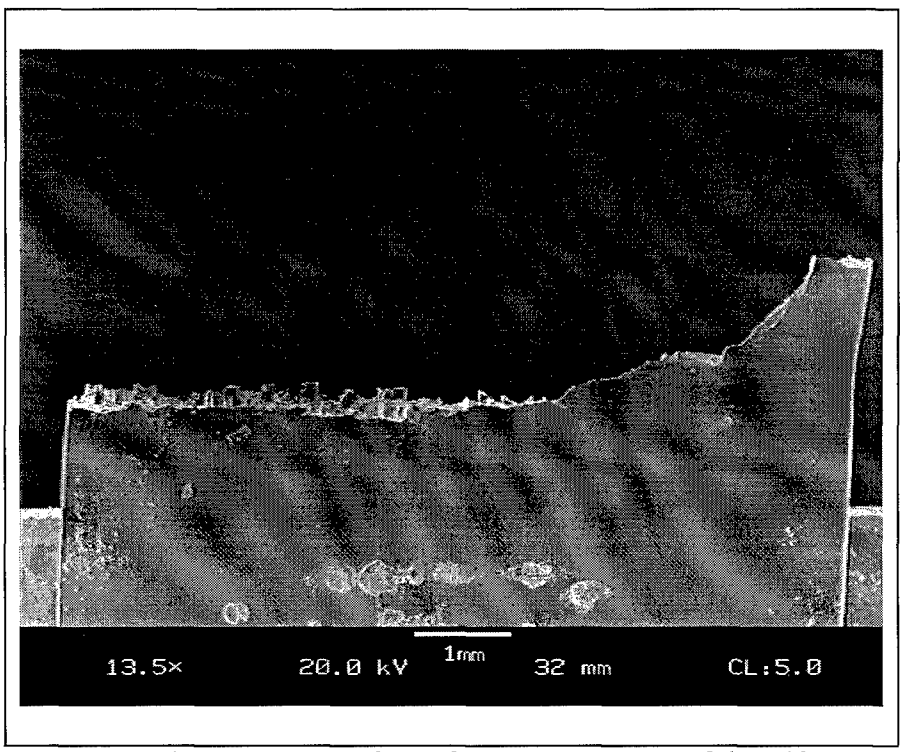

Figure 4.45 Fracture Surface of R.S. Test at 50% of the Life

Figure 4.46 shows the tilted fracture surface of the specimen 96-889 tested for the residual strength under the fatigue load with the 0.01Hz frequency. This figure shows that the fatigue area is initiated from both surfaces and edges (1 mm and 2 mm on the right hand side, 1.5 mm and 2.3 mm on the left hand side, two spots: 0.5 mm and 0.8 mm on both edges). The fracture surface is fairly flat but most of the area experiences ductile failure as evidenced by matrix necking, fiber pull out and dimpling. This suggests that fatigue behavior was dominated by matrix creep and dimpling due to void coalescence.

Matrix cracking initiated from the damaged or weak surfaces or edges where damaged fibers are located. Weak fibers due to fiber-matrix debonding, bad manufacturing, or fibers damaged by machining within the matrix cracking area broke early in the test. At low frequency, it is evident that the specimens experienced more creep and ductility than cleavage because they have an irregular fracture surface with several matrix cracks which may have initiated at different levels. Figure 4.49 shows a certain site with ×368 magnification in the static failure area. Matrix ductility caused by matrix necking and void coalescence is evident.

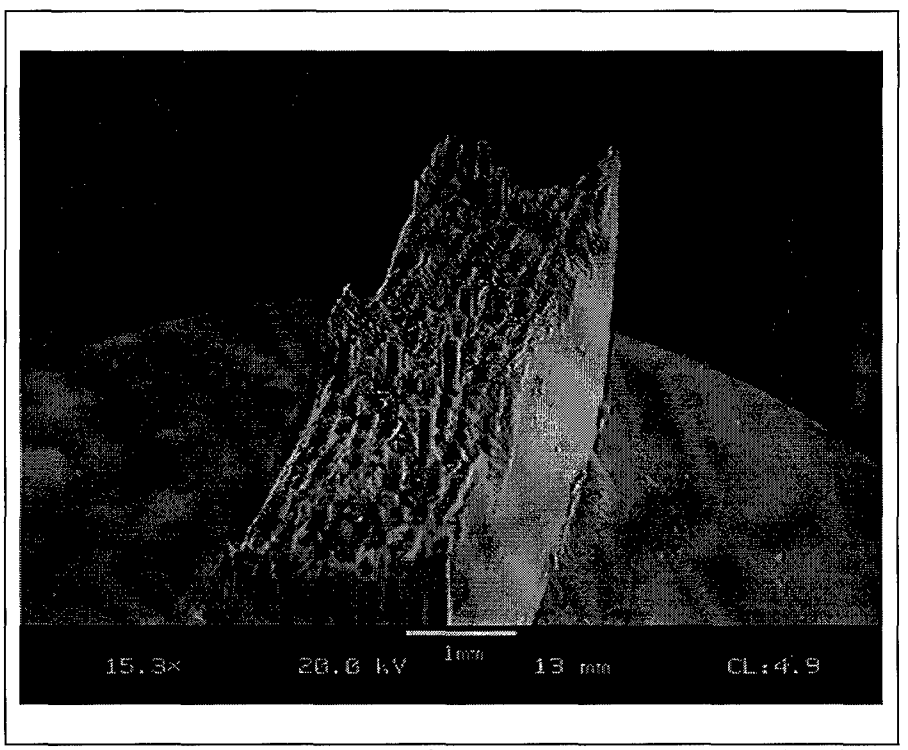

Figure 4.46 Titlted Fracture Surface of R.S. Test at 46% of the Life

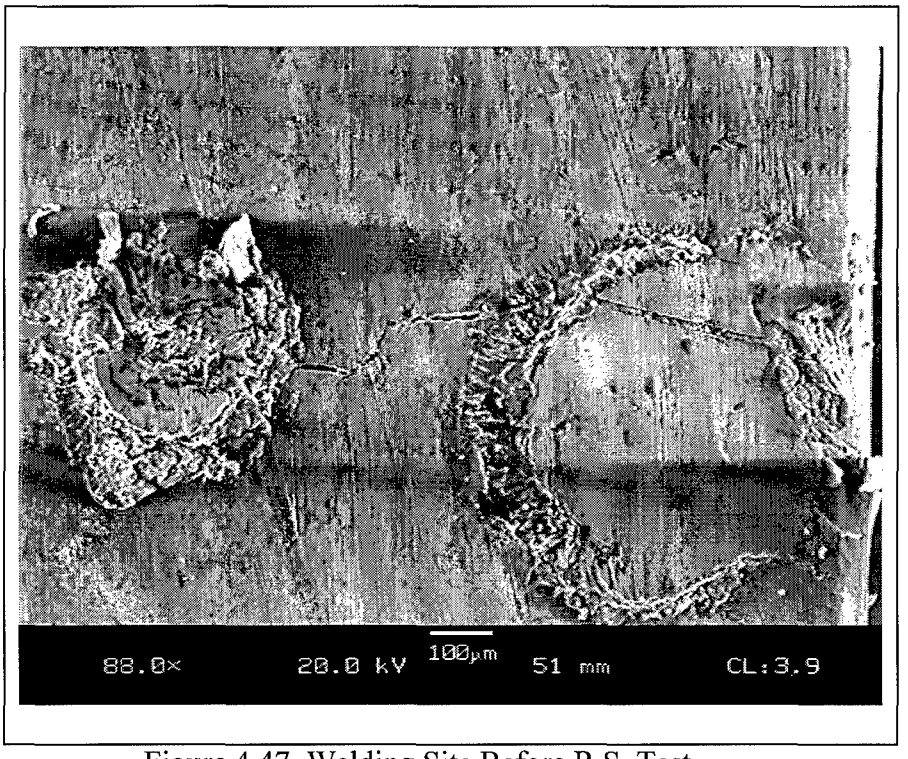

Figure 4.47 Welding Site Before R.S. Test

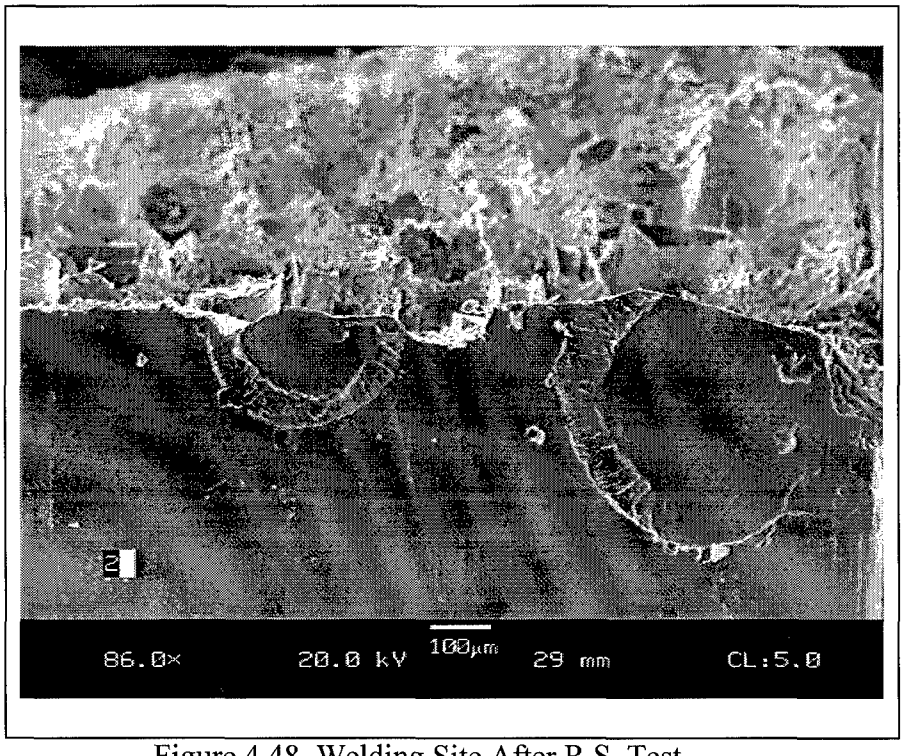

Figure 4.48 Welding Site After R.S. Test

In contrast to the 1Hz test (matrix-dominated mode), the 0.01Hz fracture surfaces were much more difficult to quantitatively identify the fatigue versus static areas. In order to distinguish the areas, the SEM machine and microscopic observation of the

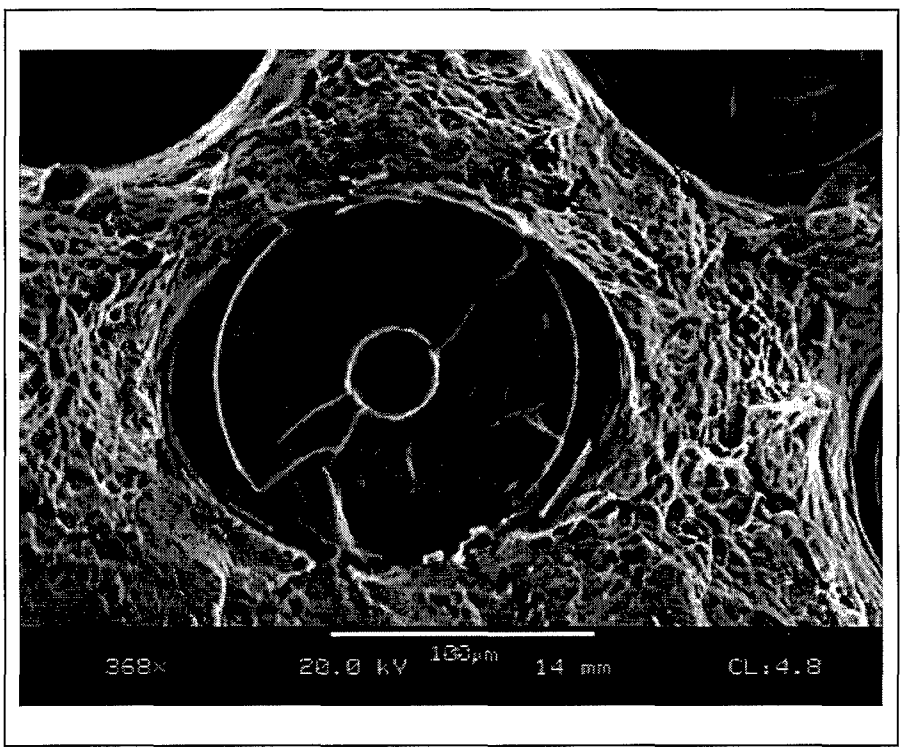

Figure 4.49 Static Region

fracture surface were used. In the photo taken by the SEM without tilt, as the ductility of the area increases, the area is brighter. This is because coalesced voids reflect more light than a cleaved area. Figure 4.50 shows that there are some reflectivity distinctions in the sample photo.

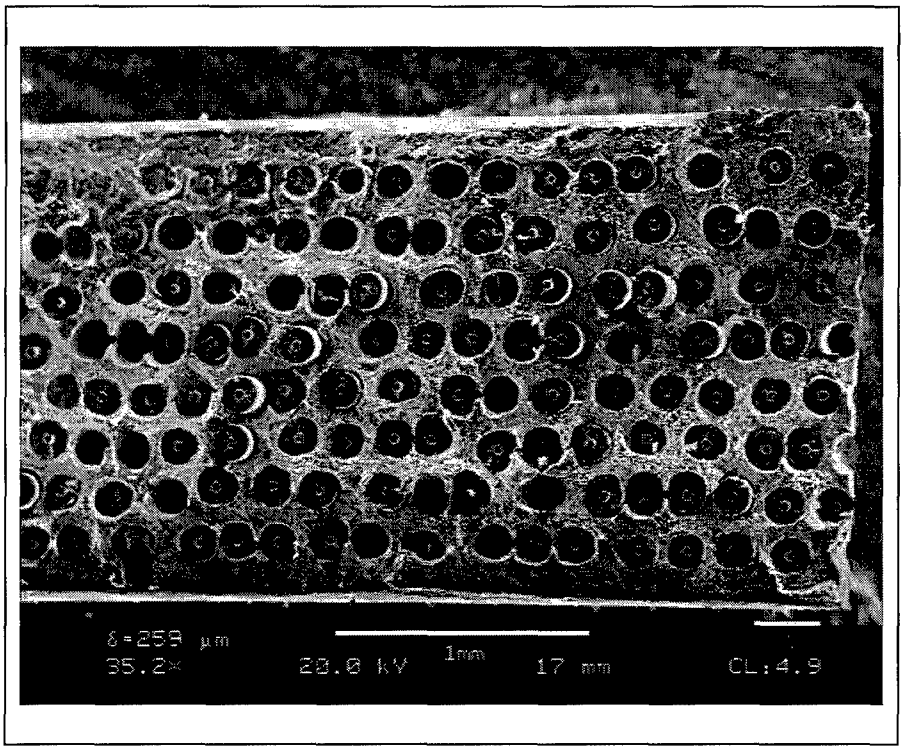

Figure 4.50 Differences of Brightness on the Fracture Surface

The fracture area was divided into three categories. The dark area which is located at the corner of the right top and shallow area along the below edge represents the matrix cracking area, and the bright area shows the static overload region. Table 4.10 shows the estimated data plot based on the above distinction. In the table, transit area represents the second case on the estimating procedure. The relationship between the relative areas and the residual strength is not nearly as consistent for the 0.01Hz results as observed previously for the 1Hz. However, the error associated with identifying the relative areas is significant for 0.01Hz. Because specimen 95-062 was severely damaged from the welding, it had a relatively large matrix cracking area and held less residual

strength due to an extensively progressed fatigue crack. The static area well represents the residual strength in this case.

Table 4.10 Measured Data of the Fatigue and Static Area for 0.01Hz Tests

Specimen ID	Applied Cycles	Applied Cycles (%)	Matrix Crack Area (%)	Transit Area (%)	Static Area (%)	Residual Strength (MPa)
96-889	5003	46	14	54	32	1238
95-062	5333	58	20	58	22	992
95-065	7247	67	15	46	39	1129
96-890	9004	83	18	48	34	1250

4.4 Frequency Effect Comparisons

In the previous sections, the behavior of the SCS-6/Ti-6-4 composite was presented under isothermal fatigue with two different frequencies. To understand the difference in the residual strength under the different test frequencies, macroscopic and microscopic observation over the life of the specimen were discussed, and the fatigue and static areas of the fracture surfaces were measured. In this section, the frequency effects on the fatigue life and the residual strength of the specimen will be analyzed. Table 4.11 shows the results of the residual strength tests for both 1Hz and 0.01Hz.

4.4.1 Frequency Effects on Fatigue Life

Comparisons will be focused here to show how the two different frequencies affect the mechanisms of deformation and damage and then how the mechanisms work differently regarding the residual strength.

Table 4.12 shows values of the mean strains and moduli of the specimens at a specific percent of their lives. Each mean strain and cycle was normalized by the mean strain of the last cycle and the number of the first cycle, respectively. In the 0.01Hz tests, the mean strain increased to 22.5% on an average during the first 10% of the life and then smoothly increased up to 35% on an average at 80% of the life. Finally, the specimen experienced a catastrophic increase (additional 35%) in strain during the final stages of its life. On the other hand, the mean strain of the 1Hz test gradually increased to 26% on an average of its initial strain to failure even though the mean strain had experienced relatively fast increase during the first 10% of its life. Figure 4.51 pictorially shows the changes of the mean strains over the entire fatigue life. The mean strains of 0.01Hz specimen had increased over three times of the mean strains of the 1Hz tests at 10% of their lives and both of them reached 25% ~ 35% of their initial mean strain up to 80% of their lives. Another distinction is in the characteristics of the variation of increasing strain from approximately 80% of the lives to the failure. The 1Hz specimen (039) failed without much increase in mean strain (only 4% ~ 5%) during the last 20% of the fatigue loading while the mean strain of the 0.01Hz test (specimen 95-712) had increased over 30% compared to its initial mean strain during the last 20% of life.

Table 4.11 Test Results

Test Type	Specimen	Parent Plate	Freq (Hz)	Cycle (N)	CTE (10^{-6}/°C)	σ_{ult}, σ_{res} (MPa)
fatigue-RS	95-034	PRDA 5-1L	10	Slip-bad	6.792	900
Static	95-035	PRDA 5-2L	---	---	5.574	1182
fatigue	95-036	PRDA 5-3L	1	30697	6.417	900
fatigue	95-037	PRDA 5-4L	1	31058	5.808	900
fatigue-RS	95-038	PRDA 5-5L	1	19792	5.761	1126
fatigue	95-039	PRDA 5-6L	1	48102	5.808	900
fatigue	95-040	PRDA 5-7L	1	21248	5.714	900
	Average				**5.982**	
fatigue	95-061	PRDA 7-2L	1	8004	6.276	900
fatigue-RS	95-062	PRDA 7-3L	0.01	5222	5.808	992
fatigue	95-063	PRDA 7-4L	0.01	1552	5.948	900
fatigue	95-064	PRDA 7-5L	0.01	7283	6.206	900
fatigue-RS	95-065	PRDA 7-6L	0.01	7247	5.550	1129
fatigue	95-066	PRDA 7-7L	1	28708	5.550	900
	Average				**5.889**	
Static	96-884	PRDA 10-1	---	Grip-fail	**	---
fatigue-RS	96-885	PRDA 10-2	1	12505	5.644	1431.4
fatigue-RS	96-886	PRDA 10-3	1	25007	5.574	1277.2
fatigue-RS	96-887	PRDA 10-4	1	40003	5.480	940.77
Static	96-888	PRDA 10-5	---	---	5.714	1355.8
fatigue-RS	96-889	PRDA 10-6	0.01	5003	5.550	1238
fatigue-RS	96-890	PRDA 10-7	0.01	9003	5.527	1250.3
fatigue-RS	96-891	PRDA 10-8	---	Untested	5.761	---
	Average				**5.6071**	

Table 4.12 Mean Strain and Cycles at each percent life.

Freq	Sample	$N_{10\%}$	$MS_{10\%}$	$N_{80\%}$	$MS_{80\%}$	$N_{\sim 100\%}$	$MS_{\sim 100\%}$
0.01	890:*R*	1240	22	8680	29	9002:86%	33:86%
0.01	712:*F*	1516	23	8431	41	10501:100%	78:100%
1	887:*R*	5069	5.4	38759	26.4	40003:83%	30:83%
1	039:*F*	5016	9.8	38082	25.5	48102:100%	28.4:100%

- *R*: Residual Strength Test , F: Fatigue Test
- $N_{10\%}$: Cycles at the percent of the life
- $MS_{10\%}$: Mean Strain at the percent of the life

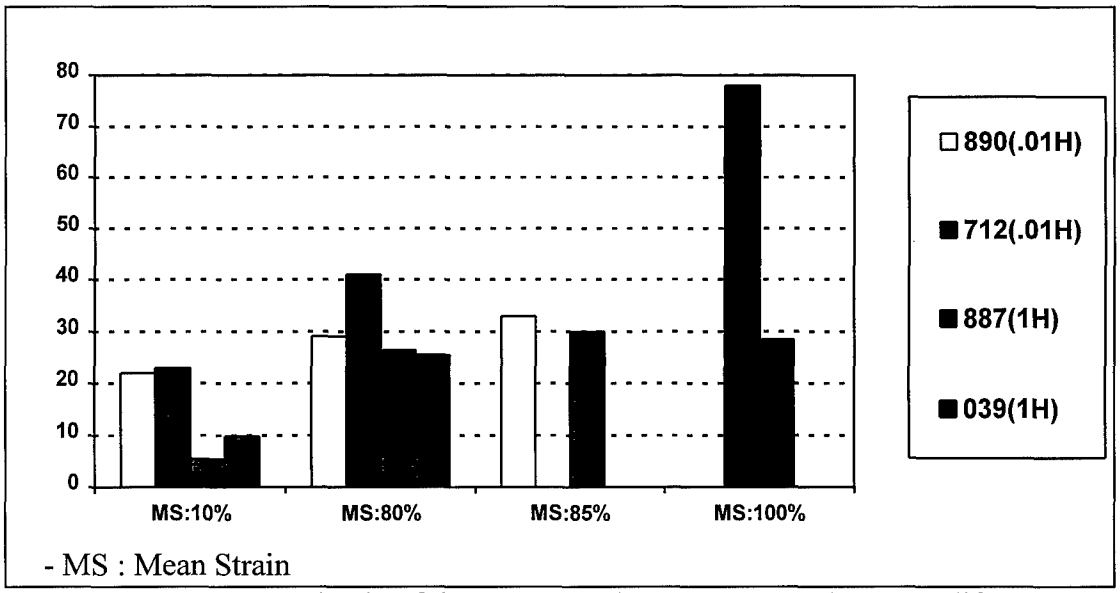

Figure 4.51 Mean Strain of the 0.01Hz and 1Hz tests at each percent life

Figures 4.52 and 4.53 show the stress-strain responses of the 0.01Hz and 1Hz fatigue tests, respectively. In Figure 4.52, a permanent residual strain (ε_p) is present upon unloading during the first cycle. The stress-strain responses on the subsequent fatigue cycles are linear, but extensive incremental increase in the permanent deformation was observed along with a relaxation of the maximum stress (900MPa) within 10% of its life. Small incremental increases followed up to 80% of its life. Then, the strains increase rapidly with a greater rate of the maximum strain than minimum strain. In Figure 4.53 (1Hz), the permanent residual strain (ε_p) at the first cycle is absent, and the stress-strain responses on the subsequent fatigue cycles are also linear and parallel, but an incremental increase in the permanent deformation is apparent

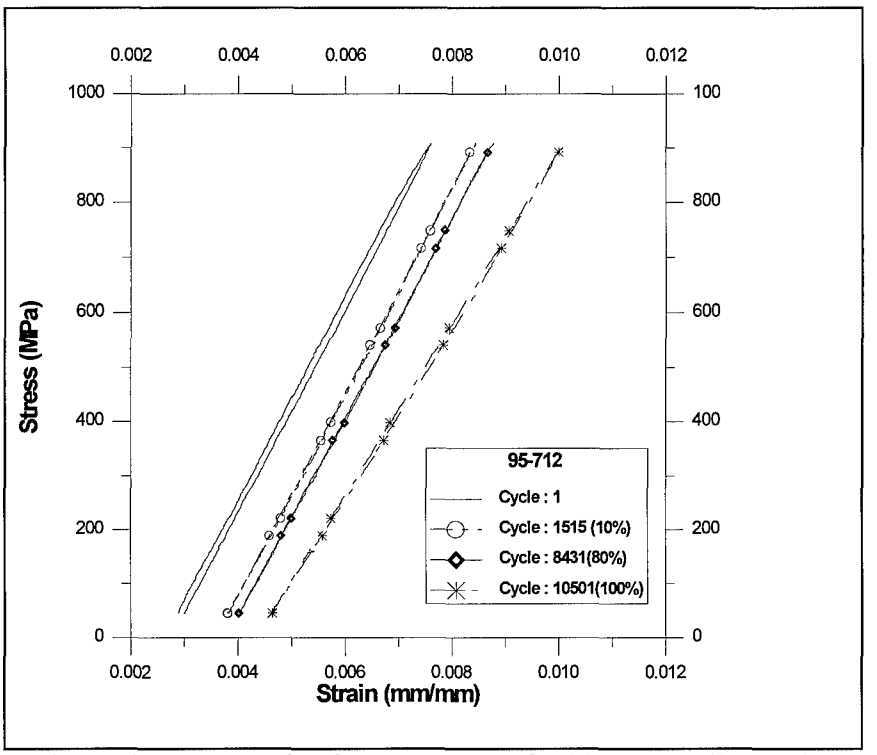

Figure 4.3.2 Stress-Strain Responses of 0.01Hz Test (95-712).

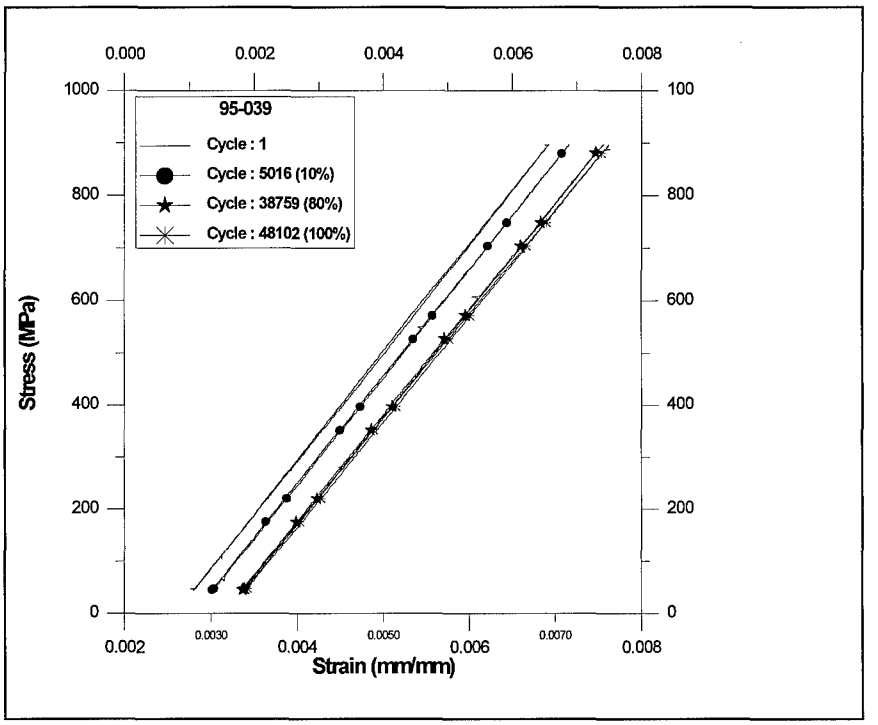

Figure 4.53 Stress-Strain Responses of 1Hz Test (95-038).

Figure 4.54 is presented to compare the mean strain and modulus responses under the two different frequencies. As discussed above, the mean strains of the 0.01Hz test indicated fiber dominant behavior while those of

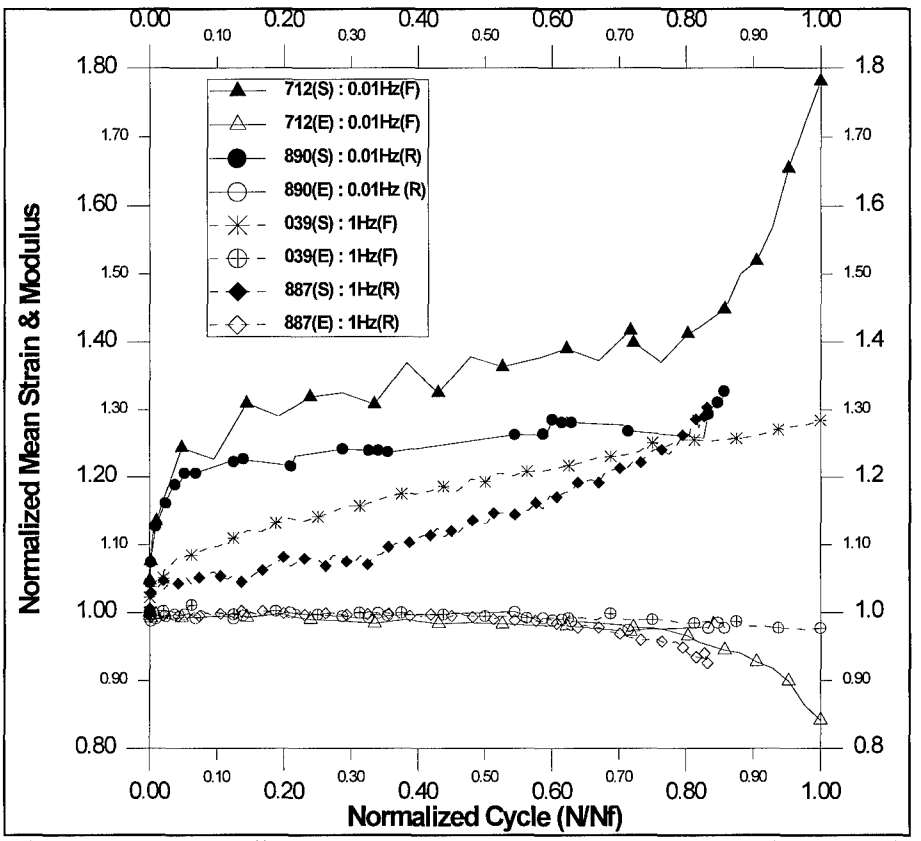

Figure 4.54 Normalized Mean Strain & Modulus vs. Normalized Cycle.

the 1Hz tests indicated matrix dominant behavior. The moduli did not decrease as much as the mean strains. After 80% of the life, only the modulus of the 0.01Hz test rapidly decreased to failure.

In the microscopic evaluation, the samples of the 1Hz tests revealed that the fracture is quite irregular and composed of several relatively flat fatigue cracking regions that extend from the edge and/or surface of the specimen. These fatigue cracking regions were not located on the same cracking plane, and overload failure morphology was found in the adjoined regions. Conversely the samples of the 0.01Hz tests revealed irregular fiber breakage and matrix deformation.

4.4.2 Frequency Effects on the Residual Strength

Figure 4.55 is presented to illustrate deformation and damage mechanisms of the fatigue tests with two different frequencies and how these affect the residual strength. The responses of the mean strain and modulus of the specimens were partitioned into three stages, which are stages I ~ stage III. The stages were operative only in the 0.01Hz tests. For the 1Hz test, the increase of the mean strain from a few cycles to 10% of the life was relatively fast, but the knee point from fast portion to steady portion much varied from specimen to specimen. In spite of this variation, introducing the stage was considered to be a useful method to compare tests performed at different frequencies. A matrix dominant damage occurred in the 1Hz frequency test and a fiber dominant damage was evident in the 0.01Hz test.

In the first stage of the matrix dominated failure mode (1Hz test), matrix creep mainly influenced the increase of the strain and a little decrease of the modulus. A relaxation of the thermal residual stress between fiber and matrix contributed to the respective increase or decrease. The matrix experienced slight plasticity in this stage like

an intergranular decohesion, transgranular decohesion and/or small void and their coalescence. During this process, the matrix was hardening due to the high frequency effect, so it would turn out to be slightly brittle even though it is difficult to quantify. In this region, the matrix did not crack, but in some instances fibers could crack due to their statistical scatter of the fiber strength [31]. It has been shown by Nicholas and Ahmad that cracked fibers alone are not enough to produce any measurable changes in the stiffness of a MMC [27]. As a result, the residual strength will not be affected in this stage (Figure 4.56).

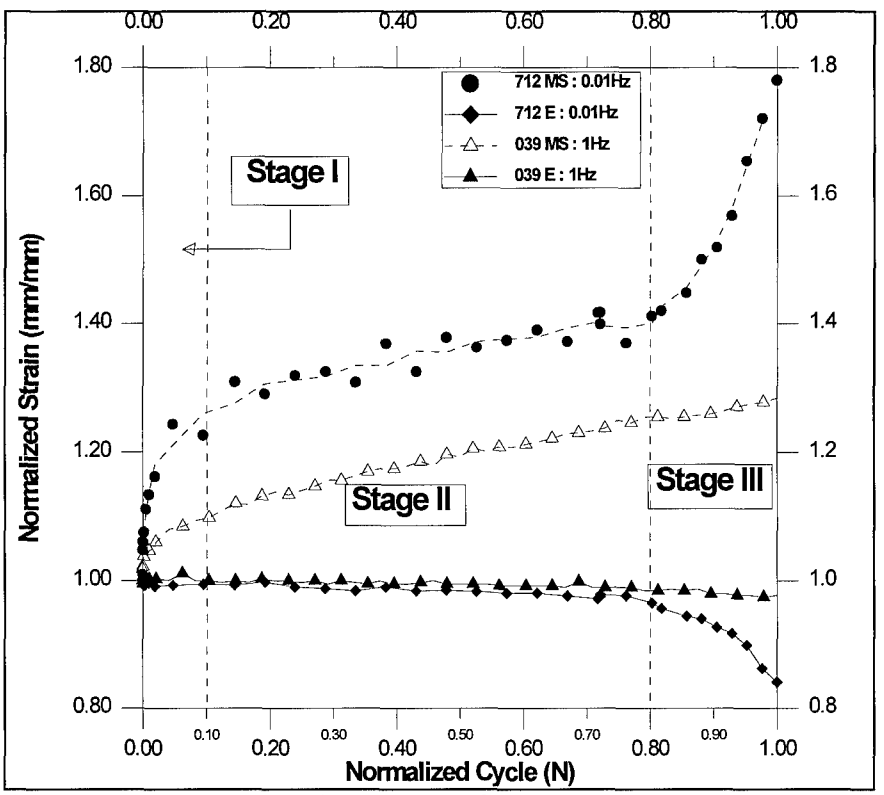

Figure 4.55 Three Stage of Fatigue Life.

At the second and third stage, matrix crack growth dominated the damage and caused a simultaneous change in the strain and modulus. At the end of the third stage, the overloaded fibers and matrix suddenly fractured with a typical plastic failure (extensive void coalescence and necking). Theoretically, any residual strength remaining in these stages should correspond to the real size of the uncracked ligament. But the residual strength did not decrease until 50% ~ 60 % of life (Figure 4.56). However, if the fibers were bridging the matrix crack, any reduction in the residual strength would be smaller due to the fibers carring the load. This may be one reason the quantified fatigue area was not proportional to the residual strength.

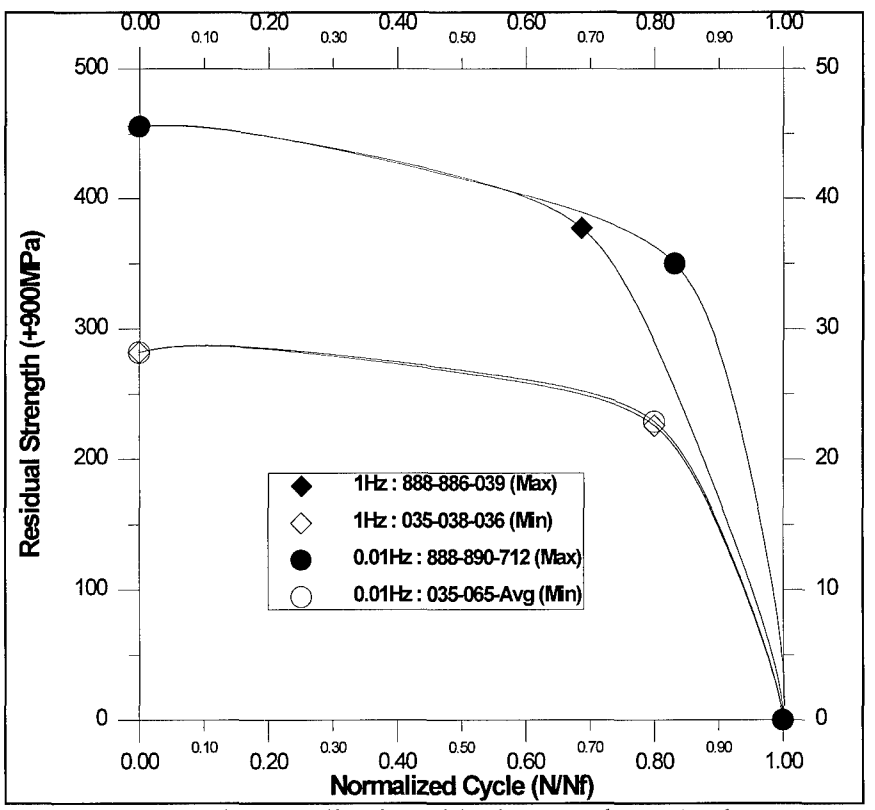

Figure 4.56 Normalized Residual Strength vs. Cycle

In the first stage of the fiber dominated failure mode (0.01Hz test), the specimen experienced extensive matrix creep due to the low frequency. This strain growth with the relaxation of the thermal residual strength caused the fast increase and decrease of the mean strain and modulus, respectively. As discussed above, the rate of the mean strain's growth was over three times that of the 1Hz test. As shown in Figure 4.3.2, the fact that the curves shifted to the right with a greater rate suggests that the matrix suffered repeated plastic deformation. In this stage, after the matrix experienced extensive plasticity, it became brittle and the interfacial reaction zone may have been damaged too, but the majority of the fibers can be considered to be unbroken owing to the insufficiency of the maximum load (900 MPa). Therefore, the residual strength was not affected (Figure 4.56). In the second stage, additional cyclic loading advanced the debonding between fibers and matrix. Individual fibers may exceed their failure strengths and produce isolated cracks. These cracks will tend to form on the same plane due to local stress risers near fiber cracks. In the third stage, the scattered and confined crack areas start to coalesce. It is indicative of the crack propagation that the extensive modulus drop and the mean strain increase simultaneously in stage III. The residual strength will be severely influenced in this region with a catastrophic decrease (Figure 4.56).

The Figure 4.57 and 4.58 show the frequency effect of the residual strength versus the number of cycles and time for the 1Hz and 0.01Hz tests. The curves indicate that the material retains its strength up to 80% of each life independent of the frequency. Thus, if the fatigue life is extended, the material will also be maintained longer. Pittman showed that the SCS-6/Ti-6-4 composite exhibited a gradual transition from cycle-dependence to

time-dependence as the frequency changed from 1Hz to 0.01Hz. Therefore, the knee point located in between the steady portion and the rapid decrease portion (approximately 80% of the life) will effect a change in its duration over the fatigue life. The residual strength of the 1Hz test had held its strength during 38% more cycles than that of the 0.01Hz test. It is difficult to show how much the cycle-dependency dominates the residual strength in this figure due to the lack of data at other frequencies, though. When this figure is compared with Figure 4.58, the time-dependency is clearly shown in the lower frequency. In Figure 4.58, the composite tested at 0.01Hz kept its strength about 70% longer than that of the 1Hz test.

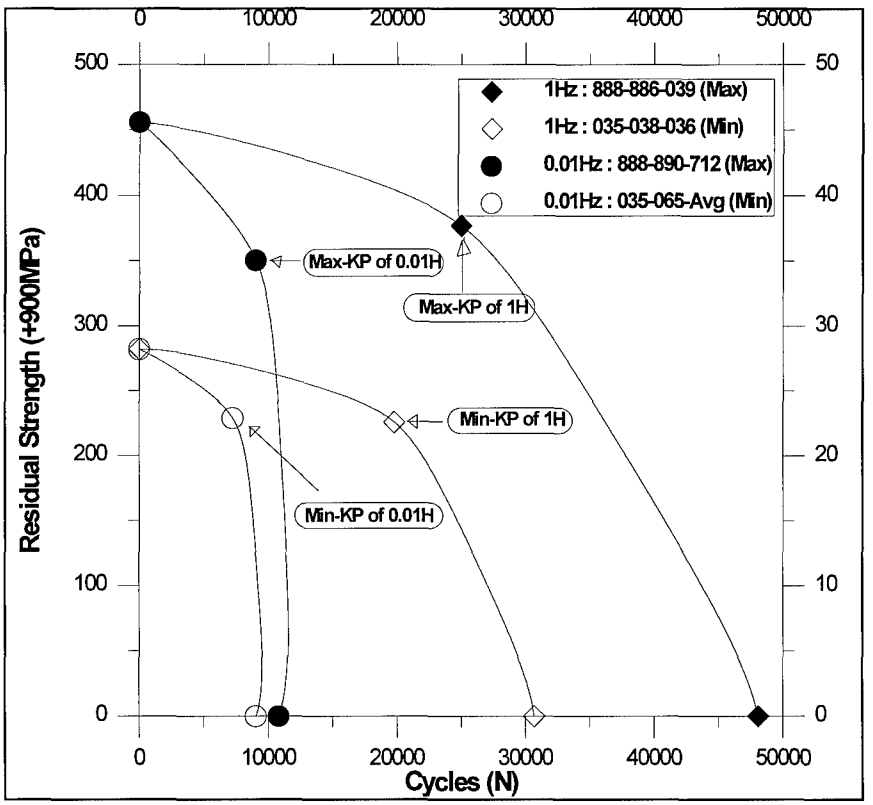

Figure 4.57 The residual strength bands (σ_{Max}-σ_{Res})vs. Cycle.

There are two possible reasons for the shorter life at the lower frequency. The specimen is exposed to the high temperature environment for a much longer duration. During this duration, oxidation may contribute to promote crack initiation and accelerate crack propagation. On the other hand, the lower frequency allowed more creep. Oxidation and creep are considered to be main differences between low and high frequency and, therefore to cause the time-dependency.

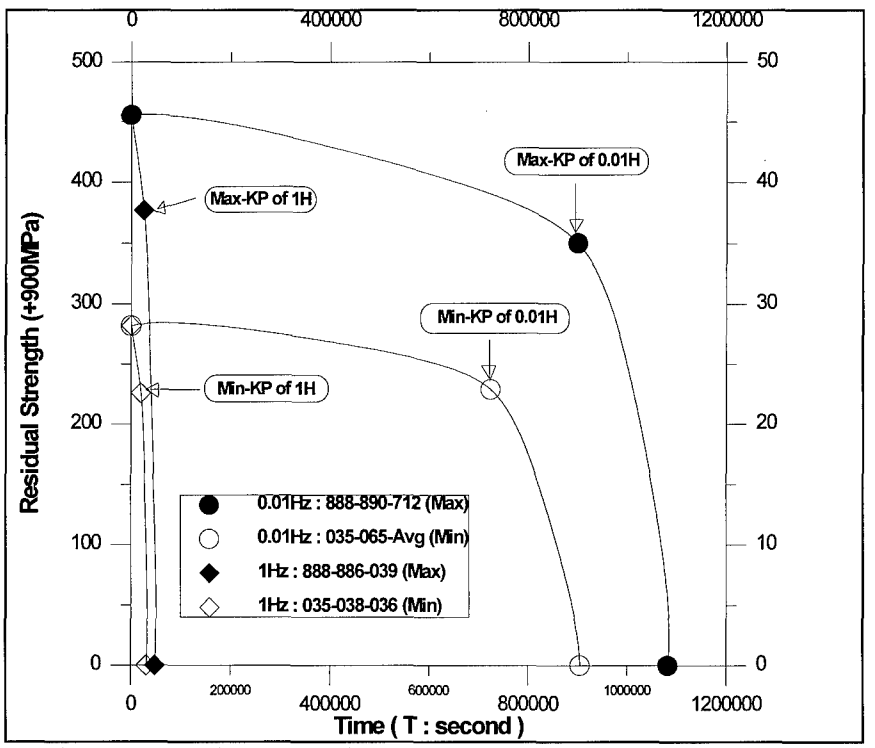

Figure 4.58 The residual strength bands (σ_{Max}-σ_{Res})vs. Cycle.

5. Summary, Conclusions and Recommendations

The purpose of this study was to investigate the residual strength and the frequency effects on the residual strength of an unidirectional laminate of SCS-6/Ti-6-4, a titanium alloy matrix based composite.

Three static tests were accomplished to obtain the Young's modulus, yield stress and ultimate tensile strength at the elevated temperature (427°C), and seventeen load-controlled isothermal fatigue tests were performed at two different frequencies through a systematic series of experiments. To obtain the residual strength, the fatigue tests were stopped at a specific percent of the life and a static test was used to obtain the residual strength. Among these seventeen residual strength tests, only eight residual strength measurements were successfully completed owing to variations from specimen to specimen and additional damage caused by thermocouple welding or machining. The failed specimens were used to obtain estimates of fatigue life variation. Modulus and strain histories, as well as stress-strain data during cycling provided macroscopic evidence of various fatigue mechanisms on both the specimens fatigued to failure and the specimens fatigued for the residual strength tests, while microscopic physical observations identified primary and secondary causes of specimen failure.

Tests conducted at the 1Hz frequency exhibited matrix dominated fatigue response. For the specimens under this test condition, macroscopic observation revealed that the strains increased rapidly within the first 10% of the life, but the rate varied from

specimen to specimen. Then, the strain grew continuously and slowly until failure. However, the modulus did not decrease in proportion to the increasing rate of the strain up to failure. In the microscopic observation, it was evident brittle behavior (flat matrix crack) prevailed on the fracture surface and ductile behavior was found in the adjoining area due to stress overload. These fracture surfaces subjected to the matrix-dominated fatigue responses easily allowed quantification of the fatigue area formed during a specific cyclic loading.

Tests conducted at the 0.01Hz frequency exhibited fiber-dominated fatigue response. The strain increased faster than in the 1Hz test within the first 10% of life owing to extensive matrix creep, and then kept steady up to 80% of life. During the final stage of life, it experienced a rapid increase in strain. The modulus behavior was a mirror image of the strain but the slope was not as high as that of the strain, which suggests that the matrix creep itself does not much affect the reduction in stiffness. Microscopic observation revealed that the fracture surface was fairly flat with extensive plasticity (ductility: void coalescence, matrix necking and fiber pull out). Because the fibers break first and then matrix fails, the ductile fracture surface made quantification of the fatigue area difficult.

Based on the understanding of these fatigue responses at the two different frequencies, the plotting of the residual strength versus cycles or time was performed in several ways. The residual strength band over the fatigue life was introduced to cover the scattered data caused from variations of the strength and fatigue life of the specimens. In these plots, two bands were used to represent both the minimum residual strength curve

and the maximum residual strength curve. Each band had a knee point at approximately 80% of its fatigue life and after this knee point the residual strength experienced a catastrophic drop up to the cycles to failure. There was no evidence of dependence of the residual strength on frequency. Similar to the fatigue response shifting from cycle-dependency to time-dependency whenever the test frequency changes from high to low, the residual strength shifts in proportion to the cycle or time-dependency. So, the residual strength can be considered to have a fatigue life dependency.

Comparisons between the fatigue area and residual strength was performed to estimate how much the residual strength decreased as the fatigue area increased. Due to a vast variation from specimen to specimen, correlating the fatigue area to the residual strength was difficult, but there are obvious trends of increasing fatigue area with reduction in residual strength. Further research is required to better quantify the fatigue or static area. Also, more research into the specimen to specimen variation is required to improve the confidence in the scatter bands.

Appendix - Additional Photographs of Fractured Specimens

Photographs of all fractured specimens are presented below.

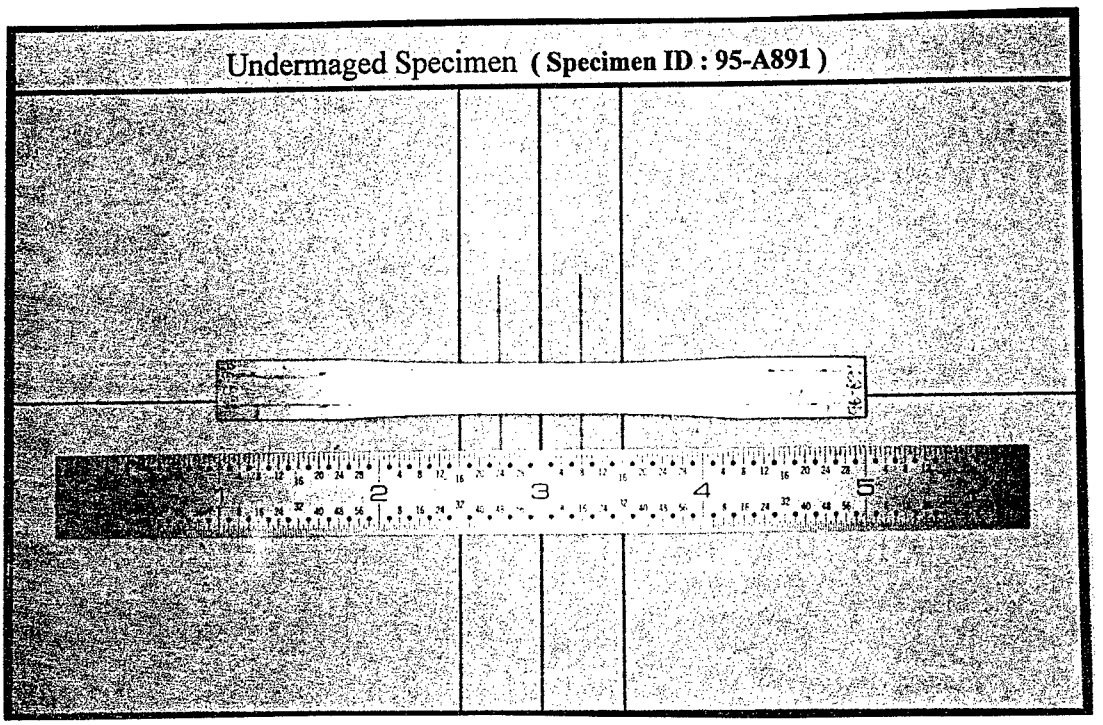

Figure A.1 Specimen Nos. 96-891 (Undamaged Specimen)

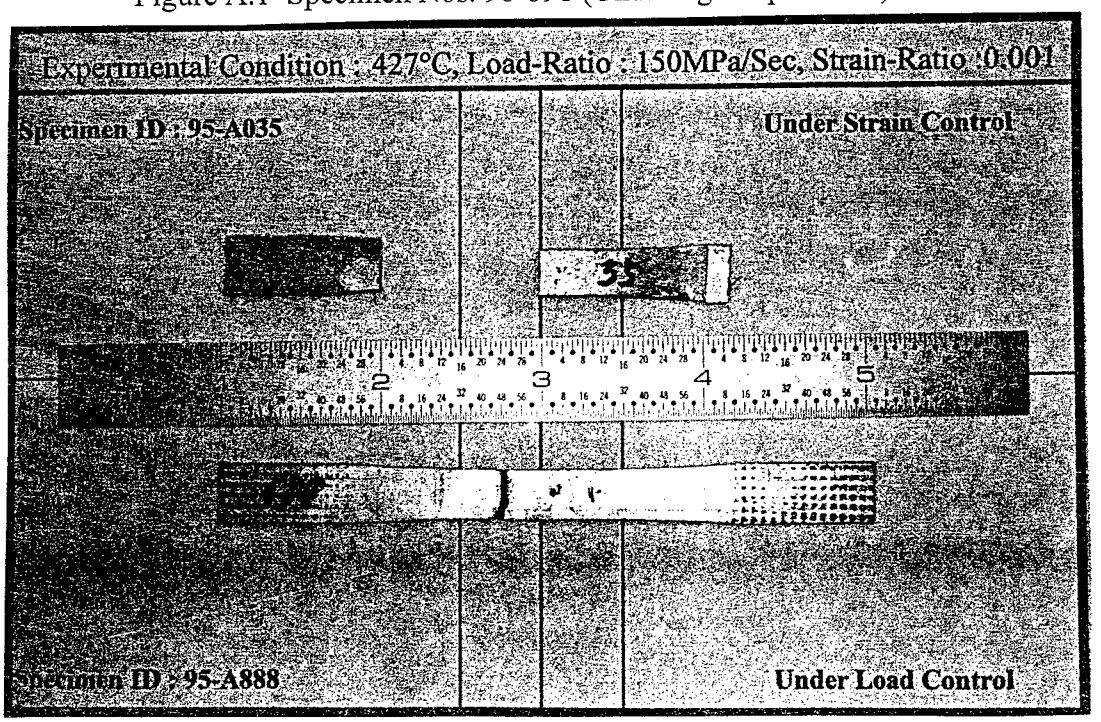

Figure A.2 Specimen Nos. 95-035 and 96-888 (Static Test)

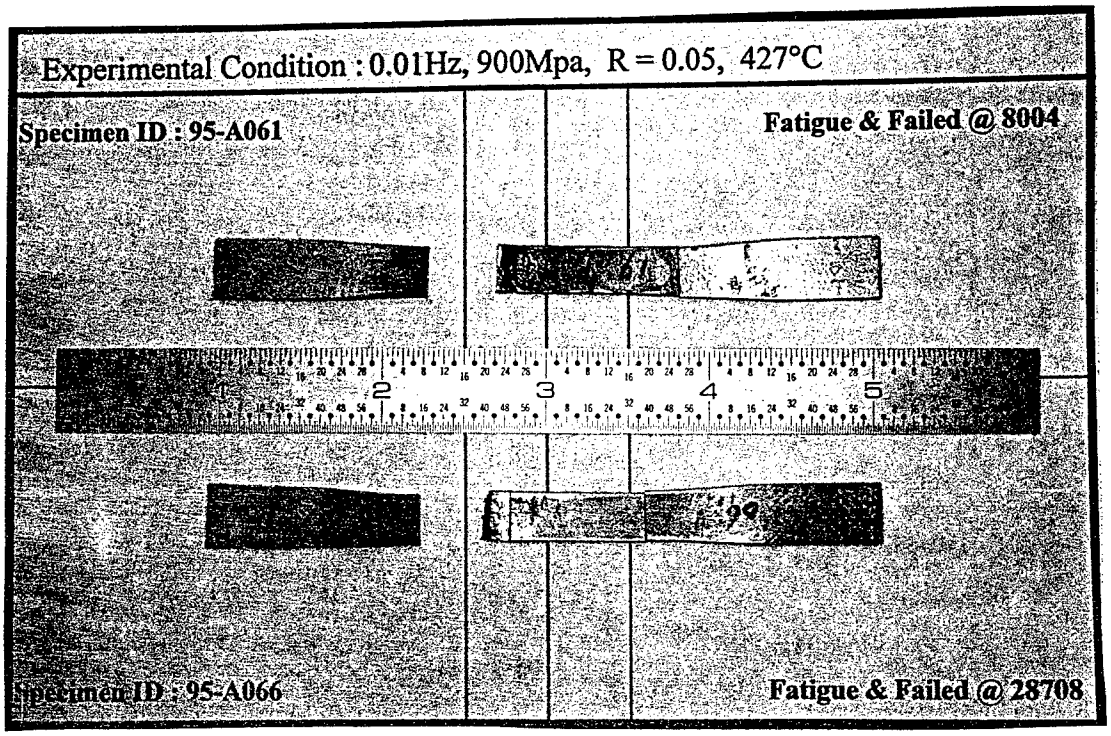

Figure A.3 Specimen Nos. 95-061 and 95-066 (1Hz Test)

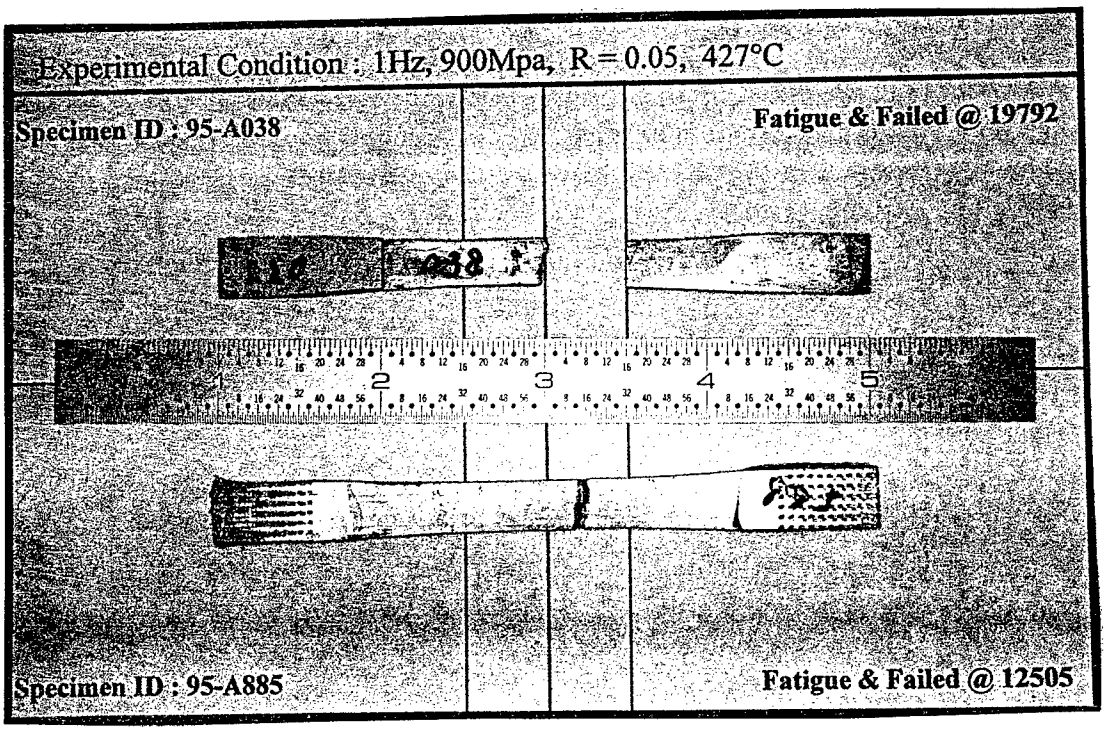

Figure A.4 Specimen Nos. 95-038 and 95-885 (1Hz Test)

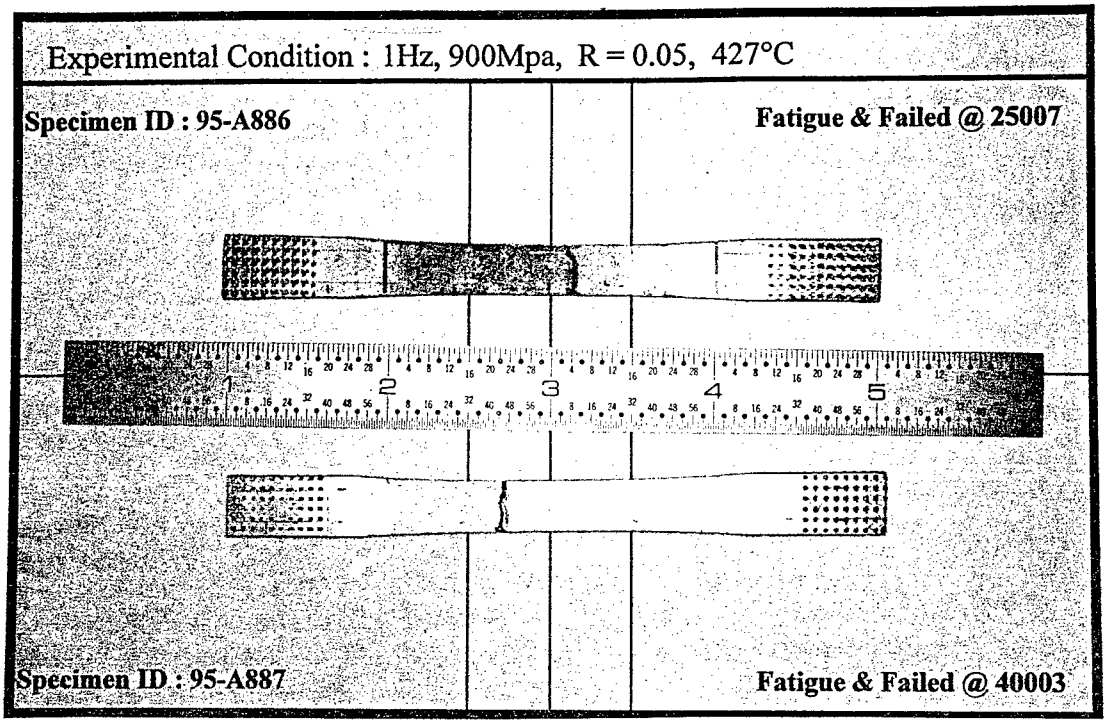

Figure A.5 Specimen Nos. 96-886 and 96-887 (1Hz Test)

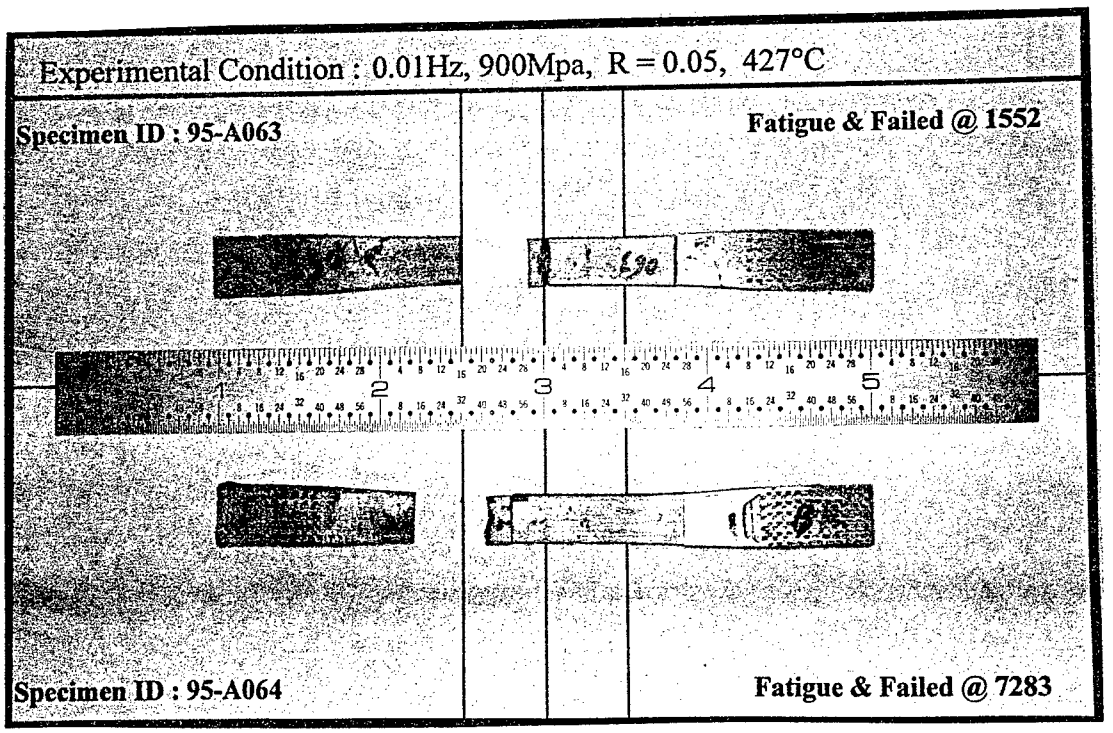

Figure A.6 Specimen Nos. 95-063 and 95-064 (0.01Hz Test)

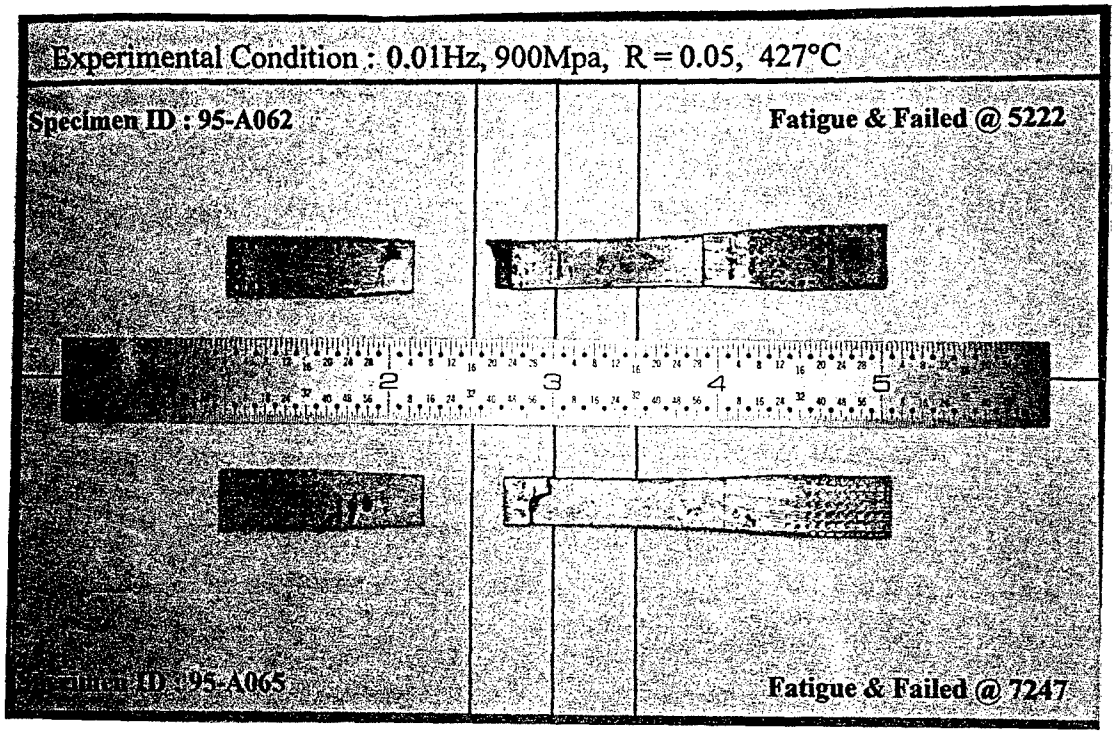

Figure A.7 Specimen Nos. 95-062 and 95-065 (0.01Hz Test)

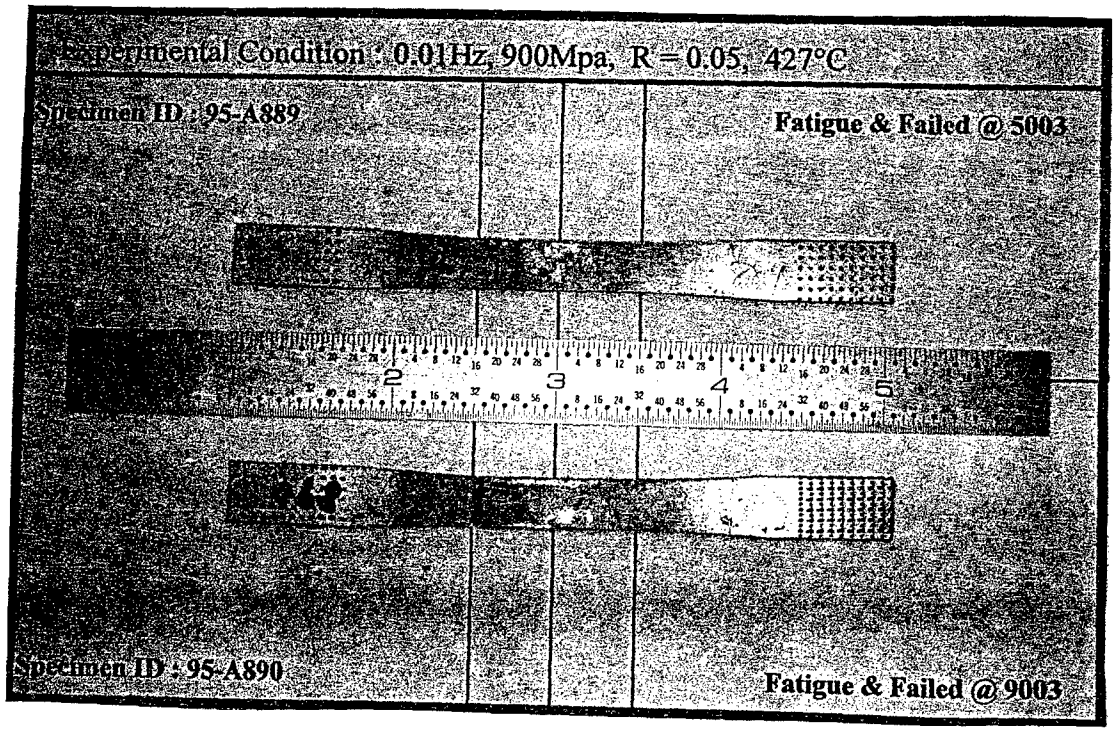

Figure A.8 Specimen Nos. 96-889 and 96-890 (0.01Hz Test)

Bibliography

1. Aboudi, J., "Elastoplasticity Theory for Composite Materials," Solid Mechanics Archives, Vol.11 1986, pp. 141-183.

2. Aboudi, J., " Closed Form Constitutive Equations for Metal Metrix Composites," International Journal of Engineering Science, Vol. 25, 1987, pp. 93 - 103.

3. Barney, C., Beevers, C.J., and Bowen, P., " Fatigue Crack Growth in SiC Continuous Fiber Reinforced Ti-6Al-4V Alloy Metrix Composite," Composites, Vol 2, 1992.

4. Bhatt, R. T. and Grimes, H. H., "Fatigue Behavior of SiC Reinforced Ti(6AI-4V) at 650 °C," Metallurgical Transactions A, Vol. 13A, November 1982, pp. 1933-19388.

5. El-Soudani, Sami, M., and Gambone, Mary, L., " Strain-Controlled fatigue Testing of SCS-6/Ti-6Al-4-V Metal-Matrix Composite,"

6. Ermer, Capt Paul G. Investiaation of the Failure Modes in a Metal Matrix Composite Under Thermal Cycling. MS Thesis, AFIT/GAE/ENY/89D-07. School of Engineering, Air Force Institute of Technology (AU), Wright-Patterson AFB OH, December 1989.

7. Forsyth,P.J.E. The Physical basis of Metal Fatigue. New York: American Elsevier Publishing Company, Inc., 1969.

8. Gabb, T. P. et al., "Isotherrnal and Nonisotherrnal Fatigue Behavior of a Metal Matrix Composite," Journal of Composite Materials, Vol. 24, June1990, pp. 667-686.

9. Gayda, J. and Gabb, T.P. "Effect of Heating Mode and Specimen Geometry on Fatigue Properties of a Metal Matrix Composite", NASA Conference Publication 10051,HITEMP Review October, 1990. pp 31-1-8.

10. Hertzberg, Richark W., Deformation and Fracture Mechanisms of Engineering Materials. 3d Ed., John Willy & Sons, Inc.: New York, 1989.

11. Highsmith, A. L., Shin, D., and Naik, R.A. " Local Stresses in Metal Matrix Composites Subjected to Thermal and Mechanical Loading," Thermal and Mechanical Behavior of Metal Matrix Composites and ceramic Matrix Composites, ASTM STP 1080, J.M. Kennedy, H.H. Moeller, and W.S. Johnsion, Eds., American Society for Testing and Materials, Philadelphia, 1990, pp.3-19.

12. Jacques, E. Schoutens, Kaman Tempo, "Introduction to Metal Matrix Composite Materials", DOD Metal Matrix Composites Information Analysis Center, Second Printing, MMC No.272, Chapter two,1982

13. Jeng, S.M., Yang, J.-M., and Yang, C.J. "Fracture Mechanisms of Fiber-Reinforced Titanium Alloy Matrix Composites Part II : Tensile Behavior," Matreial Science and Engineering, Vol 138, 1991, pp169-180.

14. Jeng, S.M., Alassoeur, P., and Yang J.-M., "Fracture mechanisms of fiber-reinforced titanium alloy matrix composites Part IV: Low cycle fatigue," Matreial Science and Engineering, Vol 148, 1991, pp67-77

15. Jeng, S.M., and Yang, J.-M., " Damage Mechanisms of SCS- 6/Ti-6AL-4V Composites Under Thermal-Mechanical Fatigue," Matreial Science and Engineering, Vol 156, 1992, pp 117-124.

16. Johnson, W. S., "Fatigue Testing and Damage Development in Continuous Fiber Reinforced Metal Matrix Composites," Metal Matrix Composites: Testing, Analysis, and Failure Modes, W. S. Johnson, Ed., American Society for Testing and Materials, Philadelphia, 1989.

17. Johnson, W.S., Lubowinski, S.i. and Highsmith, A.L.. "Mechanical Characterization of Unnotched SCS6/Ti-15-3 Metal Matrix Composites at Room Temperature," Thermal and Mechanical Behavior of Metal Matrix and Ceramic Matrix Composites, ASTM STP 1080, J.M. Kennedy, H.H. Moeller, and W.S. Johnson, Eds., American Society of Testing and Materials, Philadelphia, 1990, pp. 193-218.

18. Krishnaohanrao, Y.,Kutumbarao, V.V., Rama Rao,P. Fracture Michanism Maps for Titanium and its Alloy. Defence Metallurgica Laboratory, Hyderabad, India. Acta Metallurgica, Vol. 3, Sept. 1986, p.1783-1806.

19. Learch, B.A. and Hull, D.R., " As-Received Microstructure of SiC/ Ti-15-3 Composite," NASA TM- 100938, August 1988.

20. Majundar, B.S., and Bradley A. Lerch. " Fatigue Mechanisms in a Ti-Based Fiber-Reinforced MMC and Approaches to life Prediction." Submitted to Titanium Composites Workshop, La Jolla, California, June 1993.

21. Majumdar, B.S, and Newaz G.M., " Inelastic Deformation of MetalMatrix Composites: Plasticity and Damage Mechanism" Philosophical Magazine, 1992, Vol. 66, No. 2, 187-212.

22. Majumdar, B.S, and Newaz G.M., "Fatigue of SCS-6/Ti-15-3 Metal Matrix Composite," Battelle Memorial Institute, Columbus, OH,1993.

23. Mall, S., Ermer, P.G., " Thermal Fatigue Behavior of a Unidirectional SCS/Ti-15-3 Metal Matrix Composie. " Journal of Composite Materials, Vol. 25,December 1991, pp. 1668 - 1686.

24. Mallick, P. K., Fiber-reinforced Composites: Materials, Manufacturing, and Design (Second Edition), Michael Dekker, Inc., New York, 1993.

25. Micricon User's Manual. Research Inc., Minneapolis, MN, 1986.

26. Nicholas, T. et al., " Frequency and Stress Ratio Effects on Fatigue of Unidirectionsl SCS-6/Ti-24Al-11Nb Composite at 650° C," Fatigue 93, Vol.2, J. -P. Bailon and J. I. Dickson, Eds., EMAS, 1993, pp.995-1000.

27. Newaz G.M., Majumdar B.S., " Thermal Cycling Response of Quasi-
Isotropic Metal Matrix Composites," Battelle Memorial Institute, Columbus, OH. Submitted to The Journal of Engineering Materials and Technology - ASME.

28. Pernot, Capt John J., Crack Growth Rate Modelina of A Titanium-Aluminide Alloy Under Thermal-Mechanical Cycling. Dissertation, AFIT/DS/AA/91/3. School of Engineering, Air Force Institute of Technology (AU), Wright-Patterson AFB OH, December 1991.

29. Pittman, R.N., " Freqency Effects on Fatigue Behavior of a Unidirectional Metal Metrix Composite at Elevated Temperature," MS thesis, AFIT/GAE/ENY/95D-20, Graduate School of Engineering, Air Force Institute of Technology, Wright-Patterson AFB, OH., July, 1995.

30. Portner, Capt Barry D. Investigation of the Fatigue Damage Mechanisms in a Metal Matrix Composite Under Elevated. MS Thesis, AFIT/GAE/ENY/90D-07. School of Engineering, Air Force Institute of Technology (AU), Wright-Patterson AFB OH, December 1990.

31. Sanders, B. P. and Mall, S., "Longitudinal Fatigue Response of a Metal Matrix Composite Under Strain Controlled Mode at Elevated Temperature," Journal of Composites Technology & Research, Vol. 16, No. 4, October 1994, pp. 304-313.

32. Schmidt, C.G., Kanazawa, C.H., and Shockey, D.A., " Residual Strength of a Thermomechanically Fatigued TIMETAL 21S/SCS-6 Composite," Journal of Materials Engineering and Performance, Vol 4, 1995, pp. 624-626.

33. Schubbe, Capt Joel J. Investigation of the Damage Mechanisms in a Cross Ply Metal Matrix Comiposite Under Thermo-Mechanical Loading. MS Thesis, AFIT/GAE/ENY/90D-07. School of Engineering, Air Force Institute of Technology (AU), Wright-Patterson AFB OH, December 1990.

34. Sen-Tzer Chiou, " Residual Strength After Fatigue of Unidirectional and Cross-Ply Metal Matrix Composites at Elevated Temperature," MS thesis, AFIT/GAE/ENY/96J-20, Graduate School of Engineering, Air Force Institute of Technology, Wright-Patterson AFB, OH., July, 1996.

35. Skelton, R.P., Fatigue at igh Temperature. New York: Applied Science Publishers, 1983.

37. S. M. Jeng , P. Alassoeur , J. -M. Yang., "Fracture mechanisms of fiber-reinforced titanium alloy matrix composites Part IV: Low cycle fatigue," Material Science and Engineering, A148, 1991, P. 67~77

38. Sullivan, B.J., Buesking, K.W., " Effects of Carbon Interface Morphology on the Residual Stresses in Silicon Carbide/Titanium Composites." 21st Carbon Conference, Buffalo, NY, June 13-18, 1993.

39. Talreja, R. Faticfue of comnuite Materials, Technomic Publishing Company, 1987.

Vita

Major Sang-Myung Lee [redacted] a. He graduated from Kang Won High School in 1982 and entered the Republic of Korea (ROK) Military Academy that winter. In 1986, he was commissioned as a Second Lieutenant and received a Bachelor of Art in Chinese. His first tour of duty was at 26 Division, Uy Jeng Bu. There he was a platoon leader. In 1988, he entered the Korea Army Aviation School, and he has served as a helicopter pilot after graduation of that school. In 1989, he accomplished his second tour duty as an Education Officer, in Hong Chen, then he graduated from the ROK Army Aviation School for Office Advanced Course in October of the same year. Between November of 1989 and December of 1992, he stationed at 36 Army Aviation Corps, Poh Chen, Keng Ki Do, as a Personnel Officer, Aviation Schedule Officer and pilot. In 1993, he was selected to abroad education case, and then entered the graduate School of Engineering of the Air Force Institute of Technology in May 1994.

[redacted]

REPORT DOCUMENTATION PAGE

Form Approved
OMB No. 0704-0188

1. AGENCY USE ONLY *(Leave blank)*	2. REPORT DATE	3. REPORT TYPE AND DATES COVERED
	DECEMBER 1996	Mater's Thesis

4. TITLE AND SUBTITLE

RESIDUAL STRENGTH AND FATIGUE CHARACTERIZATION OF SCS-6/TI-6-4

5. FUNDING NUMBERS

6. AUTHOR(S)

SANG-MYUNG LEE, Major, ROKA

7. PERFORMING ORGANIZATION NAME(S) AND ADDRESS(ES)

Air Force Institute of Technology
2750 P Street
WPAFB, OH 45433-6583

8. PERFORMING ORGANIZATION REPORT NUMBER

AFIT/GAE/ENY/96D-7

9. SPONSORING / MONITORING AGENCY NAME(S) AND ADDRESS(ES)

WL/MLLN
2230 Tenth Street, Ste 1
WPAFB, OH 45433-6583

10. SPONSORING / MONITORING AGENCY REPORT NUMBER

11. SUPPLEMENTARY NOTES

12a. DISTRIBUTION / AVAILABILITY STATEMENT

Approved for Public release, distribution unlimited

12b. DISTRIBUTION CODE

A

13. ABSTRACT *(Maximum 200 words)*

This study investigated the residual strength of unidirectional laminate of SCS-6/Ti-6-4, a titanium alloy matrix based composite at elevated temperature 427°C under tension-tension load controlled mode (σ_{max} = 900MPa, R-ratio=0.05) with 1Hz and 0.01Hz frequencies. Two specimens were tested for a ultimate tensile strength and modulus of the materials and then were fatigued to failure. Based on the strength and fatigue life, specimens were fatigued to various fractions of the fatigue life and then loaded monotonically to failure. Macroscopic and microscopic observation were performed to characterize damage. Under both 1Hz and 0.01Hz test frequencies, the residual strength degraded so slowly up to 70~80% of the fatigue life and then dropped catastrophically to the end of the life. The critical failure behavior revealed in these material was able to be banded by the maximum and minimum curve so that most variation of the residual strength could be include within these ranges.

14. SUBJECT TERMS

Metal-matrix composite (MMC), Residual Strength, Frequency Effects, SCS-6/Ti-6-4, Isothermal Fatigue, Fiber Cracks, Matrix Crack, Creep

15. NUMBER OF PAGES

122

16. PRICE CODE

17. SECURITY CLASSIFICATION OF REPORT	18. SECURITY CLASSIFICATION OF THIS PAGE	19. SECURITY CLASSIFICATION OF ABSTRACT	20. LIMITATION OF ABSTRACT
Unclassified	Unclassified	Unclassified	UL

GENERAL INSTRUCTIONS FOR COMPLETING SF 298

The Report Documentation Page (RDP) is used in announcing and cataloging reports. It is important that this information be consistent with the rest of the report, particularly the cover and title page. Instructions for filling in each block of the form follow. It is important to ***stay within the lines*** to meet ***optical scanning requirements***.

Block 1. Agency Use Only *(Leave blank)*.

Block 2. Report Date. Full publication date including day, month, and year, if available (e.g. 1 Jan 88). Must cite at least the year.

Block 3. Type of Report and Dates Covered. State whether report is interim, final, etc. If applicable, enter inclusive report dates (e.g. 10 Jun 87 - 30 Jun 88).

Block 4. Title and Subtitle. A title is taken from the part of the report that provides the most meaningful and complete information. When a report is prepared in more than one volume, repeat the primary title, add volume number, and include subtitle for the specific volume. On classified documents enter the title classification in parentheses.

Block 5. Funding Numbers. To include contract and grant numbers; may include program element number(s), project number(s), task number(s), and work unit number(s). Use the following labels:

C	- Contract	**PR**	- Project
G	- Grant	**TA**	- Task
PE	- Program Element	**WU**	- Work Unit Accession No.

Block 6. Author(s). Name(s) of person(s) responsible for writing the report, performing the research, or credited with the content of the report. If editor or compiler, this should follow the name(s).

Block 7. Performing Organization Name(s) and Address(es). Self-explanatory.

Block 8. Performing Organization Report Number. Enter the unique alphanumeric report number(s) assigned by the organization performing the report.

Block 9. Sponsoring/Monitoring Agency Name(s) and Address(es). Self-explanatory.

Block 10. Sponsoring/Monitoring Agency Report Number. *(If known)*

Block 11. Supplementary Notes. Enter information not included elsewhere such as: Prepared in cooperation with...; Trans. of...; To be published in.... When a report is revised, include a statement whether the new report supersedes or supplements the older report.

Block 12a. Distribution/Availability Statement. Denotes public availability or limitations. Cite any availability to the public. Enter additional limitations or special markings in all capitals (e.g. NOFORN, REL, ITAR).

DOD - See DoDD 5230.24, "Distribution Statements on Technical Documents."
DOE - See authorities.
NASA - See Handbook NHB 2200.2.
NTIS - Leave blank.

Block 12b. Distribution Code.

DOD - Leave blank.
DOE - Enter DOE distribution categories from the Standard Distribution for Unclassified Scientific and Technical Reports.
NASA - Leave blank.
NTIS - Leave blank.

Block 13. Abstract. Include a brief *(Maximum 200 words)* factual summary of the most significant information contained in the report.

Block 14. Subject Terms. Keywords or phrases identifying major subjects in the report.

Block 15. Number of Pages. Enter the total number of pages.

Block 16. Price Code. Enter appropriate price code *(NTIS only)*.

Blocks 17. - 19. Security Classifications. Self-explanatory. Enter U.S. Security Classification in accordance with U.S. Security Regulations (i.e., UNCLASSIFIED). If form contains classified information, stamp classification on the top and bottom of the page.

Block 20. Limitation of Abstract. This block must be completed to assign a limitation to the abstract. Enter either UL (unlimited) or SAR (same as report). An entry in this block is necessary if the abstract is to be limited. If blank, the abstract is assumed to be unlimited.

★U.S.GPO:1993-0-336-043